การศึกษาโครงสร้างและพลวัตของไอออนโพแทสเซียมและไอออนแคลเซียมที่ซอลเวตอยู่ในสารละลายน้ำโดยใช้การจำลองพลวัตเชิงโมเลกุลที่ผสมผสานกลศาสตร์ควอนตัมและกลศาสตร์โมเลกุลแบบดั้งเดิมและบนพื้นฐานของวิธีโอเนียม-เอกซ์เอส

นายศุภชัย วันประโคน

วิทยานิพนธ์นี้เป็นส่วนหนึ่งของการศึกษาตามหลักสูตรปริญญาวิทยาศาสตรดุษฎีบัณฑิต
สาขาวิชาเคมี
มหาวิทยาลัยเทคโนโลยีสุรนารี
ปีการศึกษา 2554

STRUCTURE AND DYNAMICS OF THE HYDRATED K^+ AND Ca^{2+}: A COMPARATIVE STUDY OF THE CONVENTIONAL QM/MM MD AND QM/MM MD BASED ON ONIOM-XS METHOD

Supachai Wanprakhon

A Thesis Submitted in Partial Fulfillment of the Requirements for the Degree of Doctor of Philosophy in Chemistry

Suranaree University of Technology

Academic Year 2011

STRUCTURE AND DYNAMICS OF THE HYDRATED K^+ AND Ca^{2+}: A COMPARATIVE STUDY OF THE CONVENTIONAL QM/MM MD AND QM/MM MD BASED ON ONIOM-XS METHOD

Suranaree University of Technology has approved this thesis submitted in partial fulfillment of the requirements for the Degree of Doctor of Philosophy.

Thesis Examining Committee

_____

(Asst. Prof. Dr. Kunwadee Rangsriwatananon)

Chairperson

_____

(Assoc. Prof. Dr. Anan Tongraar)

Member (Thesis Advisor)

_____

(Prof. Dr. Kritsana Sagarik)

Member

_____

(Assoc. Prof. Dr. Albert Schulte)

Member

_____

(Asst. Prof. Dr. Viwat Vchirawongkwin)

Member

_____

(Prof. Dr. Sukit Limpijumnong)

Vice Rector for Academic Affairs

_____

(Assoc. Prof. Dr. Prapun Manyum)

Dean of Institute of Science

ศุภชัย วันประโคน : การศึกษาโครงสร้างและพลวัตของไอออนโพแทสเซียมและไอออนแคลเซียมที่ซอลเวตอยู่ในสารละลายน้ำโดยใช้การจำลองพลวัตเชิงโมเลกุลที่ผสมผสานกลศาสตร์ควอนตัมและกลศาสตร์โมเลกุลแบบดั้งเดิมและบนพื้นฐานของวิธีโอเนียม-เอกซ์เอส (STRUCTURE AND DYNAMICS OF THE HYDRATED K^+ AND Ca^{2+}: A COMPARATIVE STUDY OF THE CONVENTIONAL QM/MM MD AND QM/MM MD BASED ON ONIOM-XS METHOD) อาจารย์ที่ปรึกษา : รองศาสตราจารย์ ดร.อนันต์ ทองระอา, 134 หน้า.

การจำลองพลวัตเชิงโมเลกุลที่ผสมผสานกลศาสตร์ควอนตัมและกลศาสตร์โมเลกุลแบบดั้งเดิม (conventional QM/MM MD) และการจำลองพลวัตเชิงโมเลกุลที่ผสมผสานกลศาสตร์ควอนตัมและกลศาสตร์โมเลกุลบนพื้นฐานของวิธีโอเนียม-เอกซ์เอส (ONIOM-XS) ได้ถูกดำเนินการเพื่อศึกษาสมบัติเชิงโครงสร้างและเชิงพลวัตของไอออนโพแทสเซียม (K^+) และไอออนแคลเซียม (Ca^{2+}) ที่ซอลเวตอยู่ในสารละลายน้ำ โดยเทคนิคการจำลองดังกล่าวนี้ ส่วนของไอออนและน้ำที่อยู่ล้อมรอบไอออนจะถูกอธิบายด้วยกลศาสตร์ควอนตัมในระดับฮาร์ทรี-ฟอร์ค (HF) โดยใช้เบซิสเซตชนิด LANL2DZ และ DZV+ สำหรับไอออนและน้ำตามลำดับ ในขณะที่ส่วนที่เหลือของระบบจะถูกอธิบายโดยใช้ฟังก์ชันศักย์คู่ ผลการศึกษาพบว่า ค่าเลขไฮเดรชันเฉลี่ยของไอออนโพแทสเซียมและไอออนแคลเซียมในน้ำที่ได้จากการคำนวณโดยเทคนิค ONIOM-XS มีค่าเท่ากับ 6.3 และ 7.6 ตามลำดับ เปรียบเทียบกับผลที่ได้จากเทคนิค QM/MM แบบดั้งเดิม ซึ่งมีค่าเท่ากับ 7.0 และ 7.8 เมื่อพิจารณาร่วมกับข้อมูลด้านพลวัตซึ่งเทคนิคการจำลองทั้งสองให้ผลการศึกษาที่แตกต่างกันอย่างมีนัยสำคัญ แสดงให้เห็นความสามารถของเทคนิค ONIOM-XS ที่ทำนายสมบัติเชิงโครงสร้างและเชิงพลวัตของไอออนทั้งสองชนิดได้น่าเชื่อถือมากกว่าเทคนิค QM/MM แบบดั้งเดิม

สาขาวิชาเคมี ลายมือชื่อนักศึกษา_____

ปีการศึกษา 2554 ลายมือชื่ออาจารย์ที่ปรึกษา_____

SUPACHAI WANPRAKHON : STRUCTURE AND DYNAMICS OF THE HYDRATED K^+ AND Ca^{2+}: A COMPARATIVE STUDY OF THE CONVENTIONAL QM/MM MD AND QM/MM MD BASED ON ONIOM-XS METHOD. THESIS ADVISOR : ASSOC. PROF. ANAN TONGRAAR, Ph.D. 134 PP.

POTASSIUM ION/ CALCIUM ION/ ONIOM-XS/ QM/MM

Molecular dynamics (MD) simulations based on conventional QM/MM scheme and ONIOM-XS method were performed to investigate structural and dynamical properties of K^+ and Ca^{2+} in water. Regarding to the detailed analyses of the ONIOM-XS MD trajectories, the average hydration numbers for K^+ and Ca^{2+} were found to be 6.3 and 7.6, respectively, compared to the corresponding values of 7.0 and 7.8 derived by the conventional QM/MM simulations. Together with the significant difference found in the comparison of the dynamics details, the ONIOM-XS method clearly showed its capability in predicting more reliable detailed knowledge of these hydrated ions.

School of Chemistry Student's Signature_____

Academic Year 2011 Advisor's Signature_____

ACKNOWLEDGEMENTS

First of all, I would like to gratitude my thesis advisor, Assoc. Prof. Dr. Anan Tongraar for his exceptional generous support, academic guidance, advice and encouragement during my study. I would like to thank Prof. Dr. Kritsana Sagarik for his encouragement and help. I would like to thank committee members for their time and useful comments and suggestions.

I am thankful to Prof. Dr. Jiali Gao for his kindness and sincere suggestions for my research work and life when I visited at the University of Minnesota, United States of America. I would also like to thank my colleagues in Professor Gao's group for their help, giving me the wonderful experiences.

I would like to acknowledge the financial support from the Thailand Research Fund (TRF) through the Royal Golden Jubilee (RGJ) Ph.D. program (Grant No. PHD/0123/2549). Special thanks should go to the School of Chemistry, Institute of Science, Suranaree University of Technology (SUT) for powerful research facilities.

I would like to take this opportunity to express my deepest gratitude to all of my friends in the computational chemistry research group and my friends in School of Chemistry, SUT for their friendship, wonderful encouragement and kind assistance in work and life.

Finally, I would like to express my deepest gratitude to my parents for their unconditional love, wonderful encouragement and all supports.

Supachai Wanprakhon

CONTENTS

CONTENTS (Continued)

CONTENTS (Continued)

LIST OF TABLES

LIST OF TABLES (Continued)

LIST OF TABLES (Continued)

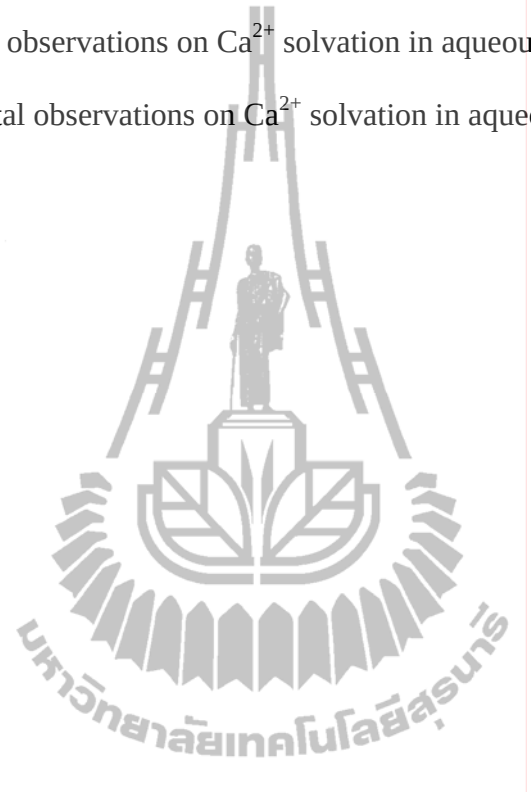

LIST OF FIGURES

LIST OF FIGURES (Continued)

Figure **Page**

LIST OF FIGURES (Continued)

LIST OF FIGURES (Continued)

LIST OF FIGURES (Continued)

Figure **Page**

LIST OF FIGURES (Continued)

Figure **Page**

LIST OF FIGURES (Continued)

Figure **Page**

LIST OF ABBREVIATIONS

XRD	=	X-ray diffraction
ND	=	Neutron diffraction
EXAFS	=	Extended X-ray absorption fine structure
MC	=	Monte Carlo
MD	=	Molecular dynamics
CPMD	=	Car-Parrinello molecular dynamics
QM/MM	=	Quantum mechanics/molecular mechanics
QMSTAT	=	Quantum mechanics/statistical mechanics
Ca^{2+}	=	Calcium ion
K^{+}	=	Potassium ion
KOH	=	Potassium hydroxide
KCl	=	Potassium chloride
KF	=	Potassium fluoride
KBr	=	Potassium bromide
KI	=	Potassium iodide
$CaCl_2$	=	Calcium choride
$Ca(NO_3)_2$	=	Calcium nitrate
$CaBr_2$	=	Calcium bromide
CaI_2	=	Calcium iodide
HF	=	Hartree-Fock

LIST OF ABBREVIATIONS (Continued)

DFT	=	Density functional theory
QCDF	=	Quasi-component distribution functions
MCY	=	Matsuoka-Clementi-Yoshimine configuration interaction potential for rigid water-water interactions
SPC/E	=	Simple point charge effective pair water model
CF2	=	Central force model version 2
LANL2DZ	=	Los Alamos ECP plus DZ
BLYP	=	Becke hybrid functional combined with Lee-Yang-Parr correlation function
B3LYP	=	Becke three-parameter hybrid functional combined with Lee-Yang-Parr correlation function
AMOEBA	=	Atomic multipole optimized energetics for biomolecular applications
OPLS	=	Optimized potentials for liquid simulations
CHARMM	=	Chemistry at Harvard molecular mechanics
SWM4-DP	=	Simple water model with four sites and drude polarizability
M	=	Molarity
CN	=	Coordination number
r_{min}	=	First minimum of peak
r_{max}	=	First maximum of peak
MP2	=	Second-order Møller-Plesset

LIST OF ABBREVIATIONS (Continued)

CCSD	=	Coupled cluster calculations using both single and double substitutions from Hatree-Fock determinant
ONIOM	=	Our own n-layered integrated molecular orbital and molecular mechanics
ONIOM-XS	=	An extension of the ONIOM method for molecular simulation in condensed phase
DZV+	=	Double zeta valence with diffuse function
CPU	=	Central processing unit
BJH	=	Flexible water model developed by Bopp, Jancsó and Heinzinger
RDF	=	Radial distribution function
ADF	=	Angular distribution function
VACF	=	Velocity autocorrelation functions
MRT	=	Mean resident times
Ψ	=	wavefunction
V	=	Potential field
$\hat{H}$	=	Hamiltonian operator
m_e	=	Mass of electron
m_k	=	Mass of nucleus
e	=	Electron charge

LIST OF ABBREVIATIONS (Continued)

Z	=	Atomic number
∇	=	Laplacian operator
Φ	=	Trial function
ψ	=	Product of a molecular orbital
χ	=	Spin orbital
etc	=	et cetera
MO	=	Molecular orbital
LCAO-MO	=	Linear combination of atomic orbitals to molecular orbital
STO	=	Slater-type orbital
GTO	=	Gaussian-type orbital
ECP	=	Effective core potential
PP	=	Pseudopotential
$\hat{J}_a$	=	Coulomb integral operator
$\hat{K}_a$	=	Exchange integral operator
SCF	=	Self-consistent field
RHF	=	Restricted Hatree-Fock
UHF	=	Unrestricted open-shell Hatree-Fock
CI	=	Configuration interaction
MP	=	Many-body perturbation
CC	=	Coupled cluster

LIST OF ABBREVIATIONS (Continued)

GGA	=	Generalized gradient approximation
NVE	=	Microcanonical ensemble
NVT	=	Canonical ensemble
μVT	=	Grand canonical ensemble
μ	=	Chemical potential
E_{tot}	=	Total interaction energy
E_{MM}	=	Interaction within MM region
E_{QM-MM}	=	Interaction between QM and MM regions
$(\Psi_{QM}\left\|\hat{H}\right\|\Psi_{QM})$	=	Interaction within QM region
F_i	=	Force acting on each particle
$S_m(r)$	=	Smoothing function
F_{QM}	=	QM force
F_{MM}	=	MM force
r_1	=	Distance characterizing the start of QM region
r_0	=	Distance characterizing the end of QM region
n_1	=	Number of particles in the QM sphere
n_2	=	Number of particles in the MM region
l	=	Number of particles in the the switching layer
$E^{ONIOM-XS}$	=	The potential energy of the entire system for ONIOM-XS

LIST OF ABBREVIATIONS (Continued)

$\bar{s}(\{r_1\})$	=	An average over a set of switching functions for individual exchanging particle in the switching layer
Aug-cc-pVDZ	=	Additional diffuse basis function and correlation consistent polarized valence double zeta
BO	=	Born-Oppenheimer
BOMD	=	Born-Oppenheimer molecular dynamics
BSSE	=	Basis set superposition error
ΔE_{HF}	=	Stabilization energies of the HF calculations
ΔE_{CCSD}	=	Stabilization energies of the CCSD calculations
ΔE_{diff}	=	Stabilization energies of cation-water complexes after BSSE corrections
D	=	Diffusion coefficient
FT-IR	=	Fourier transform infrared spectroscopy
IR	=	Infrared
ξ	=	x axis
η	=	y axis
ζ	=	z axis
V	=	Instantaneous velocity
S	=	Velocity of the center-of–mass

LIST OF ABBREVIATIONS (Continued)

R	=	Velocity component perpendicular to the molecular plane
P	=	Velocity component in the molecular plane
U	=	Projection of P on the normalized instantaneous O-H vectors
W	=	A unit vector perpendicular to it in the molecular plane
Rξ	=	Rotation around approximated x axis
Rη	=	Rotation around approximated y axis
Rζ	=	Rotation around approximated z axis
Å	=	Angstrom
au	=	Atomic unit
cm^{-1}	=	Wavenumber
fs	=	Femtosecond
K	=	Kelvin
kcal/mol	=	Kilocalorie per mole
ps	=	Picosecond
□	=	Degree
λ	=	wavelength
t_{sim}	=	Simulation time
N_{ex}	=	Number of exchange events
S_{ex}	=	Sustainability coefficient

LIST OF ABBREVIATIONS (Continued)

t^*	=	Time for observing the number of exchange water molecules
I_a	=	Associative-like interchange mechanism
I_d	=	Dissociative-like interchange mechanism
τ_{H_2O}	=	MRT of water molecules

CHAPTER I

INTRODUCTION

1.1 Literature reviews

Comprehensive information on the structure and dynamics of ions solvated in aqueous electrolyte solutions is essential in order to understand the crucial role of these ions in solution chemistry and biochemistry (George, 1958; Williams R. J, 1971). Among simple ions, potassium (K^+) and calcium (Ca^{2+}) are ubiquitous in nature, and the interactions of these ions with water are responsible for a diverse number of chemical and biological processes (Kollman and Kuntz, 1972). During the past decades, a number of experimental and theoretical attempts have been made to elucidate the details of these ions in aqueous solutions. Nevertheless, the characteristics of these hydrated ions derived by various theoretical (Bako, Hutter and Palinkas, 2002; Bernal-Uruchurtu and Ortega-Blake, 1995; Felice, Eric, Markus, François and Giulia, 2005; Floris, Persico, Tani and Tomasi, 1994; Grossfield, Ren and Ponder, 2003; Impey, Madden and McDonald, 1983; Kalko, Sese and Padro, 1996; Lamoureux and Roux, 2006; Lavanya, Marco and Michele, 1999; Lee and Rasaiah, 1996; Lim, Pribil, Ellmerer, Randolf and Rode, 2010; Mezei and Beveridge, 1981; Naor, Nostrand and Dellago, 2003; Obst and Bradaczek, 1996; Pálinkás and Heinzinger, 1986; Periole, Allouche, Daudey and Sanejouand, 1997; Rempe, Asthagiri and Pratt, 2004; Schwenk, Loeffler and Rode, 2001; Todorova,

Hünenberger and Hutter, 2008; Tofteberg, Öhrn and Karlström, 2006; Tongraar, Liedl and Rode, 1997; Tongraar, Liedl and Rode, 1998; Tongraar, T-Thienprasert, Rujirawat and Limpijumnong, 2010) and experimental techniques (Badyal, Barnes, Cuello and Simonson, 2004; Cummings, Enderby and Howe, 1980; Dang, Schenter, Glezakou and Fulton, 2006; Fulton, Heald, Badyal and Simonson, 2003; Hewish, Neilson and Enderby, 1982; Jalilehvand, Spangberg, Lindqvist-Reis, Hermansson, Persson and Sandstrom, 2001; Licheri, Piccaluga and Pinna, 1976; Neilson, Mason, Ramos and Sullivan, 2001; Neilson and Skipper, 1985; Pálinkás, Radnai and Hajdu, 1980; Smirnov, Yamagami, Wakita and Yamaguchi, 1997; Soper and Weckström, 2006; Spangberg, Hermansson, Lindqvist-Reis, Jalilehvand, Sandstrom and Persson, 2000) appear to reflect ambiguities, even for the fundamental data as the average coordination numbers. Previous theoretical and experimental observations on the K^+ and Ca^{2+} solvation in aqueous solutions are summarized in Tables A.1-A.4 (see Appendix A).

In terms of computer simulations, Monte Carlo (MC) and molecular dynamics (MD) simulations are well-established tools for studying ion-solvent complexes. In the past decades, most of earlier simulation works had relied on classical pair potentials for describing interactions of each interacting atoms or molecules in the system. However, it has been shown that classical pair potentials, although providing rather accurate structural details, often fail to predict the dynamic properties of such systems (Tongraar and Rode, 2001; Tongraar, Sagarik and Rode, 2001). On the other hand, it is known that the quality and accuracy of the simulation results depend crucially on the quality of the potential function employed in the simulations.

To accurately describe the properties of hydrated ions, it has been demonstrated that the interaction potentials must include polarizability and many-body (non-additive) contributions (Tongraar, Liedl and Rode, 1997). The non-additive contributions in ion-water complexes are generally related to the strength of binding energies between the ion and water. These many-body effects have been demonstrated to be large for the case of highly charge ions or strongly interacting systems (Remsungnen and Rode, 2004). It has been shown that the neglect of these terms in the potentials resulted in wrong structural and dynamical properties of many hydrated ions, especially for the description of their first hydration shell (Tongraar, Liedl and Rode, 1998; Tongraar and Rode, 2004). With regard to this point, various schemes have been proposed, for example, the polarizable continuum model (PCM) (Tomasi and Persico, 1994), which incorporates the many-body interactions in an average way, or a direct approach by calculating the energy hypersurface of many-body interactions and then fitting them to an analytical function (Probst, Spohr, Heinzinger and Bopp, 1991). In general, both exemplary models can provide significant improvement of the results. However, for the PCM model, a major weakness is that it cannot reproduce specific interaction with the surrounding solvent, such as hydrogen bonds (Erras-Hanauer, Clark and Eldik, 2003). For the second model, the construction of many-body potentials is rather difficult, and is hardly feasible for large molecular systems because of their complicated orientation dependence (Schwenk, Loeffler and Rode, 2001; Texler and Rode, 1997).

In principle, *ab initio* quantum mechanical methods can be seen as an ideal method for a correct treatment of multiple intermolecular interactions of the systems. However, the performance of quantum mechanics for a condensed-phase system

consisting of a large number of particles is still beyond the current computational feasibility. Thus, an alternative approach is to apply a so-called combined *ab initio* quantum mechanical and molecular mechanical (QM/MM) method (Field, Bash and Karplus, 1990; Singh and Kollman, 1986). In recent years, several hybrid QM/MM models have been proposed, incorporating either a semiempirical (Cummins and Gready, 1997; Gao, 1996), density functional (Car and Parrinello, 1985; Stanton, Hartsough and Merz, 1995) or even an *ab initio* Hartree-Fock (Muller and Warshel, 1995; Singh and Kollman, 1986) methodology with commonly used molecular mechanical force fields. Recently, a "Born-Oppenheimer *ab initio* QM/MM MD technique" has been introduced and applied for studying the structural and dynamical properties of various ions in solutions (Kerdcharoen, Liedl and Rode, 1996; Remsungnen and Rode, 2004; Rode, Schwenk and Tongraar, 2004; Tongraar and Rode, 1999; Tongraar and Rode, 2001; Tongraar and Rode, 2004; Tongraar, T-Thienprasert, Rujirawat and Limpijumnong, 2010). Based on the QM/MM technique, the active-site region (*i.e.*, the solvation shell around the ion) is treated quantum mechanically, while the environment consisting of further solvent molecules is described by classical MM potentials. By this technique, the complicated many-body contributions as well as the polarization effects, at least within the solvation sphere of the ion, can be reliably included. Despite the technique's successes, however, there are some unsolved problems that undermine the validity of this approach. For example, according to the conventional QM/MM scheme, a smoothing function is applied only for the exchanging particles that are crossing the QM-MM boundary. Such treatment is not realistic since an immediate exchange of particles between the QM and MM regions also affects the forces acting on the remaining QM particles. In

addition, the conventional QM/MM framework cannot clearly define the energy expression during the solvent exchange process (Kerdcharoen and Morokuma, 2002; Kerdcharoen and Morokuma, 2003).

To solve these problems, a more sophisticated QM/MM MD technique based on ONIOM-XS method has been proposed (Kerdcharoen and Morokuma, 2002; Kerdcharoen and Morokuma, 2003). This technique allows forces on all QM particles to be smoothed during particle exchange, and thus, clearly defines the system's energy expression. Recently, the ONIOM-XS MD technique has been successfully applied for systems of Li^+ (Kerdcharoen and Morokuma, 2002) and Ca^{2+} (Kerdcharoen and Morokuma, 2003) in liquid ammonia, proving its capability in providing reasonable energetic information and the coordination number.

In this work, the QM/MM MD technique based on ONIOM-XS method, abbreviated throughout this work as ONIOM-XS MD, will be applied for studying the hydration shell structure and dynamics of K^+ and Ca^{2+} in aqueous solution. The results obtained by the ONIOM-XS MD simulations will be compared to the corresponding data obtained by the conventional QM/MM scheme, as well as to the available experimental data.

1.2 Research objectives

1. To apply the more sophisticated ONIOM-XS MD technique for studying the solvation structure and dynamics of the hydrated K^+ and Ca^{2+} ions.

2. To investigate the validity of the conventional QM/MM technique for the treatment of such particular systems, by comparing the QM/MM results with those obtained by the more accurate ONIOM-XS MD technique.

1.3 Scope and limitation of the study

This work focuses on the performance of the more accurate ONIOM-XS MD technique for elucidating the structural and dynamical properties of K^+ and Ca^{2+} in aqueous solution. The results obtained by the ONIOM-XS MD simulations will be analyzed and compared to those obtained by the conventional QM/MM scheme. In this respect, the observed differences between the conventional QM/MM and ONIOM-XS MD simulations will be considered as the deficiency of the conventional QM/MM scheme for the treatment of such particular systems. With regard to both conventional QM/MM and ONIOM-XS MD simulations, the QM treated region refers to the sphere which includes the ion and its surrounding water molecules, which is treated at Hartree-Fock level of accuracy using DZV+ basis set for water and LANL2DZ basis set for K^+ and Ca^{2+}, while the rest of the system is described by classical pair potentials (Tongraar, Liedl and Rode, 1997; Tongraar, Liedl and Rode, 1998). In this work, the QM size with diameter of 8.4 Å was chosen, consisting of central ion of interest and about 12-16 surrounding water molecules. Regarding to the computational expense for QM force calculations, the selection of QM method, QM size and basis sets employed in the simulations is considered to be suitable, compromising between the quality of the simulation results and the requirement of CPU time. The structural properties of the hydrated K^+ and Ca^{2+} will be characterized through a set of radial distribution functions (RDFs) and their corresponding

integration numbers, together with detailed analysis on angular distribution functions (ADFs) and orientations of water molecules surrounding the ions. The corresponding dynamics details will be analyzed by mean of velocity autocorrelation functions (VACFs) and mean residence times (MRTs) of water molecules as well as water exchange processes at the ion. The results obtained by the conventional QM/MM and ONIOM-XS MD simulations will also be compared to the available experimental data.

1.4 References

Badyal, Y. S., Barnes, A. C., Cuello, G. J. and Simonson, J. M. (2004). Understanding the effects of concentration on the solvation structure of Ca^{2+} in aqueous solution. II: Insights into longer range order from neutron diffraction isotope substitution. **The Journal of Physical Chemistry A**. 108: 11819-11827.

Bako, I., Hutter, J. and Palinkas, G. (2002). Car-Parrinello molecular dynamics simulation of the hydrated calcium ion. **The Journal of Chemical Physics**. 117: 9838-9843.

Bernal-Uruchurtu, M. I. and Ortega-Blake, I. (1995). A refined Monte Carlo study of Mg^{2+} and Ca^{2+} hydration. **The Journal of Chemical Physics**. 103: 1588-1598.

Car, R. and Parrinello, M. (1985). Unified approach for molecular dynamics and density-functional theory. **Physical Review Letters**. 55: 2471-2474.

Cummings, S., Enderby, J. E. and Howe, R. A. (1980). Ion hydration in aqueous $CaCl_2$ solutions. **Journal of Physics C: Solid State Physics**. 13: 1-7.

Cummins, P. L. and Gready, J. E. (1997). Coupled semiempirical molecular orbital and molecular mechanics model (QM/MM) for organic molecules in aqueous solution. **Journal of Computational Chemistry**. 18: 1496-1512.

Dang, L. X., Schenter, G. K., Glezakou, V.-A. and Fulton, J. L. (2006). Molecular simulation analysis and x-ray absorption measurement of Ca^{2+}, K^{+} and Cl^{-} ions in solution. **The Journal of Physical Chemistry B**. 110: 23644-23654.

Erras-Hanauer, H., Clark, T. and Eldik, R. (2003). Molecular orbital and DFT studies on water exchange mechanisms of metal ions. **Coordination Chemistry Reviews**. 238-239: 233-253.

Felice, C. L., Eric, S., Markus, A., François, G. and Giulia, G. (2005). A first-principles molecular dynamics study of calcium in water. **ChemPhysChem**. 6: 1745-1749.

Field, M. J., Bash, P. A. and Karplus, M. (1990). A combined quantum mechanical and molecular mechanical potential for molecular dynamics simulations. **Journal of Computational Chemistry**. 11: 700-733.

Floris, F. M., Persico, M., Tani, A. and Tomasi, J. (1994). Hydration shell structure of the calcium ion from simulations with *ab initio* effective pair potentials. **Chemical Physics Letters**. 227: 126-132.

Fulton, J. L., Heald, S. M., Badyal, Y. S. and Simonson, J. M. (2003). Understanding the effects of concentration on the solvation structure of Ca^{2+} in aqueous solution. I: The perspective on local structure from EXAFS and XANES. **The Journal of Physical Chemistry A**. 107: 4688-4696.

Gao, J. (1996). Methods and applications of combined quantum mechanical and molecular mechanical potentials. **Reviews in Computational Chemistry** (pp. 119-185): John Wiley & Sons, Inc.

George, W. B. (1958). Structure in ionic solutions. II. **The Journal of Chemical Physics**. 28: 464-469.

Grossfield, A., Ren, P. and Ponder, J. W. (2003). Ion solvation thermodynamics from simulation with a polarizable force field. **Journal of the American Chemical Society**. 125: 15671-15682.

Hewish, N. A., Neilson, G. W. and Enderby, J. E. (1982). Environment of Ca^{2+} ions in aqueous solvent. **Nature**. 297: 138-139.

Impey, R. W., Madden, P. A. and McDonald, I. R. (1983). Hydration and mobility of ions in solution. **Journal of Physical Chemistry**. 87: 5071-5083.

Jalilehvand, F., Spangberg, D., Lindqvist-Reis, P., Hermansson, K., Persson, I. and Sandstrom, M. (2001). Hydration of the calcium ion. An EXAFS, large-angle x-ray scattering, and molecular dynamics simulation study. **Journal of the American Chemical Society**. 123: 431-441.

Kalko, S. G., Sese, G. and Padro, J. A. (1996). On the effects of truncating the electrostatic interactions: Free energies of ion hydration. **The Journal of Chemical Physics**. 104: 9578-9585.

Kerdcharoen, T., Liedl, K. R. and Rode, B. M. (1996). A QM/MM simulation method applied to the solution of Li^{+} in liquid ammonia. **Chemical Physics**. 211: 313-323.

Kerdcharoen, T. and Morokuma, K. (2002). ONIOM-XS: an extension of the ONIOM method for molecular simulation in condensed phase. **Chemical Physics Letters**. 355: 257-262.

Kerdcharoen, T. and Morokuma, K. (2003). Combined quantum mechanics and molecular mechanics simulation of Ca^{2+}/ammonia solution based on the ONIOM-XS method: Octahedral coordination and implication to biology. **The Journal of Chemical Physics**. 118: 8856-8862.

Kollman, P. A. and Kuntz, I. D. (1972). Cation hydration. **Journal of the American Chemical Society**. 94: 9236-9237.

Lamoureux, G. and Roux, B. (2006). Absolute hydration free energy scale for alkali and halide ions established from simulations with a polarizable force field. **The Journal of Physical Chemistry B**. 110: 3308-3322.

Lavanya, M. R., Marco, B. and Michele, P. (1999). *Ab initio* molecular-dynamics simulation of K^+ solvation in water. **The Journal of Chemical Physics**. 111: 1587-1591.

Lee, S. H. and Rasaiah, J. C. (1996). Molecular dynamics simulation of ion mobility. 2. Alkali metal and halide ions using the SPC/E model for water at 25 °C. **The Journal of Physical Chemistry**. 100: 1420-1425.

Licheri, G., Piccaluga, G. and Pinna, G. (1976). X-ray diffraction study of the average solute species in $CaCl_2$ aqueous solutions. **The Journal of Chemical Physics**. 64: 2437-2441.

Lim, L. H. V., Pribil, A. B., Ellmerer, A. E., Randolf, B. R. and Rode, B. M. (2010). Temperature dependence of structure and dynamics of the hydrated Ca^{2+} ion according to ab initio quantum mechanical charge field and classical molecular dynamics. **Journal of Computational Chemistry**. 31: 1195-1200.

Mezei, M. and Beveridge, D. L. (1981). Monte Carlo studies of the structure of dilute aqueous solutions of Li^{+}, Na^{+}, K^{+}, F^{-}, and Cl^{-}. **The Journal of Chemical Physics**. 74: 6902-6910.

Muller, R. P. and Warshel, A. (1995). *Ab initio* calculations of free energy barriers for chemical reactions in solution. **The Journal of Physical Chemistry**. 99: 17516-17524.

Naor, M. M., Nostrand, K. V. and Dellago, C. (2003). Car-Parrinello molecular dynamics simulation of the calcium ion in liquid water. **Chemical Physics Letters**. 369: 159-164.

Neilson, G. W., Mason, P. E., Ramos, S. and Sullivan, D. (2001). Neutron and x-ray scattering studies of hydration in aqueous solutions. **Philosophical Transactions of the Royal Society A: Mathematical, Physical and Engineering Sciences**. 359: 1575-1591.

Neilson, G. W. and Skipper, N. (1985). K^{+} coordination in aqueous solution. **Chemical Physics Letters**. 114: 35-38.

Obst, S. and Bradaczek, H. (1996). Molecular dynamics study of the structure and dynamics of the hydration shell of alkaline and alkaline-earth metal cations. **The Journal of Physical Chemistry**. 100: 15677-15687.

Pálinkás, G. and Heinzinger, K. (1986). Hydration shell structure of the calcium ion. **Chemical Physics Letters**. 126: 251-254.

Periole, X., Allouche, D., Daudey, J. P. and Sanejouand, Y. H. (1997). Simple two-body cation-water interaction potentials derived from *ab initio* calculations. Comparison to results obtained with an empirical approach. **The Journal of Physical Chemistry B**. 101: 5018-5025.

Probst, M. M., Spohr, E., Heinzinger, K. and Bopp, P. (1991). A molecular dynamics simulation of an aqueous beryllium chloride solution. **Molecular Simulation**. 7: 43-57.

Rempe, S. B., Asthagiri, D. and Pratt, L. R. (2004). Inner shell definition and absolute hydration free energy of K^+(aq) on the basis of quasi-chemical theory and *ab initio* molecular dynamics. **Physical Chemistry Chemical Physics**. 6: 1966-1969.

Remsungnen, T. and Rode, B. M. (2004). Molecular dynamics simulation of the hydration of transition metal ions: the role of non-additive effects in the hydration shells of Fe^{2+} and Fe^{3+} ions. **Chemical Physics Letters**. 385: 491-497.

Rode, B. M., Schwenk, C. F. and Tongraar, A. (2004). Structure and dynamics of hydrated ions--new insights through quantum mechanical simulations. **Journal of Molecular Liquids**. 110: 105-122.

Schwenk, C. F., Loeffler, H. H. and Rode, B. M. (2001). Molecular dynamics simulations of Ca^{2+} in water: Comparison of a classical simulation including three-body corrections and Born--Oppenheimer *ab initio* and density functional theory quantum mechanical/molecular mechanics simulations. **The Journal of Chemical Physics**. 115: 10808-10813.

Singh, U. C. and Kollman, P. A. (1986). A combined *ab initio* quantum mechanical and molecular mechanical method for carrying out simulations on complex molecular systems: Applications to the $CH_3Cl + Cl^-$ exchange reaction and gas phase protonation of polyethers. **Journal of Computational Chemistry**. 7: 718-730.

Smirnov, P., Yamagami, M., Wakita, H. and Yamaguchi, T. (1997). An x-ray diffraction study on concentrated aqueous calcium nitrate solutions at subzero temperatures. **Journal of Molecular Liquids**. 73-74: 305-316.

Soper, A. K. and Weckström, K. (2006). Ion solvation and water structure in potassium halide aqueous solutions. **Biophysical Chemistry**. 124: 180-191.

Spangberg, D., Hermansson, K., Lindqvist-Reis, P., Jalilehvand, F., Sandstrom, M. and Persson, I. (2000). Model extended x-ray absorption fine structure (EXAFS) spectra from molecular dynamics data for Ca^{2+} and Al^{3+} aqueous solutions. **The Journal of Physical Chemistry B**. 104: 10467-10472.

Stanton, R. V., Hartsough, D. S. and Merz, K. M. (1995). An examination of a density functional/molecular mechanical coupled potential. **Journal of Computational Chemistry**. 16: 113-128.

Texler, N. R. and Rode, B. M. (1997). Monte Carlo simulations of copper chloride solutions at various concentrations including full 3-body correction terms. **Chemical Physics**. 222: 281-288.

Todorova, T., Hünenberger, P. H. and Hutter, J. (2008). Car–Parrinello molecular dynamics simulations of $CaCl_2$ aqueous solutions. **Journal of Chemical Theory and Computation**. 4: 779-789.

Tofteberg, T., Öhrn, A. and Karlström, G. (2006). Combined quantum chemical statistical mechanical simulations of Mg^{2+}, Ca^{2+} and Sr^{2+} in water. **Chemical Physics Letters**. 429: 436-439.

Tomasi, J. and Persico, M. (1994). Molecular interactions in solution: An overview of methods based on continuous distributions of the solvent. **Chemical Reviews**. 94: 2027-2094.

Tongraar, A., Liedl, K. R. and Rode, B. M. (1997). Solvation of Ca^{2+} in water studied by Born-Oppenheimer *ab initio* QM/MM dynamics. **The Journal of Physical Chemistry A**. 101: 6299-6309.

Tongraar, A., Liedl, K. R. and Rode, B. M. (1998). Born−Oppenheimer *ab initio* QM/MM dynamics simulations of Na^{+} and K^{+} in water: From structure making to structure breaking effects. **The Journal of Physical Chemistry A**. 102: 10340-10347.

Tongraar, A. and Rode, B. M. (1999). Preferential solvation of Li^{+} in 18.45 % aqueous ammonia: A Born-Oppenheimer *ab initio* quantum mechanics/molecular mechanics MD simulation. **The Journal of Physical Chemistry A**. 103: 8524-8527.

Tongraar, A. and Rode, B. M. (2001). The role of non-additive contributions on the hydration shell structure of Mg^{2+} studied by Born-Oppenheimer *ab initio* quantum mechanical/molecular mechanical molecular dynamics simulation. **Chemical Physics Letters**. 346: 485-491.

Tongraar, A. and Rode, B. M. (2004). Dynamical properties of water molecules in the hydration shells of Na^{+} and K^{+}: *ab initio* QM/MM molecular dynamics simulations. **Chemical Physics Letters**. 385: 378-383.

Tongraar, A., Sagarik, K. and Rode, B. M. (2001). Effects of many-body interactions on the preferential solvation of Mg^{2+} in aqueous ammonia solution: A Born-Oppenheimer *ab initio* QM/MM dynamics study. **The Journal of Physical Chemistry B**. 105: 10559-10564.

Tongraar, A., T-Thienprasert, J., Rujirawat, S. and Limpijumnong, S. (2010). Structure of the hydrated Ca^{2+} and Cl^{-}: Combined x-ray absorption measurements and QM/MM MD simulations study. **Physical Chemistry Chemical Physics**. 12: 10876-10887.

Williams R. J, P. (1971). Biochemistry of group IA and IIA cations. **Bioinorganic Chemistry.** (pp. 155-173). Washington, D. C.: American Chemical Society.

CHAPTER II

QUANTUM CHEMISTRY

2.1 Introduction to quantum chemistry

Quantum chemistry is based on quantum mechanical principles, in which the fundamental behavior of matter at the molecular scale can be described through the understanding of the electron behavior. A wavefunction, which can be obtained by solving the *Schrödinger equation* (Schrödinger, 1926), is the tool of quantum chemistry for describing the properties of matter in terms of energies and positions of the nuclei and electrons. Many chemical problems can be solved by applying quantum chemistry, especially for the understanding of chemical bonding, spectral phenomena, molecular reactivity and various other fundamental chemical problems.

2.2 Schrödinger equation

In chemistry, most applications of quantum mechanics (QM) deal with the Schrödinger equation. Based on Schrödinger equation, electrons are considered as wave-like particles whose "waviness" is mathematically represented by a set of wavefunctions, Ψ. For a one-electron atom, the connection between classical waves and de Broglie's particle waves was made by Schrödinger. The classical three-dimensional wave equation can be written as

$$\nabla^2\Psi = -(\frac{2\pi}{\lambda})^2\Psi \tag{2.1}$$

where ∇ is the Laplacian operator ($\nabla \equiv \frac{\partial}{\partial x} + \frac{\partial}{\partial y} + \frac{\partial}{\partial z}$) and Ψ is the wave function describing the displacement at any point along the wave. Schrödinger substituted the de Broglie wavelength, λ, in term of energy to adapt the classical wave equation to particle waves. The Schrödinger equation is then given by

$$\nabla^2\Psi = -(\frac{8\pi^2 m}{h^2})(E - V)\Psi, \tag{2.2}$$

then

$$\left[(\frac{-h^2}{8\pi^2 m})\nabla^2 + V\right]\Psi = E\Psi, \tag{2.3}$$

which is known as *Schrödinger's time-independent* wave equation for a single particle of the mass (m) moving in the three-dimensional potential field (V). The left-hand side of the equation is called the *Hamiltonian operator* ($\hat{H}$),

$$\hat{H} \equiv \left[(\frac{-h^2}{8\pi^2 m})\nabla^2 + V\right], \tag{2.4}$$

which can often be written as

$$\hat{H}\Psi = E\Psi. \tag{2.5}$$

The equation (2.5) can be further simplified since the *Born-Oppenheimer approximation* considers the nuclei wave function can be separated and the electron distribution depends only on the instantaneous positions of nuclei and not on their velocities. Therefore, an electronic Schrödinger equation can be obtained as

$$\hat{H}^{elec}\Psi^{elec} = E^{elec}\Psi^{elec}. \tag{2.6}$$

Hence, the Hamiltonian operator for an atom with k electrons can be written as

$$\hat{H}^{elec} = \left[\left(\frac{-h^2}{8\pi^2 m_e}\right)\sum_{i=1}^{k}\nabla_i^2 - \sum_{i=1}^{k}\frac{Z}{r_i}\right] + \sum_{i=1}^{k-1}\sum_{j=i+1}^{k}\frac{1}{r_{ij}}. \tag{2.7}$$

$T_{electron}$ $V_{electron\text{-}nucleus}$ $V_{electron\text{-}electron}$

Within the Born-Oppenheimer approximation, the electronic Schrödinger equation can be solved at any given set of nuclei positions, then $T_{nucleus}$ is omitted. The Schrödinger equation for a multi-electron atom can be solved numerically. Although $V_{electron\text{-}electron}$ cannot be included as an explicit term in the Hamiltonian, its effect on Ψ can be accounted by a mathematically simpler approach that each electron interacts with an average field of the nucleus and all other electrons (see self-consistent field approximation in section 2.7). The Hamiltonian operator for a molecule with N atoms and k electrons is given by

$$\hat{H}^{elec} = \left[\left(\frac{-h^2}{8\pi^2 m_e}\right) \sum_{i=1}^{k} \nabla_i^2 \quad - \quad \sum_{j=1}^{N} \sum_{i=1}^{k} \frac{Z_j}{r_{ji}} \right]$$

$$T_{electron} \qquad V_{electron\text{-}nucleus} \qquad (2.8)$$

$$+ \sum_{i=1}^{k-1} \sum_{n=i+1}^{k} \frac{1}{r_{in}} \quad + \quad \sum_{j=1}^{N-1} \sum_{m=j+1}^{N} \frac{Z_j Z_m}{R_{jm}},$$

$$V_{electron\text{-}electron} \qquad V_{nucleus\text{-}nucleus}$$

where $V_{nucleus\text{-}nucleus}$ is typically treat as a constant.

2.3 Molecular orbital theory

Molecular quantum mechanics make use of the *Molecular Orbital (MO)* approach which applies one-electron functions or orbitals to approximate a full wavefunction. The complete wavefunction for a single electron is termed a spin orbital (χ) which is the product of a molecular orbital (ψ) and spin function (α or β). The simplest type of a wavefunction appropriate for the description of an n-electron system can be written in the form of product of spin orbitals,

$$\Psi_{product} = \chi_1(1)\chi_2(2)\ldots\chi_n(n), \qquad (2.9)$$

where $\chi_i(i)$ is the spin orbitals of electron i . However, such a wavefunction is not acceptable because it does not allow the property of antisymmetry. The multi-electron wavefunction must take into consideration the fact that electrons are indistinguishable, and therefore intercharging electron position assignments in a wavefunction cannot

lead to a different wavefunction. To ensure antisymmetry, the spin orbitals are arranged in a determinant wave function,

$$\Psi_{\text{det}} = \begin{vmatrix} \chi_1(1) & \chi_2(1) & \cdots & \chi_n(1) \\ \chi_1(2) & \chi_2(2) & \cdots & \chi_n(2) \\ \vdots & \vdots & \ddots & \vdots \\ \chi_1(n) & \chi_2(n) & \cdots & \chi_n(n) \end{vmatrix}. \tag{2.10}$$

The practical use in building up a determinant wavefunction is to choose a set of molecular orbitals, ψ_1, ψ_2, ψ_3, ..., ψ_n, and then to assign electrons of α and β spin to these orbitals. The determinant wavefunction in equation (2.10) vanishes if two columns are identical, which follows the *Pauli exclusion principle*. For some further properties of the molecular orbital wavefunctions, it is possible to force the orbitals to be *orthogonal* to each other,

$$\int \psi_i^* \psi_j dxdydz = 0, \text{ for } i \neq j, \tag{2.11}$$

and molecular orbitals may be *normalized*,

$$\int \psi_i^* \psi_i dxdydz = 1, \tag{2.12}$$

corresponding to the requirement that the probability of finding the electron anywhere in the space is unity. Thus, the determinant wavefunction (equation (2.10)) may be normalized and full many-electron molecular orbital wavefunction, for example, for

the closed-shell ground state of a molecular with *n* (even) electrons, doubly occupying *n/2* orbitals, can be written as

$$\Psi = \frac{1}{\sqrt{n!}} \begin{vmatrix} \psi_1(1)\alpha(1) & \psi_1(1)\beta(1) & \psi_2(1)\alpha(1) & \cdots & \psi_{n/2}(1)\beta(1) \\ \psi_1(2)\alpha(2) & \psi_1(2)\beta(2) & \psi_2(2)\alpha(2) & \cdots & \psi_{n/2}(2)\beta(2) \\ \vdots & \vdots & \vdots & \ddots & \vdots \\ \psi_1(n)\alpha(n) & \psi_1(n)\beta(n) & \psi_2(n)\alpha(n) & \cdots & \psi_{n/2}(n)\beta(n) \end{vmatrix}. \qquad (2.13)$$

An approximate wavefunction constructed from one electron orbital is often referred to as a *Slater determinant* (Slater, 1929).

2.4 The LCAO-MO method and basis set approach

The molecular orbitals can be built form the atomic orbitals by using a so-called "*Linear Combination of Atomic Orbitals to Molecular Orbitals* (LCAO-MO)" method. The molecular orbitals, ψ, can be composed of a set of atomic orbitals known as basis functions. If the basis functions are ϕ_1, ϕ_2, ..., ϕ_n, then an individual orbital, ψ_i, can be written as

$$\psi_i = \sum_{\mu=1}^{n} c_{\mu i}\phi_\mu, \qquad (2.14)$$

where $c_{\mu i}$ are the molecular orbital expansion coefficients, *n* is the number of atomic basis function. Here, the set of *n* function ϕ_μ is called *basis set*. The $c_{\mu i}$ can be

calculated using various approaches, most of which are based on the *linear variation* method.

The common types of basis function, or called *atomic orbital*, used in the electronic structure calculation are *Slater Type Orbitals* (STOs) (Slater, 1930) and *Gaussian Type Orbitals* (GTOs) (Boys, 1950).

The formalism of the STOs can be presented as

$$\phi_i(\zeta,n,l,m;r,\theta,\phi) = Nr^{n-1}e^{-\zeta r}Y_{lm}(\theta,\phi), \tag{2.15}$$

where N is the normalization constant and ζ is exponent. The r, θ, and ϕ are spherical coordinates, and Y_{lm} is the angular momentum part. The n, l, and m are quantum numbers referring to principal, angular momentum and magnetic, respectively. The STOs screening constants are calculated for small model molecules using rigorous self-consistent field methods, and then being generated for use with actual molecules of interest. The accuracy of STOs can be improved by combining two or more STOs (i.e. with two different values of ζ) into a single one-electron wavefunction (double ζ basis set).

The STOs are usually applied for atomic and diatomic system, which high accuracy, such as in semi-empirical methods where all three- and four-center integrals are neglected and in density functional methods that do not include exact exchange and that the coulomb energy is calculated by fitting the density into a set of auxiliary functions. However, the STOs do not satisfy in two-electron integral problem. The feasible basis functions are GTOs, which are functions of the form

$$\phi_i(\alpha, l, m, n; x, y, z) = Ne^{-\alpha r^2} x^l y^m z^n, \tag{2.16}$$

where N is a normalization constant, and α is exponent. The x, y, and z are Cartesian coordinates. The l, m, and n are now not quantum numbers but simply integral exponents at Cartesian coordinates and $r^2 = x^2 + y^2 + z^2$. The advantage of GTOs is that the product of two Gaussians at different centers is equivalent to a single Gaussian function centered at a point between the two centers. Therefore, the two-electron integral problem on three and four or more different atomic centers can be reduced to integrals over two different centers. However, the GTO gives an inferior representation of the orbitals at the atomic nuclei, which can be considered at 1s-orbital. A 1s-orbital of STO has a cusp at the atomic nucleus but a GTO does not, as shown in Figure 2.1. In this respect, the larger basis must be used to achieve the accuracy comparable to that obtained from STOs.

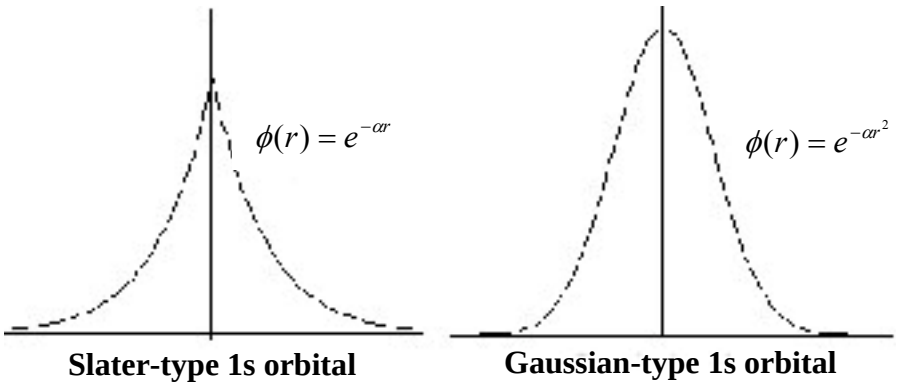

Figure 2.1 The Slater-type and Gauss-type for 1s orbital.

The most important factor for creating the molecular orbital is the set of parameters applied to the basis function, called as *basis set*. The smallest number of function possible for constructing the molecular orbital is called a *minimum basis set*. The improvement of the basis set can be made by replacing two basis functions into each basis function in the minimal basis set, called as *double zeta* (DZ). The larger basis set is a *triple zeta* (TZ), where three basis functions are used to represent each of the minimal basis sets. The compromise between the DZ and TZ basis sets is called a *split valence* (SV) basis set, in which each valence atomic orbital is represented by two basis functions while each core orbital is represented by a single basis function.

In 1969, Hehre and coworkers (Hehre, Stewart and Pople, 1969) designed the basis set by expanding the STO in terms of n primitive Gaussians, called as STO-nG basis set. The primitive Gaussian has been derived for n = 2-6. However, the STO-3G basis set is a widely used minimal basis set, as shown in Figure 2.2. The STO-3G basis set partially represents the cusp of s-type orbital at the atomic nuclei.

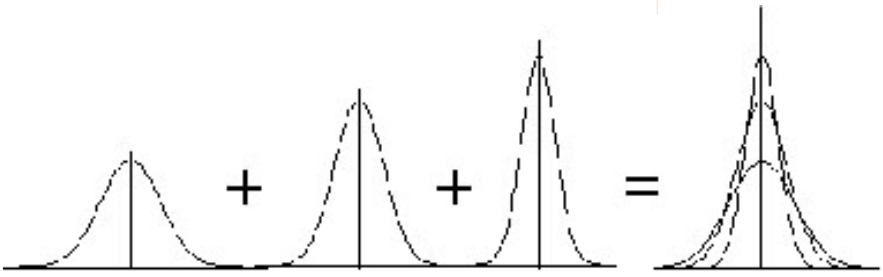

Figure 2.2 The STO-3G basis set representing the desired STO.

In addition, Hehre and coworkers have applied the split valence for having flexibility in the basis set, which can be designed as *k-nlm*G basis set. The first parameter (*k*) indicates the number of primitives used in the contracted core, while the

two values (*nl*) refer to a split valence, and three values (*nlm*) refer to a triple split valence, such as 6-311G. For the triple split valence basis, the core orbitals are a contraction of six primitives and the valence split into three functions, represented by three, one and one primitive GTOs. The Pople's style basis sets may include diffuse and/or polarization functions. The diffuse function can be denoted as + or ++ before the G, in which the first + indicates one set of diffuse s- and p-function adding on heavy atoms and the second + refer to the inclusion of diffuse s-function for hydrogen atom. The polarization function can be put after the G, which separates designation for heavy and hydrogen atoms. For example, 6-31+G(d) basis set refers to a split valence with additional diffuse sp-functions and a single d-type polarization function only on heavy atoms. The largest standard Pople style basis set is 6-311++G(3df,3pd). In addition, the polarization function can be replaced with * notation, for example, the 6-311G* basis set is identical to 6-311G(d) and 6-311G** basis set is identical to 6-311G(d,p).

Since several GTOs are often grouped together, the *contracted Gaussian function* has been applied to *Dunning-Huzinaga* (DZ) basis set (Dunning, 1970; Dunning, 1971; Huzinaga, 1965). The DZ basis set can be made by a contraction such as the (9s5p) primitive GTOs to [4s, 2p]. The contraction scheme is 6,1,1,1 for s-functions and 4,1 for the p-functions. In addition, the development of basis set by Dunning and coworker for recovering the correlation energy of the valence electrons is known as the *correlation consistent* (cc) basis sets. The general formulation can be written as cc-pV*n*Z, where *n* = D for double zeta, T for triple zeta, Q for quadruple zeta, and so on.

For the systems involving a large number of core electrons elements, it is necessary to use a large number of basis functions for describing them. However, since the deep core electrons are not much important in a chemical sense, this leads to an approximation by replacing the core electrons with analytical functions, called as an *Effective Core Potential* (ECP) or *Pseudopotentials*. In practice, such basis set is reasonably accurate and efficient, representing the combined nuclear-electronic core to the remaining electrons.

2.5 The variation theory

Since the solution of the time-independent Schrödinger equation of many-electron systems cannot be solved exactly, the variation method has been applied to determine the lowest energy, which represents the ground state of the system. If Φ is any chosen trial variation function of the electronic coordinates and is normalized, then an expectation value of the energy, E, corresponding to this function can be obtained from

$$E = \int \Phi^* \hat{H} \Phi d\tau, \tag{2.17}$$

where integration takes into account for all coordinates of all electrons, and the asterisk denotes complex conjunction. The variation method allows us to calculate an upper bound for the system's ground state energy which is often greater than exact energy,

$$E \geq E_{exact}. \tag{2.18}$$

If Φ happens to be exact wavefunction, Ψ, for the electronic ground state, it will satisfy the Schrödinger equation. Since Ψ is normalized, E will therefore be that exact energy E,

$$E = E_{exact} \int \Psi^* \Psi d\tau = E_{exact}. \tag{2.19}$$

The great advantage of the variation method in approximate quantum mechanics is that the same criteria can be applied to any trial functions to obtain approximations to correct wavefunctions. The object of the LCAO-MO based methods is to find the $c_{\mu i}$ that best approximates the actual wave function ψ_i. According to the variation theorem, this is equivalent to finding the $c_{\mu i}$ that gives rise to the lowest possible energy (minimum energy) for a given choice of Hamiltonian and basis set. We select a basis set for orbital expansion and the coefficient $c_{\mu i}$ may then be adjusted to minimize the expectation value of the energy E. The resulting value of E will then be as close to the exact energy E_{exact} as possible within the limitations imposed by the single determinant wavefunction, in an energy sense, is found by minimizing E with respect to coefficients $c_{\mu i}$. This implies variational equations of

$$\frac{\partial E}{\partial C_{\mu i}} = 0 \qquad (\text{all } \mu, i). \tag{2.20}$$

2.6 Basis set superposition error

With regard to the calculation of molecular energies using atomic basis sets, especially for weak interactions, an error occurs from the use of basis functions on adjustment molecules (Davidson and Chakravorty, 1994). The results are known as "*Basis Set Superposition Error* (BSSE)" (Boys and Bernardi, 1970). The BSSE causes overestimation of the attractive contribution to the interaction energy and consequently provides an illegitimate increase of binding energy in a molecule. Consequently, this may lead to less accurate results regarding to molecular geometry optimization and molecular charge distribution. The BSSE can be calculated with the help of *ghos*t atoms. In this respect, the amount of BSSE can be estimated using *Counterpoise Procedure* (CP) (Boys and Bernardi, 1970). The counterpoise correction is the energy lowering of single monomer in the presence of *ghost* basis functions located at the position of the atomic centers of that monomer, but without additional nuclear charges or electrons. The correction for BSSE in the molecular calculations with medium and small basis sets can result in values of interaction energies which are fairly close to those obtained by using more expensive and large basis sets. However, the counterpoise method will not provide effective improvement of the results if the atomic basis sets are very poor. The counterpoise procedure has been used as a standard tool of theoretical chemistry although some researchers have raised serious doubts on the usefulness of this procedure (Schwenke and Truhlar, 1986; Schwenke and Truhlar, 1987). The counterpoise correction can be very reasonable for the estimation of weak electronic interaction energies with small basis sets at Hatree-Fock level of accuracy. However, this approach has failed for the

estimation of strong electronic interaction energies even if with up to date basis sets, as demonstrated by a study of cyclic hydrogen fluoride trimer (Liedl, 1998).

2.7 Hartree-Fock method

The important factor in the electronic structure calculations is the electron-electron repulsions, which must be included in any accurate electronic structure calculations. The *Hartree-Fock* (HF) method has been used to treat the electron-electron repulsions in an average way. A single determinant wavefunction is substituted into the original electronic Schrödinger equation and after applying lots of algebra, it yields the Hartree-Fock equations. The resulting Hartree-Fock equations can be viewed as an alternative Schrödinger equation where the exact Hamiltonian has been replaced by an approximation. The Harmiltonian that describes this approximation is called the *Fock operator* and then the one-electron Hamiltonian operator is defined by

$$\hat{F}(1) = \hat{H}^{core}(1) + \sum_{a=1}^{N/2}(2\hat{J}_a(1) - \hat{K}_a(1)), \tag{2.21}$$

where $\hat{H}^{core}(1)$ is the exact one-electron operator,

$$\hat{H}^{core}(1) = -\frac{1}{2}\nabla_1^2 - \sum_{a=1}^{N/2}\frac{Z_a}{r_{1a}}, \tag{2.22}$$

$\hat{J}_a$ and $\hat{K}_a$ are coulomb integral and exchange integral operators, respectively,

$$\hat{J}_a(1)\phi_a(\chi_1) = (\int \phi_a^*(\chi_2)\frac{1}{r_{12}}\phi_a(\chi_2)d\chi_2)\phi_a(\chi_1), \quad (2.23)$$

and

$$\hat{K}_a(1)\phi_a(\chi_1) = (\int \phi_a(\chi_2)\frac{1}{r_{12}}\phi_a^*(\chi_2)d\chi_2)\phi_a(\chi_1). \quad (2.24)$$

The difference between the Fock operator and the exact Hamiltonian is that the coulomb operator has been replaced by an operator describing the interaction of each electron with the average field of all other electrons. Note that, the expansion of the wavefunction in term of basis functions from the application of LCAO-MO method lead to a limitation of the accuracy of the *ab initio* Hartree-Fock approach since there is limited number of basis functions available. The greater the number of basis functions, the better the wavefunction and the lower the energy. The limit of an infinite basis set is known as the *Hartree-Fock limit*. The Hartree-Fock equation for atom can be solved by numerical integration. However, complication arises when molecules are considered because there are more than one center. Thus, the Hartree-Fock equation can be written independently using *Roothaan-Hall equations*,

$$\sum_{\nu=1}^{N}(F_{\mu\nu} - \varepsilon_i S_{\mu\nu})c_{\nu i} = 0, \quad \mu = 1, 2, 3, ..., N \quad (2.25)$$

with the normalization conditions,

$$\sum_{\mu=1}^{N}\sum_{\nu=1}^{N} c_{\mu i}^{*} S_{\mu\nu} c_{\nu i} = 1, \tag{2.26}$$

where ε_i is the one-electron energy of molecular orbital ψ_i and $S_{\mu\nu}$ is the element of an $N \times N$ matrix termed the overlap matrix.

$$S_{\mu\nu} = \int \phi_{\mu}^{*}(1)\phi_{\nu}(1)dx_1 dy_1 dz_1, \tag{2.27}$$

and $F_{\mu\nu}$ is the element of another $N \times N$ matrix, called the *Fock matrix*,

$$F_{\mu\nu} = H_{\mu\nu}^{core} + \sum_{\lambda=1}^{N}\sum_{\sigma=1}^{N} P_{\lambda\sigma}\left[\langle \mu\nu | \lambda\sigma \rangle - \frac{1}{2}\langle \mu\lambda | \nu\sigma \rangle\right]. \tag{2.28}$$

In this expression, $H_{\mu\nu}^{core}$ is a matrix representing the energy of a single electron in a field of "bare" nuclei. Its elements are

$$H_{\mu\nu}^{core} = \int \phi_{\mu}^{*}(1)\hat{H}^{core}(1)\phi_{\nu}(1)dx_1 dy_1 dz_1, \tag{2.29}$$

in which

$$\hat{H}^{core}(1) = -\frac{1}{2}\left(\frac{\partial^2}{\partial x_1^2} + \frac{\partial^2}{\partial y_1^2} + \frac{\partial^2}{\partial z_1^2}\right) - \sum_{A=1}^{M}\frac{Z_A}{r_{1A}}, \tag{2.30}$$

where Z_A is the atomic number of atom A, and summation is carried out over all atoms. The quantities $\langle \mu\nu | \lambda\sigma \rangle$ and $\langle \mu\lambda | \nu\sigma \rangle$ appering in (2.28) are two-electron integrals,

$$\langle \mu\nu | \lambda\sigma \rangle = \iint \phi_\mu^*(1)\phi_\nu(1)(\frac{1}{r_{12}})\phi_\lambda^*(2)\phi_\sigma(2)dx_1dy_1dz_1dx_2dy_2dz_2, \tag{2.31}$$

and

$$\langle \mu\lambda | \nu\sigma \rangle = \iint \phi_\mu^*(1)\phi_\lambda(1)(\frac{1}{r_{12}})\phi_\nu^*(2)\phi_\sigma(2)dx_1dy_1dz_1dx_2dy_2dz_2, \tag{2.32}$$

which are multiplied by the elements of the one-electron density matrix, $P_{\lambda\sigma}$,

$$P_{\lambda\sigma} = 2\sum_{i=1}^{occ} c_{\lambda i}^* c_{\sigma i}. \tag{2.33}$$

The significance of the density matrix is that it describes the electron density of the molecules. Thus, the criterion for judging convergence of the SCF procedure can refer to the density as well as to the energy because both have to be stationary at self-consistence. In equation (2.33), the summation refers to occupy each molecular orbital, and the asterisk denotes complex conjugation (required if the molecular orbitals are not the real functions). The electronic energy, E^{elec}, is now given by

$$E^{elec} = \frac{1}{2}\sum_{\mu=1}^{N}\sum_{\nu=1}^{N} P_{\mu\nu}(F_{\mu\nu} + H_{\mu\nu}^{core}), \tag{2.34}$$

and when adding the internuclear repulsion,

$$E^{nr} = \sum_{A}^{N} \sum_{B>A}^{N} \frac{Z_A Z_B}{R_{AB}}, \tag{2.35}$$

yields an expression for the total energy.

The two-electron integrals over atomic basis functions give rise to a major practical problem in the application of the *ab initio* Hartree-Fock method due to the computational requirement which is approximated to $N^4/8$ for N basis functions. Not only time consuming of the integral calculation, but also their storage on disk is practically impossible for large systems. The *Direct SCF methods* have become available which reduce these problems significantly. In these approaches, the two-electron integrals are not stored but recalculated as required. This makes sense because the CPU of modern computers is very fast, while I/O operation takes quite long time. Secondly, only those integrals that are expected to have a significant value are actually calculated. With these tricks built into modern programs, the direct algorithms are actually faster than the conventional one for systems of more than about 100 basis functions (depending on the particular computer). On small workstations, direct SCF methods are the only practical option, even for small systems.

2.8 Electron correlation

It is known that motions of electrons are correlated and they tend to repel each electron which gives a lower energy. According to the HF method, each electron moves in the static electric field created by all of the other electrons in the system. On the other hand, the electron cannot see other electrons during the HF calculation. Thus, the significant deficiency of the HF method is that it fails to adequately treat the correlation between motions of electrons. The effects of electron correlation were usually neglected in the Hamiltonian in the previous section. This leads to limitation of the calculated HF energies. The difference between HF and exact (nonrelativistic) energies is the correlation energy,

$$E_{exact} = E_{HF} + E_{correlation}, \tag{2.40}$$

In several cases, the neglect of electron correlation effects can lead to some anomalous of qualitative information. As a consequence, the Ψ and E cannot be used to correctly predict atomic properties without somewhere accounting for electron correlation.

The electron correlation methods calculate the coefficient in front of the other determinants in different way, such as *configuration interaction* (CI) (Sherrill and Schaefer, 1999), *many-body perturbation* (MP) (Møller and Plesset, 1934), *coupled cluster* (CC) (Bartlett, 1989) and *density function theory* (DFT).

2.9 References

Bartlett, R. J. (1989). Coupled-cluster approach to molecular structure and spectra: a step toward predictive quantum chemistry. **The Journal of Physical Chemistry**. 93: 1697-1708.

Boys, S. F. (1950). Electronic wave functions. I. A general method of calculation for the stationary states of any molecular system. **Proceedings of the Royal Society of London. Series A. Mathematical and Physical Sciences**. 200: 542-554.

Boys, S. F. and Bernardi, F. (1970). The calculation of small molecular interactions by the differences of separate total energies. Some procedures with reduced errors. **Molecular Physics: An International Journal at the Interface Between Chemistry and Physics**. 19: 553-566.

Davidson, E. R. and Chakravorty, S. J. (1994). A possible definition of basis set superposition error. **Chemical Physics Letters**. 217: 48-54.

Dunning, T. H. J. (1970). Gaussian basis functions for use in molecular calculations. I. Contraction of (9*s*5*p*) atomic basis sets for the first-row atoms. **The Journal of Chemical Physics**. 53: 2823-2833.

Dunning, T. H. J. (1971). Gaussian basis functions for use in molecular calculations. III. Contraction of (10*s*6*p*) atomic basis sets for the first-row atoms. **The Journal of Chemical Physics**. 55: 716-723.

Hehre, W. J., Stewart, R. F. and Pople, J. A. (1969). Self-consistent molecular-orbital methods. I. Use of gaussian expansions of slater-type atomic orbitals. **The Journal of Chemical Physics**. 51: 2657-2664.

Huzinaga, S. (1965). Gaussian-type functions for polyatomic systems. I. **The Journal of Chemical Physics**. 42: 1293-1302.

Liedl, K. R. (1998). Dangers of counterpoise corrected hypersurfaces. Advantages of basis set superposition improvement. **The Journal of Chemical Physics**. 108: 3199-3204.

Møller, C. and Plesset, M. S. (1934). Note on an approximation treatment for many-electron systems. **Physical Review**. 46: 618-622.

Schrödinger, E. (1926). Quantisierung als eigenwertproblem. **Annalen der Physik**. 385: 437-490.

Schwenke, D. W. and Truhlar, D. G. (1986). Erratum: Systematic study of basis set superposition errors in the calculated interaction energy of two HF molecules. **The Journal of Chemical Physics**. 84: 4113-4113.

Schwenke, D. W. and Truhlar, D. G. (1987). Erratum: Systematic study of basis set superposition errors in the calculated interaction energy of two HF molecules. **The Journal of Chemical Physics**. 86: 3760-3760.

Sherrill, C. D. and Schaefer, H. F. (1999). The configuration interaction method: Advances in highly correlated approaches. **Advances in Quantum Chemistry** (Vol. 34, pp. 143-269): Academic Press.

Slater, J. C. (1930). Atomic shielding constants. **Physical Review**. 36: 57-64.

CHAPTER III

MOLECULAR DYNAMICS SIMULATIONS

3.1 Introduction to molecular dynamics simulation

Molecular dynamics (MD) technique is widely used for studying properties of various molecular systems, in particular the details related to time dependent behavior of the system. The MD simulation starts with reading in the initial configuration, velocities, accelerations and forces. The initial configuration can be obtained either from a random configuration or a lattice. The essential condition of the simulation is that there are no explicitly time-dependent or velocity dependent forces that shall act on the system. In practice, the trajectories cannot be directly obtained from Newton's equation of motion. Therefore, the *time integration algorithm* will be used to obtain the knowledge of positions, velocities and accelerations of two successive time steps. The energy of the system can be calculated through molecular mechanics (MM) or quantum mechanics (QM) method. The force of each atom in the system can be obtained from the derivative of the energy with respect to the change in the atom's position. All particles in the system will be moved by their new force to the new configurations. This process will be repeated until the system reaches its equilibrium. After that, the coordinates, velocities, accelerations, forces and so on of all particles will be collected for further structural and dynamical properties calculations. In practice, only positions and velocities are usually stored since most important and

interesting properties of the system can be obtained from these two quantities. The scheme of MD simulation is shown in Figure 3.1.

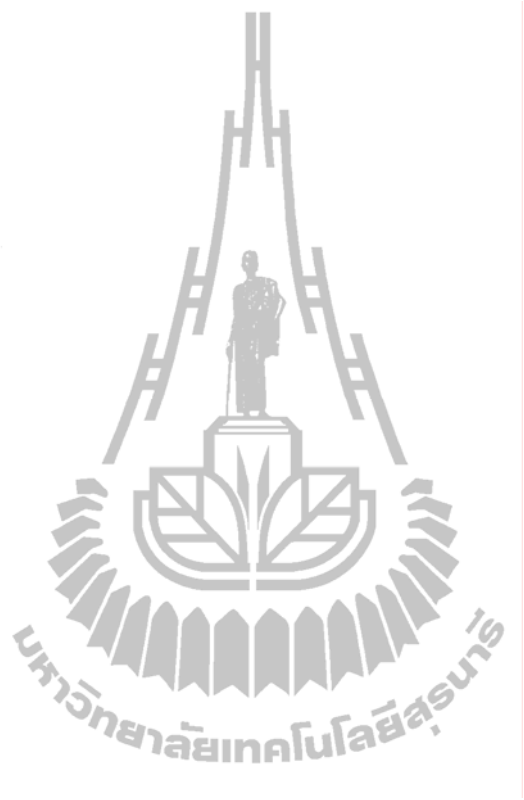

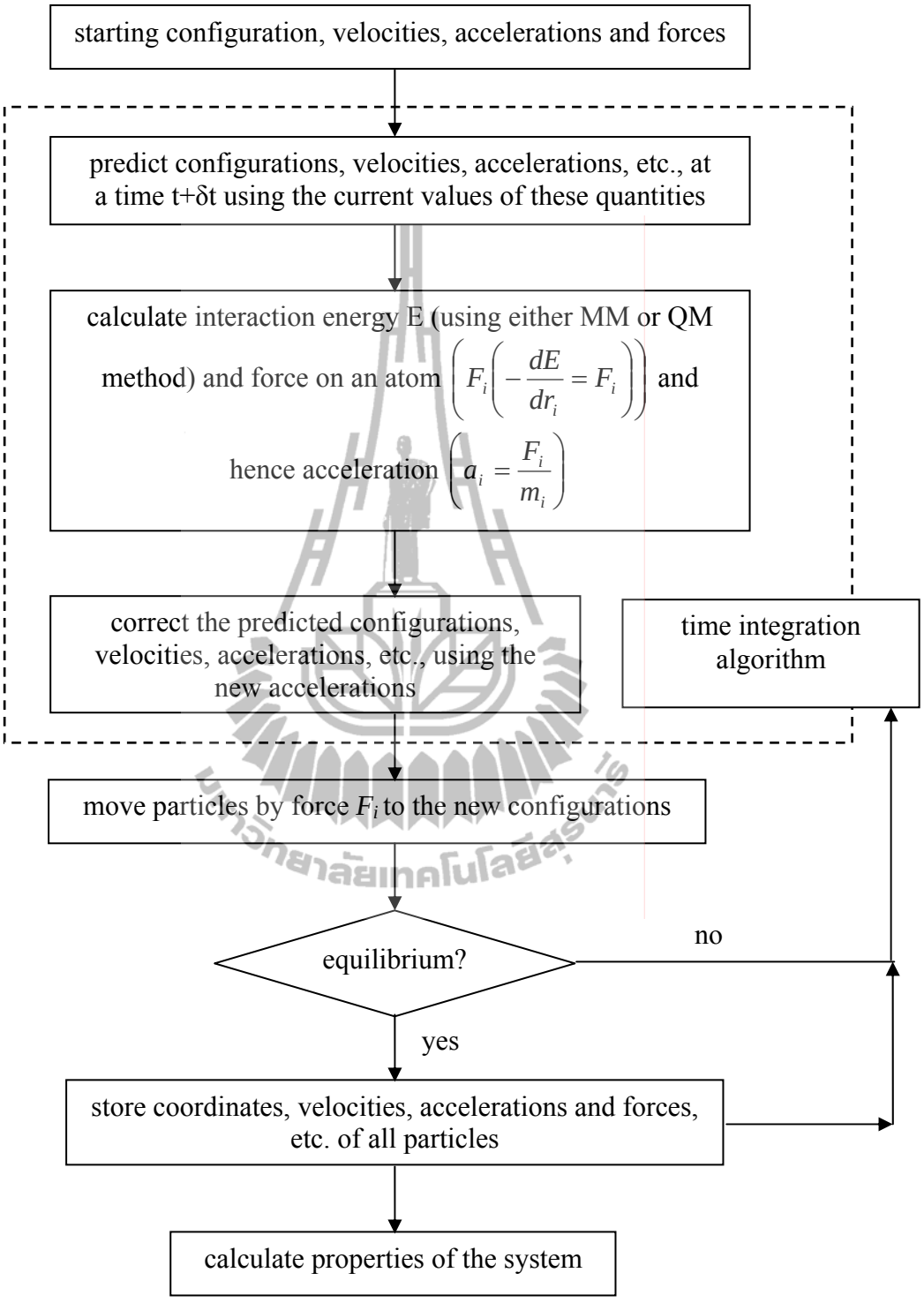

Figure 3.1 The scheme of MD simulation.

3.2 Time average and ensemble average

Basically, the properties of the system depend upon the positions and the momenta of the *N* particles that comprise the system. The value of the property *A* can thus be written as

$$A(\mathrm{p}^N(t), \mathrm{r}^N(t)), \tag{3.1}$$

where $\mathrm{p}^N(t)$ and $\mathrm{r}^N(t)$ represent particle's momenta and positions, respectively. The value of the property *A* is the average of the *A* over the time of the measurement, known as *time average*. In this regard, if the time measurement is increased to infinity, the value of the property *A* is the *true value*.

$$A_{ave} = \lim_{\tau \to \infty} \frac{1}{\tau} \int_{t=0}^{\tau} A(\mathrm{p}^N(t), \mathrm{r}^N(t)) dt. \tag{3.2}$$

In terms of computer simulation, however, the generation of an initial configuration with respect to a large number of atoms or molecules is not feasible. Boltzmann and Gibbs developed statistical mechanics, called an *ensemble*. The ensemble is a single system evolved in time which is replaced by a large number of mental copies of a system, considering all at once, each of which represents a possible state that the real system might be in. The time average is then replaced by an *ensemble average* as

$$\langle A \rangle = \iint d\mathrm{p}^N d\mathrm{r}^N A(\mathrm{p}^N, \mathrm{r}^N)\rho(\mathrm{r}^N, \mathrm{r}^N). \quad (3.3)$$

The angle bracket (< >) indicates an ensemble average or *expectation value*, *i.e.*, the average value of the property *A* over all replications of the ensemble generated by the simulation. Different macroscopic environmental constraints lead to different types of ensembles. In practice, the ensemble must be performed under some constraints, such as constant number of particles (N), volume (V), energy (E), temperature (T), chemical potential (μ), pressure (P) and so on. For example, a simple ensemble is the *microcanonical ensemble*. This ensemble is a thermodynamically isolated system, where the N, V and E are fixed throughout the simulation. The equilibrium states of NVE ensemble are characterized by the entropy. The development of NVE ensemble is the *canonical ensemble* (NVT), in which the N and V are fixed and the ensemble has a well defined temperature given by the temperature of the heat bath. The thermodynamic property derived from the NVT ensemble is Helmholtz free energy. The *grand canonical ensemble* (μVT) is the extension of NVT ensemble which allows the energy exchange, but fixes the μ, V and T.

3.3 Intermolecular potentials

The intermolecular interactions of the system are usually described by intermolecular potential. The potential energy function is the total intermolecular interaction energy comprising all of the pair, three-body, four-body up to N-body interactions,

$$V_{total} = \sum V(i,j) + \sum V(i,j,k) + \ldots + \sum V(i,j,k,\ldots,N). \quad (3.4)$$

With regard to earlier MD works, the upper terms are assumed to converge slowly and tend to have alternating signs (Kistenmacher, Popkie and Clementi, 1974). Thus, only the pair interaction has been used to describe the intermolecular interaction of the system, known as *pairwise additive approximation*. The pair potential functions can be constructed from experimental data. However, the popular way of construction the pair potential functions is to construct with respect to *ab initio* calculations.

3.4 Time integration algorithms

The engine of a molecular dynamics program is its time integration algorithms, required to integrate the equation of motion of the interacting particles and follow their trajectories. The time integration algorithms are based on finite difference method, where time is discretized on a finite grid, the time step Δt being the distance between consecutive points on the grid. Knowing the positions and some of their time derivatives at time *t*, the integration scheme gives the same quantities at a later time $t + \Delta t$. By iterating the procedure, the time evolution of the system can be followed for long times. The widely used methods for integrating the equation of motion in a molecular dynamic simulation are *Verlet algorithm* (Verlet, 1967) and *Predictor-corrector algorithm* (Gear, 1971).

3.4.1 Verlet algorithm

This method is a direct solution of the second-order equation. The basic idea is to write two third-order Taylor expansions for the position $r(t)$, one forward and another one backward in time,

$$\begin{aligned} r(t+\Delta t) &= r(t) + v(t)\Delta t + \frac{1}{2}a(t)\Delta t^2 + \frac{1}{6}b(t)\Delta t^3 + O(\Delta t^4) \\ r(t-\Delta t) &= r(t) - v(t)\Delta t + \frac{1}{2}a(t)\Delta t^2 - \frac{1}{6}b(t)\Delta t^3 + O(\Delta t^4) \end{aligned} . \tag{3.5}$$

Adding these two equations gives

$$r(t+\Delta t) = 2r(t) - r(t-\Delta t) + a(t)\Delta t^2 + O(\Delta t^4). \tag{3.6}$$

This is the basic form of the Verlet algorithm. Since we are interested in Newton's equation, *a(t)* is just the force divided by the mass, and the force is in turn a function of the position *r(t)*,

$$a(t) = -\frac{1}{m}\Delta V(r(t)). \tag{3.7}$$

As one can clearly see, the truncation error of the algorithm when evolving the system by Δt is of the order of Δt^4, even if third derivatives do not appear explicitly. This algorithm is at the same time simple to implement, it is accurate and stable, thus explaining its great popularity among molecular dynamics simulations.

A problem with this version of Verlet algorithm is that velocities are not directly generated. While they are not needed for the time evolution, knowledge of them is sometimes necessary. Moreover, they are required to compute the kinetic energy *K*, whose evaluation is necessary to test the conversation of the total energy(*E* = *K* + *V*). This is one of the most important tests to verify that a molecular dynamics simulation is proceeding correctly. One could compute the velocities from the positions by using

$$v(t) = \frac{r(t + \Delta t) - r(t - \Delta t)}{2\Delta t}. \tag{3.8}$$

However, the error associated to this expression is in the order of Δt^2 rather than Δt^4. To overcome this difficulty, some variants of the Verlet algorithm have been developed. They give rise to exactly the same trajectory, and differ in what variables are stored in memory and at what times. The *leap-frog algorithm* (Hockney, 1970) is a common numerical approach to calculate trajectories based on Newton's equation. The steps can be summarized as follows,

1. solve for a_i at t using $\quad -\frac{dE}{dr_i} = F_i = m_i a_i(t)$
2. update v_i at $t + \frac{\Delta t}{2}$ using $\quad v_i(t + \frac{\Delta t}{2}) = v_i(t - \frac{\Delta t}{2}) + a_i(t)\Delta t$
3. update r_i at $t + \Delta t$ using $\quad r_i(t + \Delta t) = r_i(t) + v_i(t + \frac{\Delta t}{2})\Delta t$

An even better implementation of the same basic algorithm is the so-calle *velocity Verlet method* (Swope, Anderson, Berens and Wilson, 1982), where positions, velocities and accelerations at time $t+\Delta t$ are obtained from the same quantities at time t in the following way,

$$\begin{aligned} r(t+\Delta t) &= r(t) + v(t)\Delta t + \frac{1}{2}a(t)\Delta t^2 \\ v(t+\frac{\Delta t}{2}) &= v(t) + \frac{1}{2}a(t)\Delta t \\ a(t+\Delta t) &= -\frac{1}{m}\nabla V(r(t+\Delta t)) \\ v(t+\Delta t) &= v(t+\frac{\Delta t}{2}) + \frac{1}{2}a(t+\Delta t)\Delta t \end{aligned} \quad . \tag{3.9}$$

3.4.2 Predictor-corrector algorithm

Predictor-corrector algorithms constitute another commonly used class of methods to integrate the equations of motion. This is often used more in molecular dynamics and consist of three steps : 1) predictor; 2) force evaluation and 3) corrector. From the positions and their time derivatives up to a certain order, all known at time *t*, one predicts the same quantities at time $t+\Delta t$. Among these quantities are, of cause, accelerations *a*. The force is computed taking the gradient of the potential at the predicted positions. The resulting acceleration will be in general different from the *predicted acceleration*. The difference between the two constitutes is an "*error signal*". This error signal is used to correct positions and their derivatives. All the corrections are proportional to the error signal, the coefficient of proportionality being a "*magic number*" determined to maximize the stability of the algorithms. The method is usually based on Taylor expansion about time *t*,

$$
\begin{aligned}
r^p(t+\Delta t) &= r(t) + \Delta t v(t) + \frac{1}{2}\Delta t^2 a(t) + \frac{1}{6}\Delta t^3 b(t) + \ldots \\
v^p(t+\Delta t) &= v(t) + \Delta t a(t) + \frac{1}{2}\Delta t^2 b(t) + \ldots \\
a^p(t+\Delta t) &= a(t) + \Delta t b(t) + \ldots \\
b^p(t+\Delta t) &= b(t) + \ldots
\end{aligned}
\quad . \qquad (3.10)
$$

The superscript p marks these as predicted values. Since r and v stand for the complete set of positions and velocities, a is short for all the accelerations and b denotes all the third time derivatives of r. From the new position r^p, we can calculate the force at time $t + \Delta t$, and hence the correct accelerations $a^c(t + \Delta t)$. These can be compared with the predicted accelerations from equation (3.10), to estimate the size of the error in the prediction step,

$$
\Delta a(t+\Delta t) = a^c(t+\Delta t) - a^p(t+\Delta t). \qquad (3.11)
$$

This error and the results of the predictor step are fed into the corrector step,

$$
\begin{aligned}
r^c(t+\Delta t) &= r^p(t+\Delta t) + c_0 \Delta a(t+\Delta t) \\
v^c(t+\Delta t) &= v^p(t+\Delta t) + c_1 \Delta a(t+\Delta t) \\
a^c(t+\Delta t) &= a^p(t+\Delta t) + c_2 \Delta a(t+\Delta t) \\
b^c(t+\Delta t) &= b^p(t+\Delta t) + c_3 \Delta a(t+\Delta t)
\end{aligned}
\quad . \qquad (3.10)
$$

The idea is that $r^c(t+\Delta t)$, $v^c(t+\Delta t)$, etc. are now better approximations of the true positions, velocities, etc. These errors do not depend on the implementation, they are intrinsic to the algorithm.

3.5 Periodic boundary conditions

The boundary effects or surface effects are often found in the computer simulation using small system size. The interactions between particles and the wall reflect in wrong properties of bulk. This problem can be solved by using the periodic boundary (PB) conditions. By the PB condition, the particles in the box are replicated in all directions to give a periodic array, which can be seen in Figure 3.2.

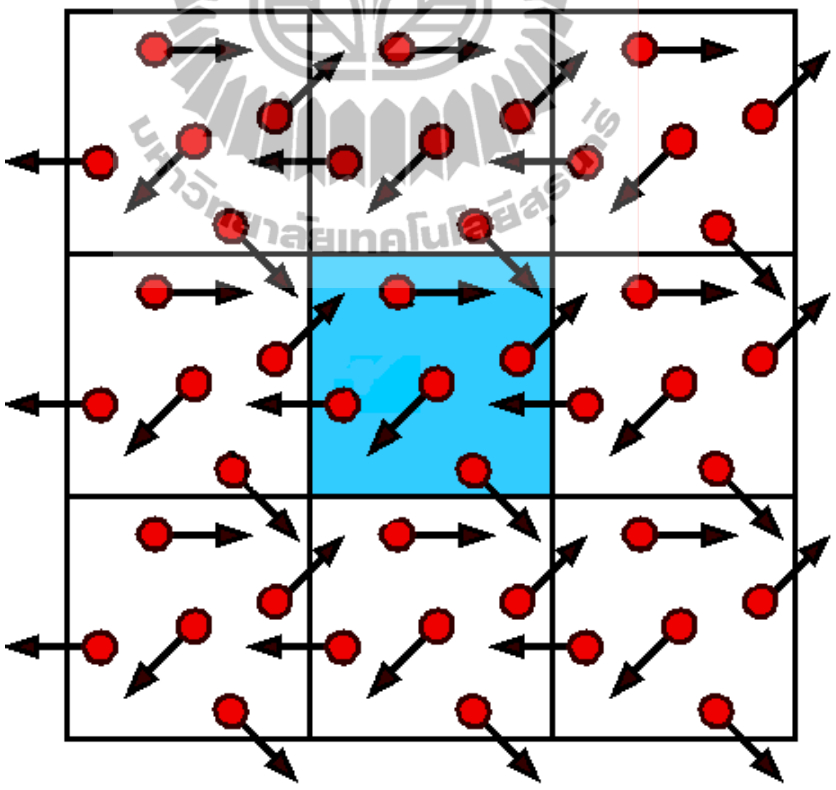

Figure 3.2 Periodic boundary conditions in two dimensions.

The main point of periodic boundary conditions is that the coordinates of the particles in the image boxes can be computed by adding or subtracting integral multiples of the box sides. If a particle leaves the box during the simulation, it is replaced by an image particle that enters from the opposite side at the same time, as illustrated in Figure 3.2. By this scheme, the number of particles within the central box remains constant.

3.6 Cut-off and minimum image convention

In general, the most time-consuming of the simulation is the calculation of the non-bond energies and forces. The simple way of reducing the expense is to use a *cut-off* and to apply the *minimum image convention*. The minimum image convention is a common form of the PB condition, in which each atom interacts with only its neighboring atoms in the system. The energies and forces are computed with respect to the closest atom or image as shown in Figure 3.3.

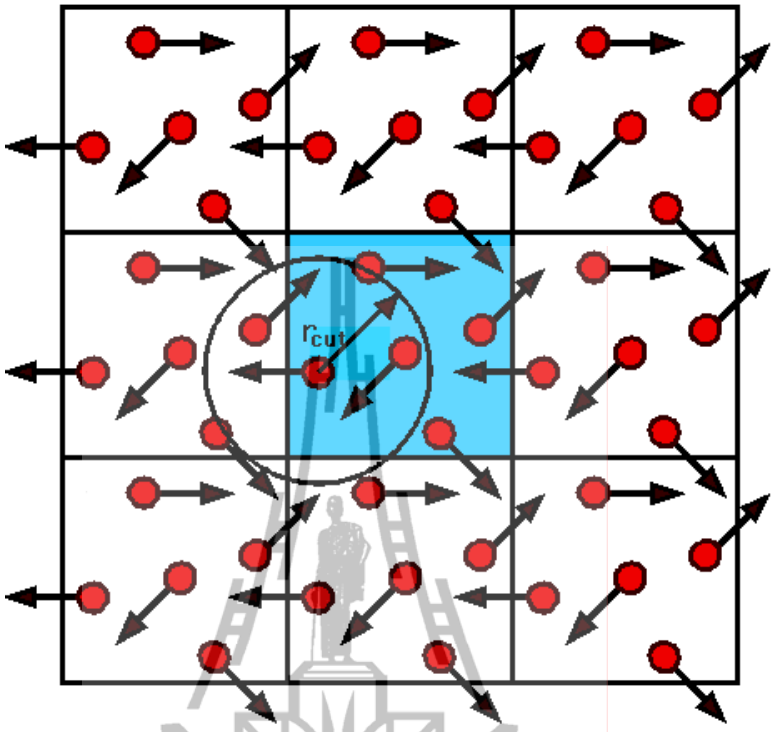

Figure 3.3 The spherical cut-off and the minimum image convention.

By using the cut-off, the interactions between all pairs of atoms that are further apart from the cut-off value are set to zero. In this regard, the cut-off distance should not be greater than half of the length of their image. However, the use of cut-off leads to a serious problem in the simulation, as can be seen in Figure 3.4.

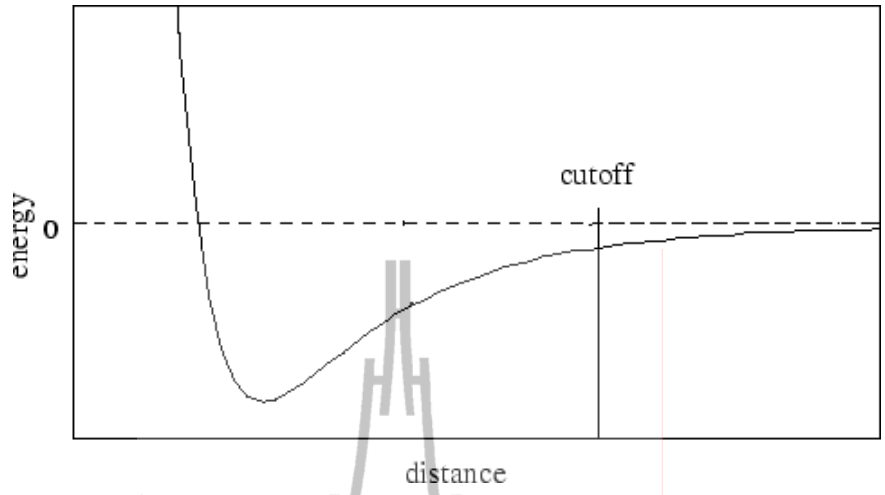

Figure 3.4 A discontinuity of the energy curve when the potential is truncated.

Once the cut-off distance is applied, this reflects in the discontinuity in both the potential energy and the force after the cut-off value. One way for solving this problem is to use a *shifted potential*, in which a constant term is subtracted from the potential at all values as

$$V'(r)\begin{cases} V(r)-V_c & r \le r_c \\ 0 & r > r_c \end{cases}, \tag{3.11}$$

where r_c is the cut-off distance and V_c corresponds to the value of the potential at the cut-off distance. In this respect, although the energy conservation can be improved by the shifted potential, the discontinuity in the force with the shifted potential still exists. At the cut-off distance, since the force will have a finite value, a suitable shifted potential would be of the form

$$V'(r)\begin{cases} V(r) - V_c - \left(\frac{dV(r)}{dr}\right)_{r=r_c}(r - r_c) & r \le r_c \\ 0 & r > r_c \end{cases}, \qquad (3.12)$$

However, the application of shifted potential is not easy for inhomogeneous systems containing many different types of atom. An alternative way is to eliminate discontinuities in the energy and force by using a *switching function.* The switched potential ($V'(r)$) is related to the true potential ($V(r)$) as

$$V'(r) = V(r)S(r). \qquad (3.13)$$

Some switching functions are applied to the entire range of the potential up to the cut-off point. In general, the switching function has a value of 1 at $r = 0$ and a value of 0 at $r = r_c$, while the switching function values between two cut-offs are varied. The example of a switching function applied to the Lennard-Jones potential is given in Figure 3.5.

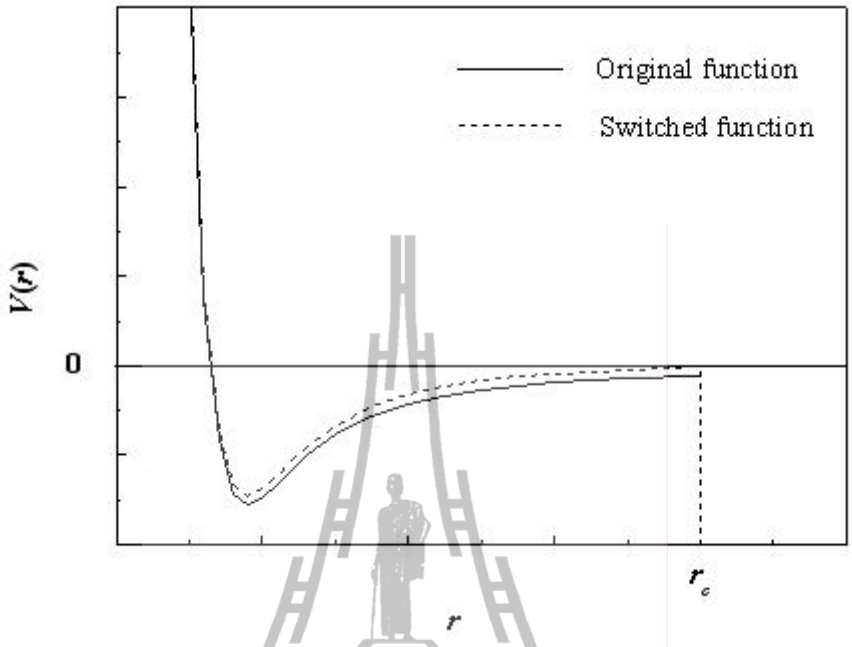

Figure 3.5 The effect of a switching function applied to the Lennard-Jones potential.

The switching function can be used to multiply the potential in a small range between the lower (r_1) an upper cut-off (r_u) distance, which takes the value 1 at the lower cut-off distance and 0 at the upper cut-off distance. The range being employed is usually small, such as between r_1 and r_u of 9 and 10 Å. The example of such application is shown in Figure 3.6.

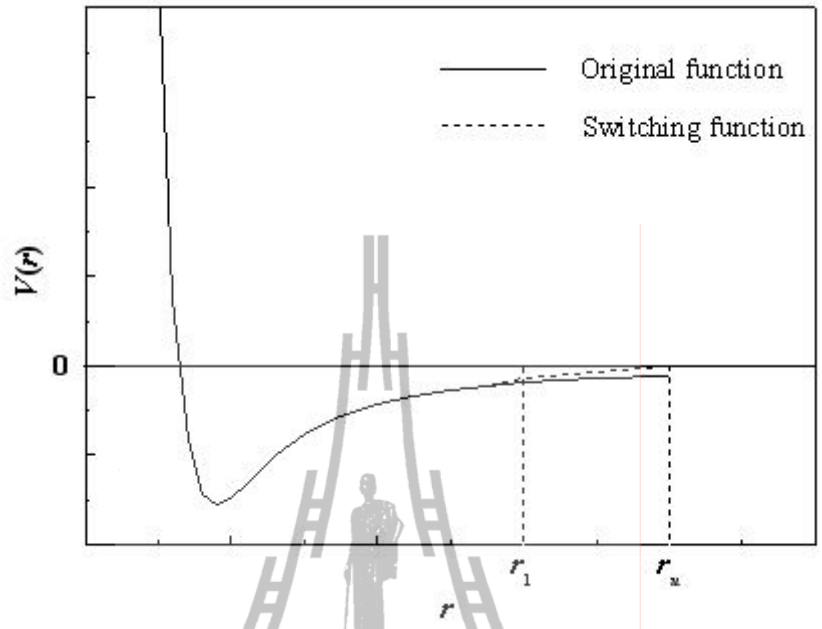

Figure 3.6 A switching function applied over a range near the cut-off and its effect on the Lennard-Jones potential.

3.7 Non-bonded neighbor lists

In practice, the use of cut-off and minimum image convention is not actually reduces the time in the MD simulation since all the non-bonded distances must be calculated and checked whether it is inside or outside the cut-off distance. A useful technique for solving this problem is to use the *non-bonded neighbor list*. The first non-bonded neighbor list has been proposed by Verlet (Verlet, 1967). The Verlet neighbor list stores all atoms within the cut-off distance (the solid circle shown in Figure 3.7) and atoms are slightly further away than the cut-off distance (the dashed circle shown in Figure 3.7). The neighbor list will frequently be updated throughout the simulation. In this respect, the distance used to calculate each atom's neighbors should be slightly larger than the actual cut-off distance in order to ensure that the

atoms outside the cut-off will not move closer than the cut-off distance before the neighbor list is updated again.

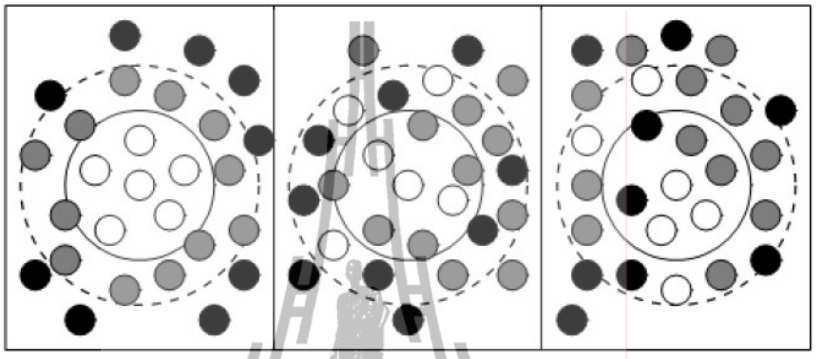

Figure 3.7 The Verlet neighbor list.

3.8 Long-range interactions

The neglect of interactions beyond the cut-off distance, especially for the strong interacting systems, may results in an incorrect description of molecular properties. One way to treat the long-range interactions is to use a large simulation cell, but this could be very time-consuming. There are many suitable methods for treating the long-range interactions. The first method is the *Ewald summation method*, which derived by Ewald in 1921 (Ewald, 1921). This method studies the energetics of ionic crystals, *i.e.*, a particle interacts with all the other particles in the simulation box and with all of their images in an infinite array of periodic cells. The charge-charge contribution to the potential energy of the Ewald summation method could be of the form

$$V = \frac{1}{2} \sum_{|\mathrm{n}|=0}{}' \sum_{i=1}^{N} \sum_{j=1}^{N} \frac{q_i q_j}{4\pi\varepsilon_0 \left| r_{ij} + \mathrm{n} \right|}, \tag{3.14}$$

where the prime on the first summation indicates that the series does not include the interaction $i = j$ for $\mathrm{n} = 0$, q_i and q_j are charges and n is a cubic lattice point. The Ewald summation method is the most correct way to accurately include all the effects of long-range forces in the computer simulation. However, this method is rather expensive to implement since the equation (3.32) converges extremely slowly.

The another method for the treatment of long-range interactions is the *reaction field method* (Foulkes and Haydock, 1989). This method constructs the sphere around the molecule with a radius equal to the cut-off distance. By this scheme, all interactions within the sphere are calculated explicitly, while those outside of the sphere are modeled as a homogeneous medium of dielectric constant (ε_s). The electrostatic field due to the surrounding dielectric is given by

$$E_i = \frac{2(\varepsilon_s - 1)}{\varepsilon_s + 1} \left(\frac{1}{r_c^3} \right) \sum_{j; r_{ij} \le r_c} \mu_j, \tag{3.15}$$

where μ_j are the dipoles of the neighboring molecules that are located within the cut-off distance (r_c) of the molecules i. The interaction between molecule i and the reaction field equals to $E_i \cdot \mu_i$.

3.9 Conventional QM/MM MD technique

According to the conventional QM/MM MD approach, the system is partitioned into two parts, namely QM and MM regions, as shown in Figure 3.8.

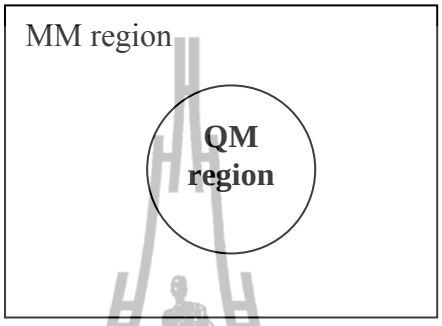

Figure 3.8 System's partition.

The system's interaction energy (E_{total}) can be calculated from

$$E_{total} = (\Psi_{QM} \left| \hat{H} \right| \Psi_{QM}) + E_{MM} + E_{QM-MM}, \quad (3.16)$$

where the first term on the right-hand side corresponds to the interactions within the QM region derived by means of quantum mechanics, while the last two terms represent the interactions within the MM and between the QM and MM regions, respectively. The later two terms are evaluated on the basis of pairwise additive approximations.

During the QM/MM simulations, forces acting on each particle in the system are switched according to which region the solvent molecule is entering or leaving the QM region and is defined as

$$F_i = S_m(r)F_{QM} + (1 - S_m(r))F_{MM}, \tag{3.17}$$

where F_{QM} and F_{MM} are quantum mechanical and molecular mechanical forces, respectively. $S_m(r)$ is a smoothing function described by

$$\begin{aligned} S_m(r) &= 1 && \text{for } r < r_1, \\ S_m(r) &= \frac{(r_0^2 - r^2)^2(r_0^2 + 2r^2 - 3r_1^2)}{(r_0^2 - r_1^2)^3} && \text{for } r_1 < r \le r_1, \\ S_m(r) &= 0 && \text{for } r > r_0, \end{aligned} \tag{3.18}$$

where r_1 and r_0 are the distances characterizing the start and the end of the QM region, applied within an interval of 0.2 Å to ensure a continuous change of forces at the transition between the QM and MM regions.

3.10 Combined QM/MM MD based on ONIOM-XS method

According to the conventional QM/MM technique, however, some unsolved problems have been demonstrated. First, only the exchanging particles which crossings between QM and MM regions are treated by a smoothing function, *i.e.*, not the whole particles in the QM region. With regards to this point, it is not reliable because immediate addition or deletion of a particle in the QM region due to the solvent exchange also affects the forces acting on the remaining particles in the QM region. Thus, the conventional QM/MM simulation may provides numerical instability of forces whenever the solvent exchange process occurs in the system.

Second, the conventional scheme cannot clearly define the appropriate energy expression when the solvent exchange process occurs during the simulation.

To solve these problems, a more sophisticated QM/MM technique based on ONIOM-XS method has been proposed (Kerdcharoen and Morokuma, 2003). The ONIOM (Own N-layered Integrated molecular Orbital and molecular Mechanics) method was originally proposed by Morokuma et al. (Svensson et al., 1996). The extension of the ONIOM method for the treatment of condensed-phase system was firstly applied by Kerdcharoen and co-worker, called ONIOM-XS (XS = eXtension to Solvation)

According to the QM/MM MD technique based on ONIOM-XS method, the system is comprised of a "high-level" QM sphere, *i.e.*, a sphere which contains the ion and its surrounding solvent molecules, and the remaining "low-level" MM bulk solvents. A thin switching shell located between the QM and MM regions is then introduced in order to smooth the transition due to the solvent exchange.

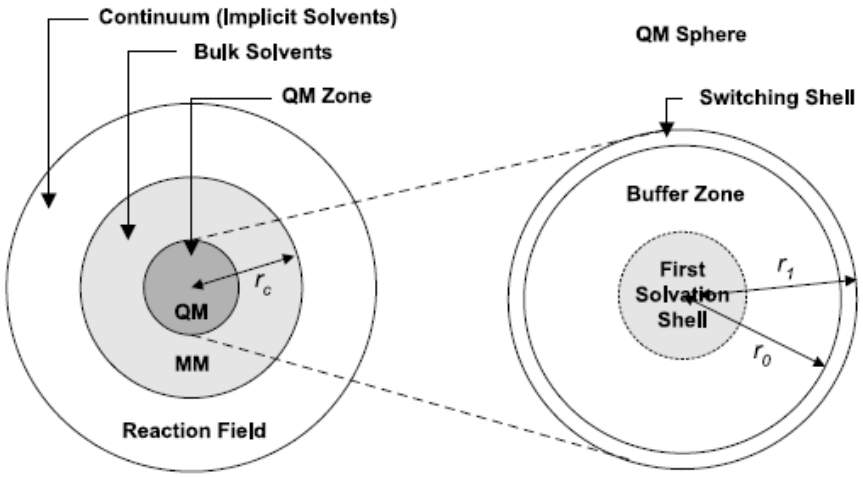

Figure 3.9 Schematic diagram of the ONIOM-XS method.

Given n_1, l and n_2 as number of particles in the QM sphere, the switching layer and the MM region, respectively, and $N(= n_1+l+n_2)$ as the total number of particles, the potential energy of the system can be written in two ways based on the ONIOM extrapolation scheme (Svensson, Humbel, Froese, Matsubara, Sieber and Morokuma, 1996). If the switching layer is included into the high-level QM region, the energy expression is written as

$$E^{ONIOM}(n_1+l;N) = E^{QM}(n_1+l) - E^{MM}(n_1+l) + E^{MM}(N). \quad (3.19)$$

If the switching layer is considered as part of the "low-level" MM region, the energy expression is written as

$$E^{ONIOM}(n_1;N) = E^{QM}(n_1) - E^{MM}(n_1) + E^{MM}(N). \quad (3.20)$$

The potential energy of the entire system is taken as a hybrid between both energy terms (3.37) and (3.38),

$$E^{ONIOM-XS}(\{r_1\}) = (1-\bar{s}(\{r_1\}))\cdot E^{ONIOM}(n_1+l;N) + \bar{s}(\{r_1\})\cdot E^{ONIOM}(n_1;N), \quad (3.21)$$

where $\bar{s}(\{r_1\})$ is an average over a set of switching functions for individual exchanging particle in the switching layer $s_i(x_i)$,

$$\bar{s}(\{r_1\}) = \frac{1}{l}\sum_{i=1}^{l} s_i(x_i), \quad (3.22)$$

The switching function in equation (3.40) can have any form. In the present study, a polynomial form is employed,

$$s_i(x_i) = 6\left(x_i - \frac{1}{2}\right)^5 - 5\left(x_i - \frac{1}{2}\right)^3 + \frac{15}{8}\left(x_i - \frac{1}{2}\right) + \frac{1}{2}\ , \tag{3.23}$$

where $x_i = \left((r_i - r_0)/(r_1 - r_0)\right)$, r_0 and r_1 are the radius of inner and outer surfaces of the switching shell, respectively, and r_i is the distance between the center of mass of the exchanging particle and the center of the QM sphere. The switching function has an S-shape and converges to 0 and 1 at r_0 and r_1, respectively. The gradient of the energy can be written as

$$\begin{aligned}\nabla_R E^{ONIOM-XS}(\{r_1\}) \\ = (1-\bar{s}(\{r_1\}))\cdot\nabla_R E^{ONIOM}(n_1+l;N) + \bar{s}(\{r_1\})\cdot\nabla_R E^{ONIOM}(n_1;N) + \\ \frac{1}{(r_1-r_0)}\nabla\bar{s}(\{r_1\})\cdot\left(E^{ONIOM}(n_1;N) - E^{ONIOM}(n_1+l;N)\right)\end{aligned}\ . \tag{3.24}$$

3.11 References

Ewald, P. P. (1921). Die berechnung optischer und elektrostatischer gitterpotentiale. **Annalen der Physik**. 369: 253-287.

Foulkes, W. M. C. and Haydock, R. (1989). Tight-binding models and density-functional theory. **Physical Review B**. 39: 12520-12536.

Gear, C. W. (1971). **Numerical initial value problems in ordinary differential equations**. Englewood Cliffs, N.J.: Prentice-Hall.

Hockney, R. W. (1970). The potential calculation and some applications. **Methods in Computational Physics**. 9: 136-211.

Kistenmacher, H., Popkie, H. and Clementi, E. (1974). Study of the structure of molecular complexes. VIII. Small clusters of water molecules surrounding Li^+, Na^+, K^+, F^-, and Cl^- ions. **The Journal of Chemical Physics**. 61: 799-815.

Svensson, M., Humbel, S., Froese, R. D. J., Matsubara, T., Sieber, S. and Morokuma, K. (1996). ONIOM: A multilayered integrated MO + MM method for geometry optimizations and single point energy predictions. A test for diels−alder reactions and $Pt(P(t\text{-}Bu)_3)_2 + H_2$ oxidative addition. **The Journal of Physical Chemistry**. 100: 19357-19363.

Swope, W. C., Anderson, H. C., Berens, P. H. and Wilson, K. R. (1982). A computer simulation method for the calculation of equilibrium constants for the formation of physical clusters of molecules: Application to small water clusters. **Journal of Chemical Physics**. 53: 289-298.

Verlet, L. (1967). Computer "experiments" on classical fluids. I. Thermodynamical properties of Lennard-Jones molecules. **Physical Review**. 159: 98-103.

CHAPTER IV

RESULTS AND DISCUSSION

4.1 Basis set superposition errors

A well-known problem in the theory of intermolecular interactions is *Basis Set Superposition Error (BSSE)*, leading to overestimation of binding energies as well as to limit of the accuracy in the standard (finite basis) quantum chemical calculations. When the BSSE is suspected, a correction must be performed in order to avoid false results, especially the global minima of stabilization energies and the corresponding molecular geometry due to the overestimation of their interaction energies. According to the Counterpoise (CP) method, the stabilization energies with and without the BSSE correction of the optimized K^+-H_2O and Ca^{2+}-H_2O complexes were evaluated using several types of basis sets. The results of the calculations are summarized in Tables 4.1 - 4.4.

Table 4.1 Basis set superposition error in the interaction energies of K^+-H_2O complex at optimized K^+-O distance obtained from HF calculations using various basis sets.

Basis set		Uncorrected E	Corrected E	BSSE
K^+	H_2O		(kcal.mol^{-1})	
STO-3G		-35.000	-14.337	-20.663
3-21G		-27.310	-20.451	-6.859
6-31G		-23.503	-21.775	-1.728
6-311G		-23.560	-22.111	-1.449
LanL2DZ	6-31G	-23.312	-21.739	-1.573
LanL2DZ	6-311G	-22.931	-21.645	-1.286
LanL2DZ	DZ	-22.414	-21.740	-0.674
LanL2DZ	DZV	-22.407	-21.734	-0.673
LanL2DZ	DZV+	-21.579	-21.490	-0.089
LanL2DZ	AUG-cc-pVDZ	-16.009	-15.914	-0.095

Table 4.2 Basis set superposition error in the interaction energies of K^+-H_2O complex at optimized K^+-O distance obtained from B3LYP, MP2 and CCSD calculations using various basis sets.

Basis set		Uncorrected E	Corrected E	BSSE
K^+	H_2O		(kcal.mol^{-1})	
B3LYP				
LanL2DZ	DZ	-23.434	-21.865	-1.569
LanL2DZ	DZV	-23.445	-21.876	-1.569
LanL2DZ	DZV+	-21.613	-21.422	-0.191
LanL2DZ	AUG-cc-pVDZ	-15.608	-15.451	-0.157
MP2				
LanL2DZ	DZ	-22.427	-21.019	-1.408
LanL2DZ	DZV	-22.426	-21.023	-1.403
LanL2DZ	DZV+	-20.965	-20.560	-0.405
LanL2DZ	AUG-cc-pVDZ	-15.209	-14.767	-0.442
CCSD				
LanL2DZ	DZ	-22.217	-20.813	-1.404
LanL2DZ	DZV	-22.212	-20.811	-1.401
LanL2DZ	DZV+	-20.800	-20.378	-0.422
LanL2DZ	AUG-cc-pVDZ	-15.326	-14.856	-0.470

Table 4.3 Basis set superposition error in the interaction energies of Ca^{2+}-H_2O complex at optimized Ca^{2+}-O distance obtained from HF calculations using various basis sets.

Basis set		Uncorrected E	Corrected E	BSSE
Ca^{2+}	H_2O		(kcal.mol^{-1})	
	STO-3G	-76.496	-50.940	-25.556
	3-21G	-67.540	-59.003	-8.537
	6-31G	-61.813	-60.229	-1.584
	6-311G	-63.130	-61.389	-1.741
LanL2DZ	6-31G	-61.805	-60.125	-1.680
LanL2DZ	6-311G	-61.296	-59.861	-1.435
LanL2DZ	DZ	-60.360	-59.566	-0.794
LanL2DZ	DZV	-60.374	-59.547	-0.794
LanL2DZ	DZV+	-59.191	-58.623	-0.568
LanL2DZ	AUG-cc-pVDZ	-50.002	-49.380	-0.622

Table 4.4 Basis set superposition error in the interaction energies of Ca^{2+}-H_2O complex at optimized Ca^{2+}-O distance obtained from B3LYP, MP2 and CCSD calculations using various basis sets.

Basis set		Uncorrected E	Corrected E	BSSE
Ca^{2+}	H_2O		(kcal.mol^{-1})	
B3LYP				
LanL2DZ	DZ	-61.999	-60.276	-1.723
LanL2DZ	DZV	-62.022	-60.298	-1.724
LanL2DZ	DZV+	-59.111	-58.363	-0.748
LanL2DZ	AUG-cc-pVDZ	-49.573	-48.884	-0.689
MP2				
LanL2DZ	DZ	-59.771	-58.025	-1.746
LanL2DZ	DZV	-59.767	-58.028	-1.739
LanL2DZ	DZV+	-57.356	-56.251	-1.105
LanL2DZ	AUG-cc-pVDZ	-47.587	-46.632	-0.955
CCSD				
LanL2DZ	DZ	-59.227	-57.468	-1.759
LanL2DZ	DZV	-59.213	-57.460	-1.753
LanL2DZ	DZV+	-56.868	-55.801	-1.067
LanL2DZ	AUG-cc-pVDZ	-47.786	-46.803	-0.983

With regard to the data in Tables 4.1 - 4.4, it is obvious that the use of small basis sets, such as STO-3G or 3-21G, leads to rather large BSSE values. On the other hand, the use of very poor atomic basis sets, *i.e.*, by means of size and quality, the CP method will not provide improvement of the results. In contrast, the CP corrections with medium-size basis sets could give values of interaction energies close to those obtained by using more expensive and larger ones. As can be seen in Tables 4.1 - 4.4, the use of medium-size basis sets, like DZV+, for H_2O, and Los Alamos ECP plus DZ basis set (LANL2DZ) for K^+ and Ca^{2+} give relatively small BSSE values, and thus these basis sets will be selected for the present study. For K^+ and Ca^{2+}, the LANL2DZ basis set was chosen since the effective core potentials have the major advantage that they can account for relativistic effects and are very efficient computationally, especially for large atoms.

4.2 Effects of electron correlation

In general, the HF SCF wavefunction takes into account the interactions between electrons only in an average way. In fact, it must be considered as the instantaneous interactions between electrons since the motions of electrons are correlated to each other, called "*electron correlation*". The effects of electron correlation should be checked, otherwise, it could lead to problems. In this work, the effects of electron correlation have been evaluated by comparing the binding energies of the ion-water complexes obtained by the HF and the CCSD methods. The results of the HF and CCSD calculations are given in Table 4.5.

Table 4.5 The contributions of electron correlation to binding energies, ΔE_{diff}, of ion-water complexes after BSSE corrections, using DZV+ basis set for H_2O and Los Alamos ECP plus DZ basis set for cations. (energies are in kcal.mol^{-1}, distance are in Å, ΔE_{HF} and ΔE_{CCSD} are binding energies at HF and CCSD levels, respectively)

Ion	ΔE_{HF}	ΔE_{CCSD}	ΔE_{diff}
K^+	-21.49	-20.38	1.11
Ca^{2+}	-58.62	-55.80	2.82
Ion	R_{HF}	R_{CCSD}	ΔR
K^+	2.66	2.69	0.03
Ca^{2+}	2.33	2.36	0.03

With regard to the details in Table 4.5, it is obvious that the HF calculations reveal slight influence of the electron correlations, *i.e.*, compared to the CCSD data. It should be noted that the performance of QM/MM simulation in conjunction with correlated *ab initio* methods is still too-time consuming, even for the MP2 level. In this regard, it is assumed that the HF method employed in this study would be reliable enough to describe the interaction energies of such complexes.

4.3 Many-body interactions

One of the main advantages of the QM/MM approach is that the effects of many-body contributions, which are usually neglected in most classical MM MD simulations, can be reliably included (*i.e.*, at least within the first hydration shell of

the ions). The effects of many-body interactions must be taken into account in order to achieve sufficient agreement with experimental binding enthalpies. The influence of many-body interactions is defined by the difference of the *ab initio* interactions and the interactions that calculated based on pairwise additive approximations. To estimate the influence of many-body contributions in the K^+-H_2O and Ca^{2+}-H_2O systems, energy optimizations of $K^+(H_2O)_n$ and $Ca^{2+}(H_2O)_n$ complexes, where n = 1, 2, 3, 4, 6 and 8, were carried out by HF calculations using DZV+ basis set for H_2O and the Los Alamos ECP plus DZ basis set for K^+ and Ca^{2+}. The *ab initio* interaction energy of the $K^+(H_2O)_n$ and $Ca^{2+}(H_2O)_n$ complexes can be computed using supermolecular approach as,

$$\Delta E_{ab} = E(K(H_2O)_n^+ - E(K^+) - nE(H_2O), \tag{4.1}$$

and

$$\Delta E_{ab} = E(Ca(H_2O)_n^{2+} - E(Ca^{2+}) - nE(H_2O), \tag{4.2}$$

and the pair interaction energy can be obtained from

$$\begin{aligned}\Delta E_{pair} &= \sum_i^n [E(K^+ - H_2O^i) - E(K^+) - E(H_2O)] \\ &+ \sum_{j>i}^n [E(H_2O^i - H_2O^j) - 2E(H_2O)],\end{aligned} \tag{4.3}$$

and

$$\Delta E_{pair} = \sum_{i}^{n}[E(Ca^{2+} - H_2O^i) - E(Ca^{2+}) - E(H_2O)] + \sum_{j>i}^{n}[E(H_2O^i - H_2O^j) - 2E(H_2O)], \quad (4.4)$$

In this respect, the interaction energy difference, ΔE_{diff}, and the percentage of them with respect to pair potential, %E, can be calculated by

$$\Delta E_{diff} = \Delta E_{ab} - \Delta E_{pair}, \quad (4.5)$$

and

$$\%E = \frac{\Delta E_{diff}}{abs(\Delta E_{pair})} \times 100 \quad (4.6)$$

The results of the geometry optimizations and their corresponding many-body interactions are summarized in Table 4.6.

Table 4.6 Optimized geometries and corresponding many-body effects in $K^+(H_2O)_n$ and $Ca^{2+}(H_2O)_n$ complexes using HF method with DZV+ basis set for H_2O and Los Alamos ECP plus DZ basis set for K^+, and Ca^{2+}. (distances and angles are in Å and degree, respectively)

Ion	n	R_{M-O}	R_{O-H}	$\angle_{HOH}$	ΔE_{ab}	ΔE_{pair}	ΔE_{diff}	%E
K^+	1	2.6553	0.9545	110.42	-21.58	-21.58	-	-
	2	2.6839	0.9541	110.63	-41.23	-41.85	0.62	1.48
	3	2.7097	0.9537	110.97	-58.08	-59.67	1.59	2.66
	4	2.7414	0.9532	111.29	-72.08	-74.91	2.90	3.86
	6	2.8392	0.9524	111.78	-89.56	95.74	6.18	6.45
	8	2.9852	0.9507	114.02	-138.63	-160.20	21.57	13.46
Ca^{2+}	1	2.3273	0.9624	107.15	-59.18	-59.18	-	-
	2	2.3501	0.9615	107.54	-114.30	-116.26	1.96	1.69
	3	2.3666	0.9601	108.14	-163.71	-169.57	5.85	3.45
	4	2.4048	0.9587	108.75	-204.13	-217.76	13.63	6.26
	6	2.4415	0.9558	109.75	-272.78	-302.14	29.36	9.72
	8	2.5247	0.9542	111.43	-313.56	-370.47	56.91	15.36

According to the data shown in Table 4.6, the many-body interactions are found to increase significantly with the increase of ligands in the ion-water complexes. It is apparent that the pairwise additive approximations underestimate the intermolecular repulsion, which reflect in the overestimation of the ion-water binding energies. In particular, the assumption of pairwise additivity leads to errors of 13.46% and 15.36% for the $K^+(H_2O)_8$ and $Ca^{2+}(H_2O)_8$ complexes, respectively. These values are considerably high, and thus, the QM/MM approach appears to be very suitable to provide the correct description of the K^+ and Ca^{2+} hydrates.

4.4 Selection of QM size, basis set and QM method

Since a fluid system consisting of a considerable number of molecules is too large to be studied by full *ab initio* calculations, *i.e.*, due to the limit of data storage and CPU time, the quantum mechanical treatment will be performed only for a small region of highest interest, such as within the whole first hydration shell of ions. In this respect, the size of QM region, the basis set and the QM method employed in the QM/MM simulation are crucial factors in obtaining the reliable results. In practice, these important parameters must be optimized, compromising between the quality of the simulation results and the requirement of CPU time.

For the size of QM region, one simple way is to estimate from the results of the classical MM MD simulations of the corresponding K^+-H_2O and Ca^{2+}-H_2O systems (Tongraar, Liedl and Rode, 1997; Tongraar, Liedl and Rode, 1998). According to the resulting K-O and Ca-O RDFs (data not shown), the first minimum of the K-O and Ca-O peaks are exhibited at around 4.0 Å. This implies that a QM size with diameter of 8.0 Å is desirable for the present study. In this work, since the

exchange of water molecules at the transition between the first hydration shell and the outer region is also of particular interest, a slightly larger QM size with diameter of 8.4 Å was chosen. This QM region contains the central ion and about 12-16 surrounding water molecules.

Once the QM size has been defined, the suitable choice for QM method and basis set will further be evaluated. Figures 4.1 - 4.4 provide useful data for selecting such parameters. It is obvious that the correlated methods, even for the MP2 level, with medium-size basis sets, like DZV+ for water and Los Alamos ECP plus DZ for ions, are still too-time consuming (*i.e.*, considering force calculations of a complex contains one ion and about 12-16 water molecules). In addition, as can be seen in Figures 4.2 and 4.4, the HF calculations with a relatively large basis set, like AUG-cc-pVDZ, are also extremely expensive. In this work, therefore, the HF method with medium-size basis sets, namely DZV+ for water and Los Alamos ECP plus DZ for ions, are employed. These selected parameters are considered to be reliable enough to achieve a sufficient level of accuracy in the QM/MM simulations. The B3LYP method is not taken into consideration since it has been shown that this method tends to overestimate the ion-water interactions (B. M. Rode, Schwenk, Hofer and Randolf, 2005; Bernd M. Rode, Schwenk and Tongraar, 2004).

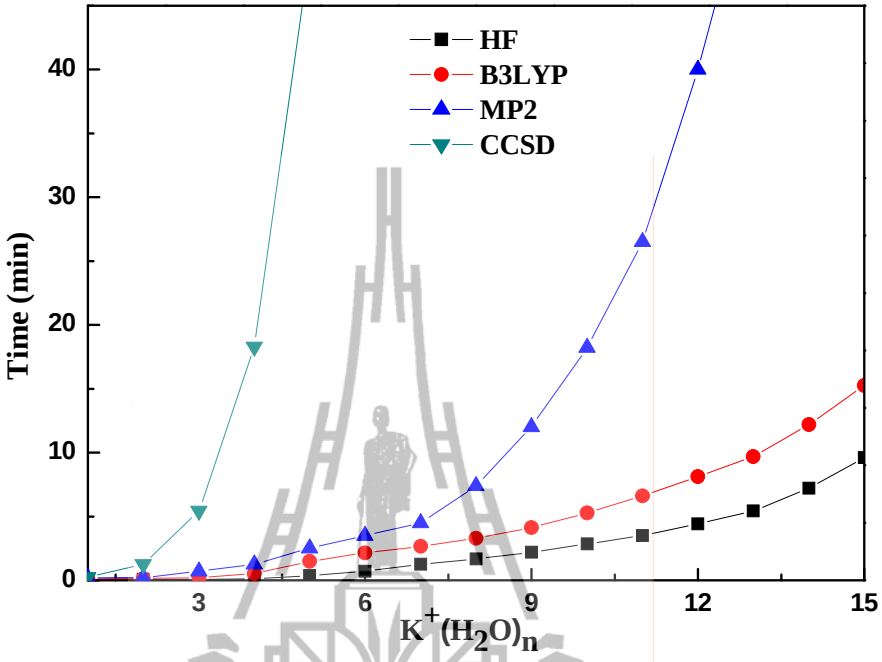

Figure 4.1 Requirements of CPU times for the HF, B3LYP, MP2 and CCSD force calculations of $K^+(H_2O)_{n,\ n=1,15}$ complexes using DZV+ basis set for H_2O and Los Alamos ECP plus DZ basis set for K^+. All calculations were performed on CCRL cluster with Intel Core™2 Quad of CPU and 4GB of Ram.

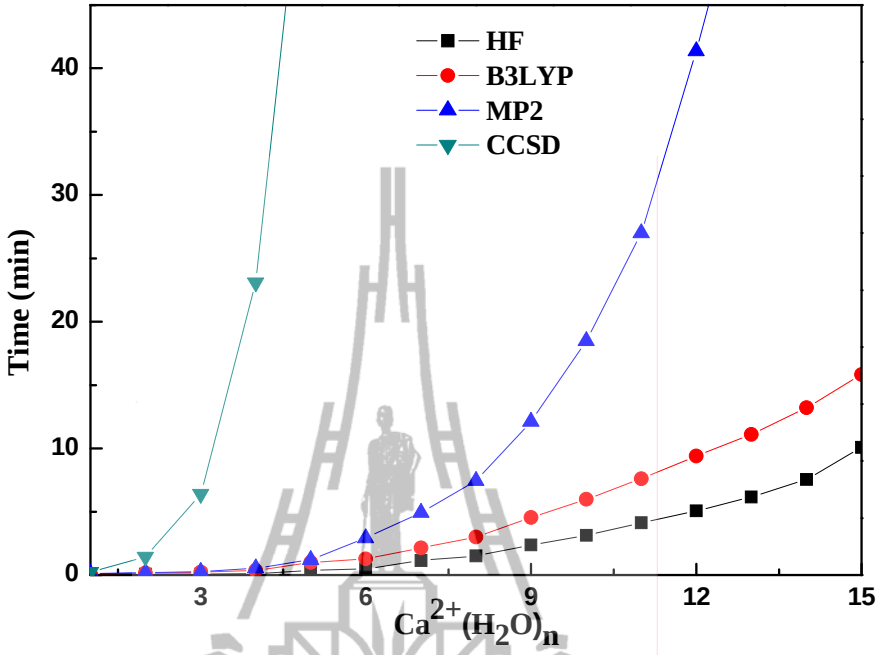

Figure 4.2 Requirements of CPU times for the HF, B3LYP, MP2 and CCSD force calculations of $Ca^{2+}(H_2O)_{n,\ n=1,15}$ complexes using DZV+ basis set for H_2O and Los Alamos ECP plus DZ basis set for Ca^{2+}. All calculations were performed on CCRL cluster with Intel Core™2 Quad of CPU and 4GB of Ram.

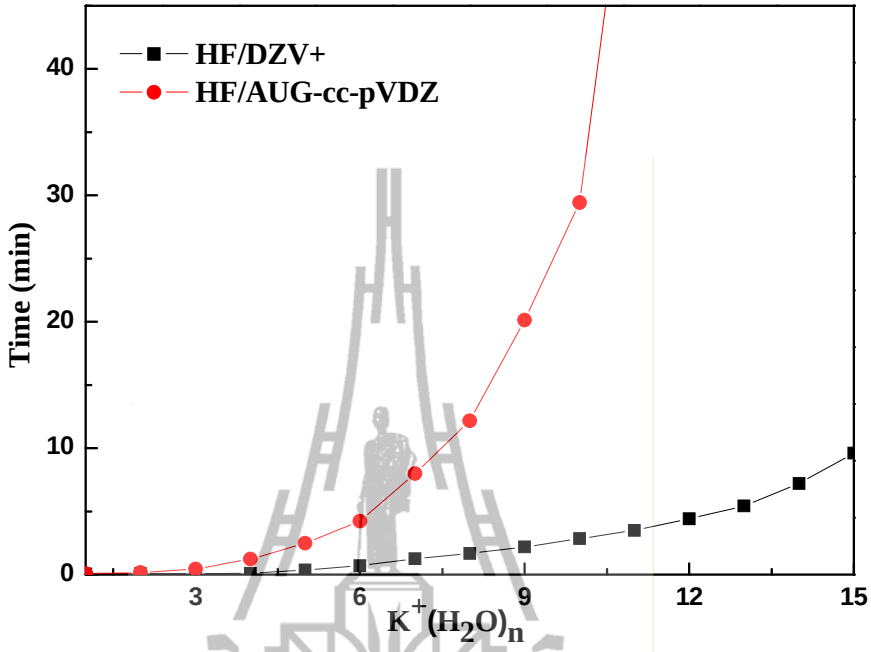

Figure 4.3 Requirements of CPU times for the HF force calculations of $K^+(H_2O)_{n,\ n=1,15}$ complexes using DZV+ and AUG-cc-pVDZ basis sets for H_2O and Los Alamos ECP plus DZ basis set for K^+. All calculations were performed on CCRL cluster with Intel Core™2 Quad of CPU and 4GB of Ram.

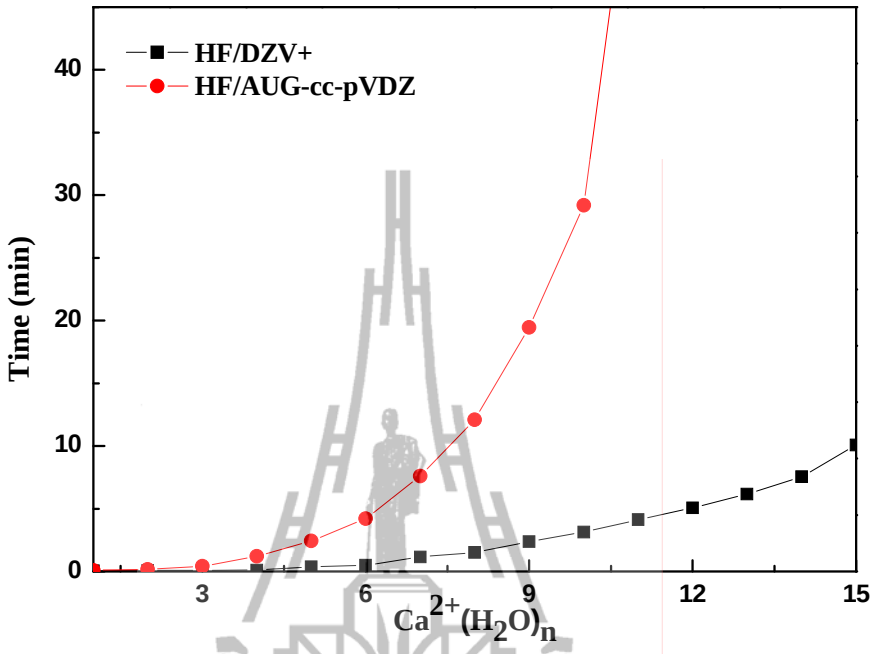

Figure 4.4 Requirements of CPU times for the HF force calculations of $Ca^{2+}(H_2O)_{n,\ n=1,15}$ complexes using DZV+ and AUG-cc-pVDZ basis sets for H_2O and Los Alamos ECP plus DZ basis set for Ca^{2+}. All calculations were performed on CCRL cluster with Intel Core™2 Quad of CPU and 4GB of Ram.

4.5 Setting of molecular dynamics simulations

In this work, two types of HF/MM MD simulations, namely the conventional HF/MM and HF/MM MD based on ONIOM-XS method (which is abbreviated throughout this work as ONIOM-XS), were performed in a canonical ensemble at 298 K with the periodic boundary conditions. A periodic box, with a box length of 18.19 Å, contains one ion and 199 water molecules, corresponding to the experimental density of pure water. A flexible model, which describes intermolecular (Stillinger

and Rahman, 1978) and intramolecular interactions (Bopp, Jancsó and Heinzinger, 1983) was employed for water. The pair potential function for K^+-H_2O and Ca^{2+}-H_2O were obtained from previous studies of K^+ and Ca^{2+} in water (Tongraar, Liedl and Rode, 1997; Tongraar, Liedl and Rode, 1998). The reaction-field method (Adams, Adams and Hills, 1979) was employed for the treatment of long-range interactions. The Newtonian equations of motions were treated by a general predictor-corrector algorithm. The time step size was set to 0.2 fs, which allows for the explicit movement of the hydrogen atoms of water molecules. The system was initially equilibrated by performing the conventional HF/MM and ONIOM-XS simulations for 20,000 time steps. Then, the conventional HF/MM and ONIOM-XS simulations were continued for 200,000 time steps, to collect configurations every 10^{th} step. The pair potential functions for describing K^+-H_2O and Ca^{2+}-H_2O interactions were obtained from previous HF/MM MD studies (Tongraar, Liedl and Rode, 1997; Tongraar, Liedl and Rode, 1998).

4.6 Determination of structural properties

The hydration shell structure of K^+ and Ca^{2+} are explained in terms of ion-O and ion-H radial distribution functions (RDFs) and their corresponding integration numbers, as depicted in Figures 4.5 and 4.6, respectively. For the aqueous K^+ solution, the first K-O peaks obtained by both the conventional HF/MM and ONIOM-XS simulations are rather broad and are not well separated from the bulk, suggesting that water molecules surrounding the ion can easily exchange with bulk waters. The first K-O maximum peak predicted by the conventional HF/MM simulation is centered at 2.83 Å, whereas a slightly shorter distance of 2.78 Å is observed in the ONIOM-XS

simulation. Integrations up to the first minimum of the K-O peaks yield the average coordination numbers of 7.0 and 6.3, respectively. With regard to the ONIOM-XS results, the first-shell coordination number and the K-O distance are closer to those of the X-ray diffraction study (Pálinkás, Radnai and Hajdu, 1980), which reported the K-O distance of 2.80 Å and the coordination number of 6. A further difference between the conventional HF/MM and ONIOM-XS simulations is recognizable in the K-H RDFs, in which the ONIOM-XS simulation reveals a slightly longer first K-H peak with a maximum at 3.28 Å, compared with the corresponding distance of 3.21 Å derived by the conventional HF/MM simulation. Overall, as compared with the conventional HF/MM results, the shape and position of the ONIOM-XS's K-O and K-H RDFs clearly reveal a more rigid structure of the K^+ first hydration shell. This finding clearly shows an important treatment of the ONIOM-XS method in obtaining a more reliable structural data for the K^+ hydrate.

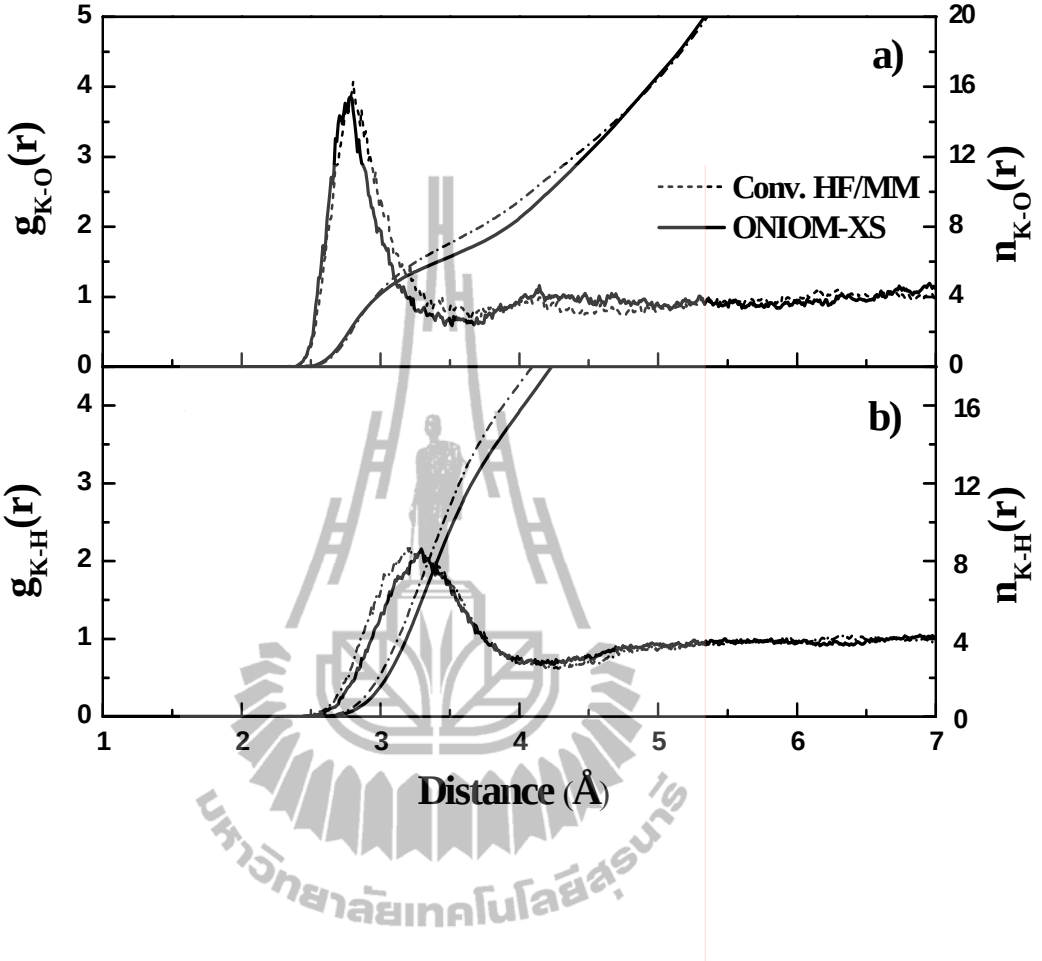

Figure 4.5 a) K-O and b) K-H radial distribution functions and their corresponding integration numbers, as obtained by the conventional HF/MM and ONIOM-XS MD simulations.

In the case of Ca^{2+} (Figure 4.6), the results obtained by both the conventional HF/MM and ONIOM-XS simulations are almost identical, with the first Ca-O maximum peaks exhibited at about 2.44 Å. The shape and height of the Ca-O and Ca-H RDFs clearly indicate a strong "structure-making" ability of Ca^{2+} in aqueous solution. The first Ca-O peaks are rather well separated from the outer region, giving the average coordination numbers of 7.8 and 7.6, respectively. The observed coordination numbers and the average Ca-O distances are in good accord with the extended X-ray absorption fine structure (EXAFS) measurements, in which the coordination numbers of Ca^{2+} were found to be of 6.8 - 8.0 with the Ca-O distances of 2.43 - 2.46 Å. The observed similarity of the conventional HF/MM and ONIOM-XS results is understandable since the ONIOM-XS method is expected to be more effective for the situation where the number of ligands that are crossing the QM/MM boundary is large, *i.e.*, a system where ion-water interactions are weak and water molecules surrounding the ion are labile. In this regard, it could be demonstrated that the conventional HF/MM scheme is reliable enough for the structural determination of such strong Ca^{2+}-water interactions, *i.e.*, a phenomenon where the immediate addition or deletion of particles in the QM region due to the solvent exchange is rare.

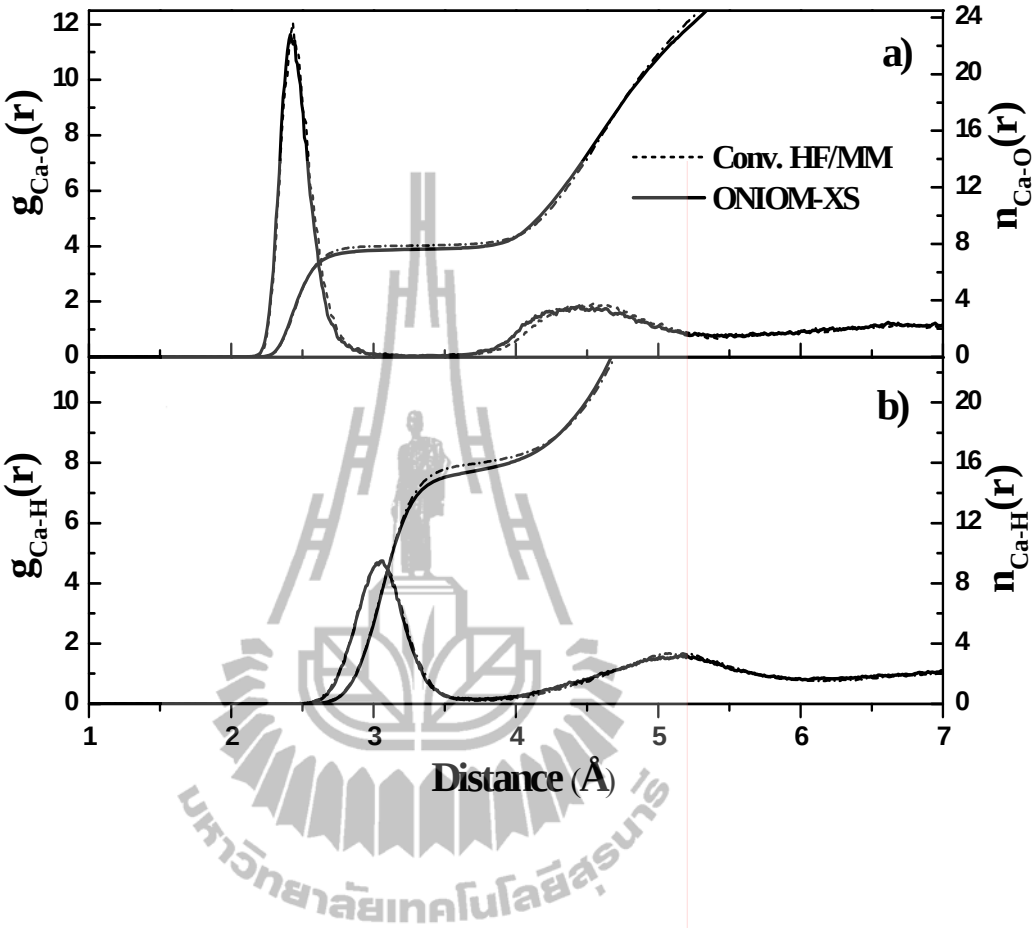

Figure 4.6 a) Ca-O and b) Ca-H radial distribution functions and their corresponding integration numbers, as obtained by the conventional HF/MM and ONIOM-XS MD simulations.

With regard to the QM/MM scheme, the selection of the QM size is found to be one of the main factors in obtaining different numbers of first-shell waters. For example, according to the analogous HF/MM simulations using similar basis sets, the coordination number of K^+ decreases significantly from 8.8 (Azam, Zaheer ul and Fatmi, 2010) and 8.3 (Tongraar, Liedl and Rode, 1998) to the value of 7.0 in the present study according to the use of different QM radii of 3.8, 4.0 and 4.2 Å,

respectively. Similarly, the coordination number of Ca^{2+} in water is found to decrease from 8.3 (Tongraar, Liedl and Rode, 1997) to 7.8 in the present work according to the use of QM radii of 3.6 and 4.2 Å, respectively. In the earlier QM/MM studies, the size of the QM region was usually set with respect to only the first hydration sphere of the ions, *i.e.*, due to the restriction of CPU time. Regarding to the results obtained by the present HF/MM simulations, it is obvious that the influence of non-additive interactions due to n-body effects beyond the first hydration shell of ions is significant, and that the use of a sufficiently large QM size is necessary in obtaining the correct coordination number of these hydrated ions. Recently, a lower K^+ coordination number of 6.2, which is close to the value of 6.3 obtained by the present ONIOM-XS simulation, was reported in the analogous HF/MM simulation with an enlarged QM radius of 6.0 Å (Azam, Hofer, Randolf and Rode, 2009). This implies that the QM size with a radius of 4.2 Å employed in this work is considered to be large enough to achieve a sufficient level of accuracy in the HF/MM simulations once the ONIOM-XS method is employed.

To further analyze the difference between the conventional HF/MM and ONIOM-XS results, the probability distributions of the coordination numbers, calculated up to first minimum of the K-O and Ca-O RDFs, are plotted in Figure 4.7a and b, respectively. For K^+, the preferred coordination number is 7 (in addition to 8 and 6 in smaller amounts) in the conventional HF/MM simulation, whereas the value of 6 (followed by 7, 8 and 5 in decreasing amounts) is preferred according to the ONIOM-XS simulation. As can be seen in Figure 4.7a, the coordination number distributions for K^+ are rather broad, ranging from 5 to 10 (HF/MM) and from 4 to 9 (ONIOM-XS), indicating that a number of different hydrated K^+ species can

simultaneously be formed in the solution. In the case of Ca^{2+}, although the preferred coordination number of 8 (followed by 7 in a smaller amount) is observed in both the conventional HF/MM and ONIOM-XS simulations, the probability distributions of the coordination numbers of 8 and 7 are significantly different, being of 81.9% and 16.7% and of 59.3% and 40.0%, respectively. This supplies information that the ONIOM-XS treatment is essential in order to obtain the correct coordination number distributions of K^+ and Ca^{2+} hydrates.

Figure 4.8a and b displays the orientation of first-shell waters, as obtained by the conventional HF/MM and ONIOM-XS simulations, calculated up to first minimum of the K-O and Ca-O RDFs, respectively. For K^+, both conventional HF/MM and ONIOM-XS simulations reveal rather broad O-K-O peak around 60-160°, which corresponds to the observed weak K^+-water interactions. For Ca^{2+}, since the first-shell waters are mainly oriented with respect to the strong influence of the ion, both conventional HF/MM and ONIOM-XS simulations show two well-pronounced peaks at around 60-100° and around 120-160°.

Further comparison on the orientation of first-shell waters, as obtained by the conventional HF/MM and ONIOM-XS simulations, is plotted in Figure 4.9a and b for the systems of K^+ and Ca^{2+}, respectively. In this context, the angle θ is defined by the ion---O axis and the dipole vector of first-shell water molecules. For K^+, the observed broad distributions of the θ angle clearly indicate weak K^+ hydration, *i.e.*, compared with the Ca^{2+} hydrate. In addition, the distributions of the angle α, as defined by the ion---O—H is also given in Figure 4.10a and b for the systems of K^+ and Ca^{2+}, respectively. As expected, the discrepancy between the conventional HF/MM and

ONIOM-XS simulations is more significant than in the case of Ca^{2+}. This clearly supports the statement that the conventional HF/MM framework is probably useful for the structural determination of strong ion-water interactions, like Ca^{2+}-water, while a more sophisticated ONIOM-XS technique is necessary for the correct treatment of relatively weak ion-water interactions, such as in the case of K^{+}.

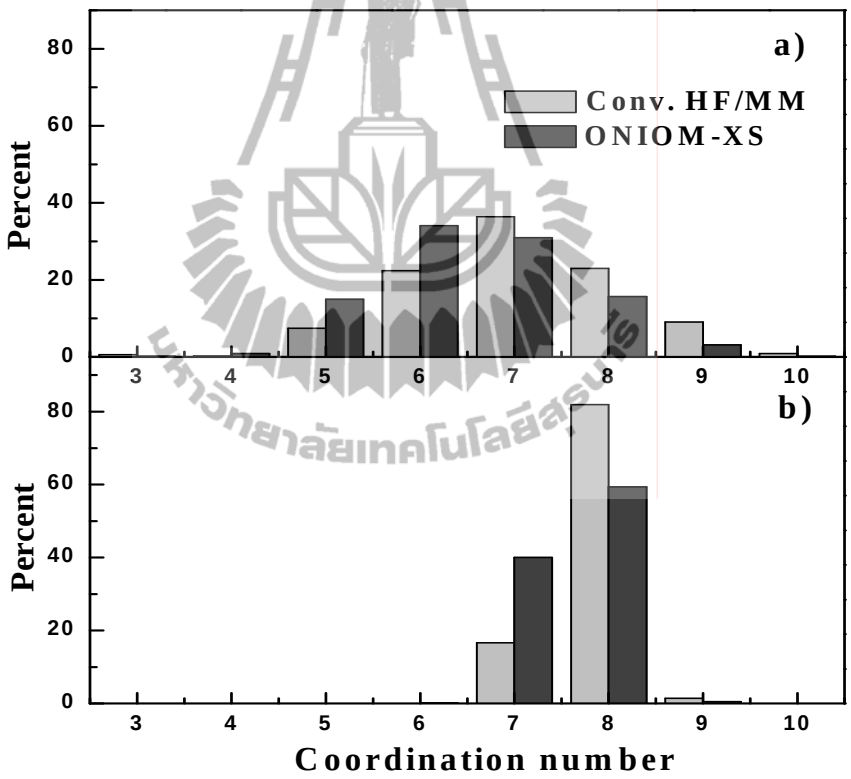

Figure 4.7 Distributions of the coordination numbers of a) K^{+} and b) Ca^{2+}, calculated within the first minimum of the K-O and Ca-O RDFs, respectively.

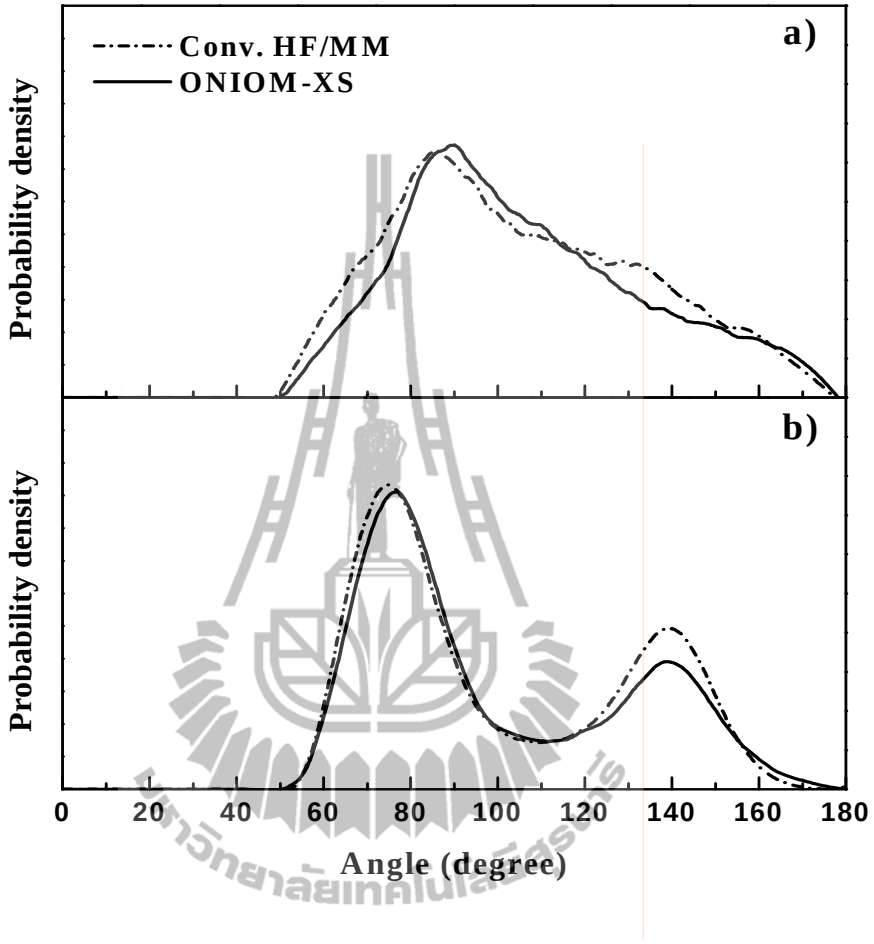

Figure 4.8 Probability distributions of O-ion-O angle in the first hydration shell of a) K^+ and b) Ca^{2+}, calculated within the first minimum of the K-O and Ca-O RDFs, respectively.

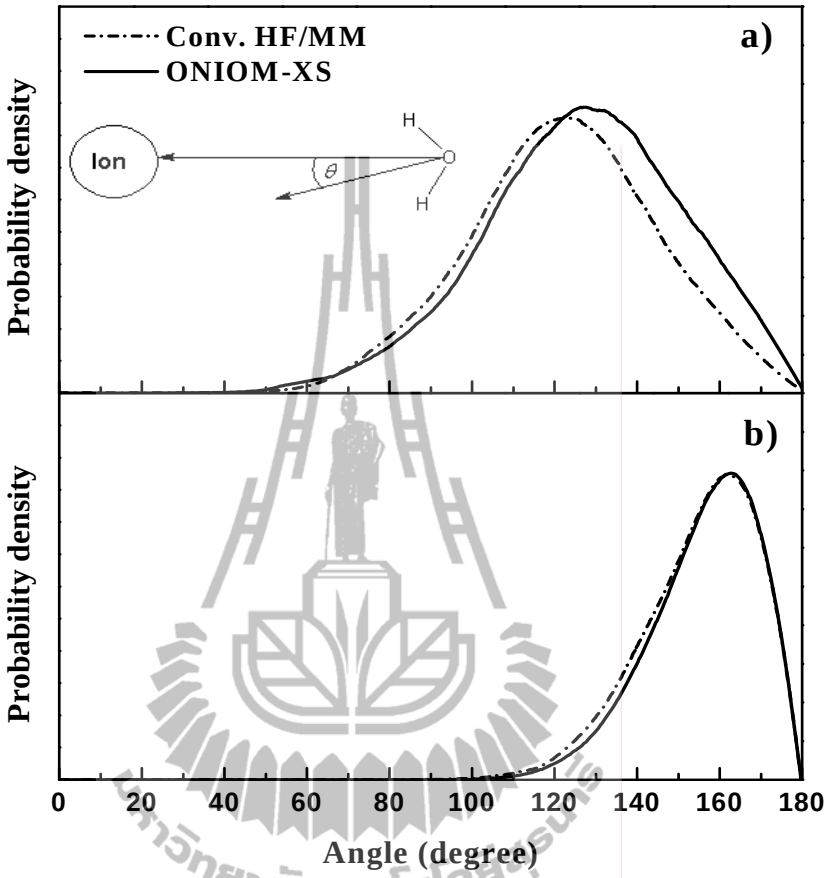

Figure 4.9 Probability distributions of θ angle in the first hydration shell of a) K^+ and b) Ca^{2+}, calculated within the first minimum of the K-O and Ca-O RDFs, respectively.

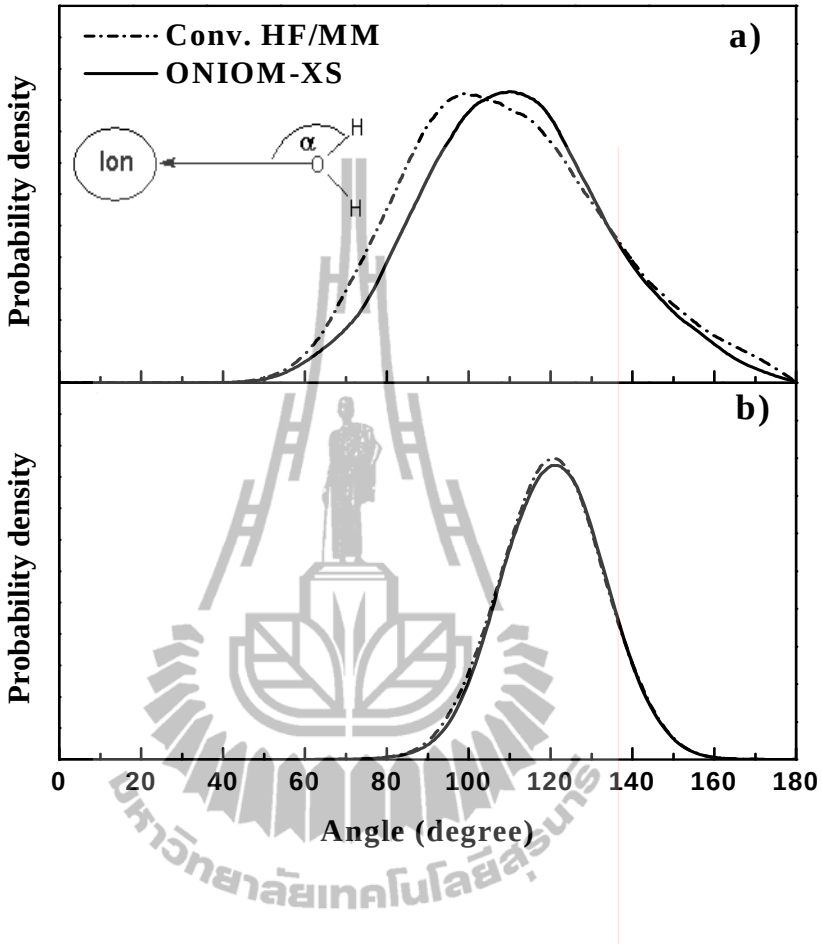

Figure 4.10 Probability distributions of α angle in the first hydration shell of a) K^+ and b) Ca^{2+}, calculated within the first minimum of the K-O and Ca-O RDFs, respectively.

4.7 Determination of dynamical properties

Since the quantities from the simulation are change over time, or time dependent, the way to measure these quantities are usually carried out in terms of time correlation function. The autocorrelation functions of the particle velocities (velocity autocorrelation functions, VACFs) and their spectral densities are usually employed to describe the particle motions in the liquid. For water, since a flexible water model has been used, the dynamical properties of waters can be described in terms of hindered translational motions, librational motions and vibrational motions, respectively. The scheme for a distorted water molecule has been proposed by Bopp (Bopp, Jancsó and Heinzinger, 1983), which can be represented in Figure 4.11.

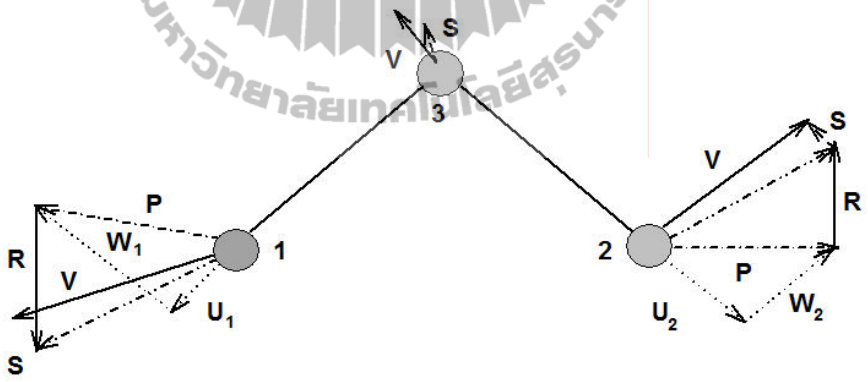

Figure 4.11 Scheme of a distorted water molecule. V: instantaneous velocity; S: velocity of the center-of–mass; R: velocity component perpendicular to the molecular plane; P: velocity component in the molecular plane; U,W: projection of P on the normalized instantaneous O-H vector and on a unit vector perpendicular to it in the molecular plane.

4.7.1 Hindered translational motions

For water, the hindered translations are studied by the center-of-mass VACFs of the water molecules. These functions can be calculated by

$$C_{VV}(t) = \frac{\sum_j \sum_{i=1}^{N_{H_2O}} \left[S_i(t_j) S_i(t_j + t) \right]}{\sum_j \sum_{i=1}^{N_{H_2O}} \left[S_i(t_j) S_i(t_j) \right]}, \tag{4.12}$$

where S_j is the velocity of center-of–mass of water. The VACFs and their Fourier transformations for water molecules in the first hydration shell of ions, as obtained by the conventional HF/MM and ONIOM-XS simulations, are shown in Figures 4.12 and 4.13 for the system of K^+-H_2O and in Figures 4.14 and 4.15 for the system of Ca^{2+}-H_2O, respectively. For the K^+-H_2O system, the VACFs obtained from both conventional HF/MM and ONIOM-XS simulations are quite similar. However, the Fourier transformation of the ONIOM-XS simulation shows a smaller influence of K^+ on the translational motions of the first-shell water molecules, *i.e.*, as can be seen from the pronounced second peak exhibits at lower frequency when compared to that of the conventional HF/MM spectra. For the Ca^{2+}-H_2O system, the VACFs and the corresponding Fourier transformations obtained from the conventional HF/MM and ONIOM-XS simulations are almost identical, which corresponds to the observed small change in the geometrical arrangement of the Ca^{2+}-H_2O complex.

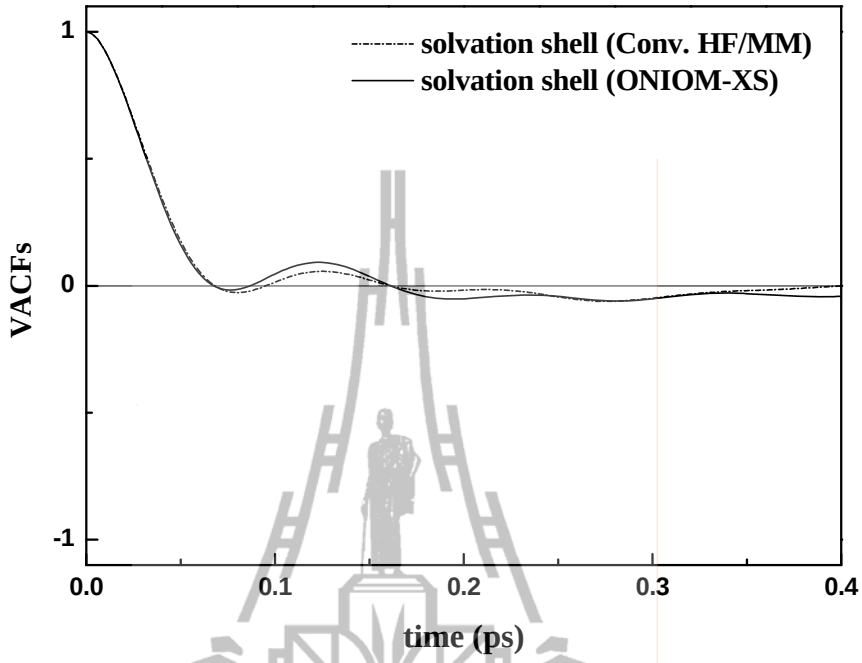

Figure 4.12 Velocity autocorrelation functions of the center-of-mass of first-shell waters for the K^+-H_2O system.

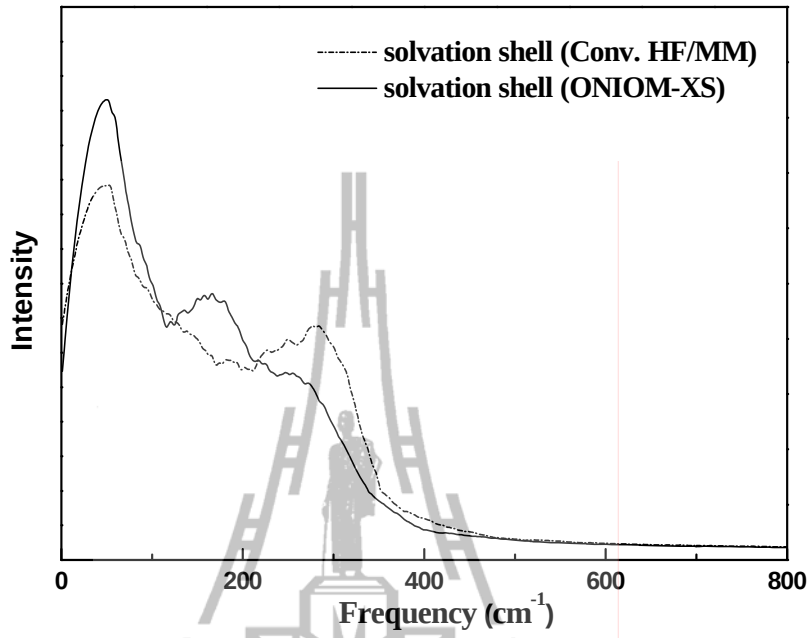

Figure 4.13 Fourier transforms of the translational motions of first-shell waters for the K^+-H_2O system, calculated from the center-of-mass VACFs of waters.

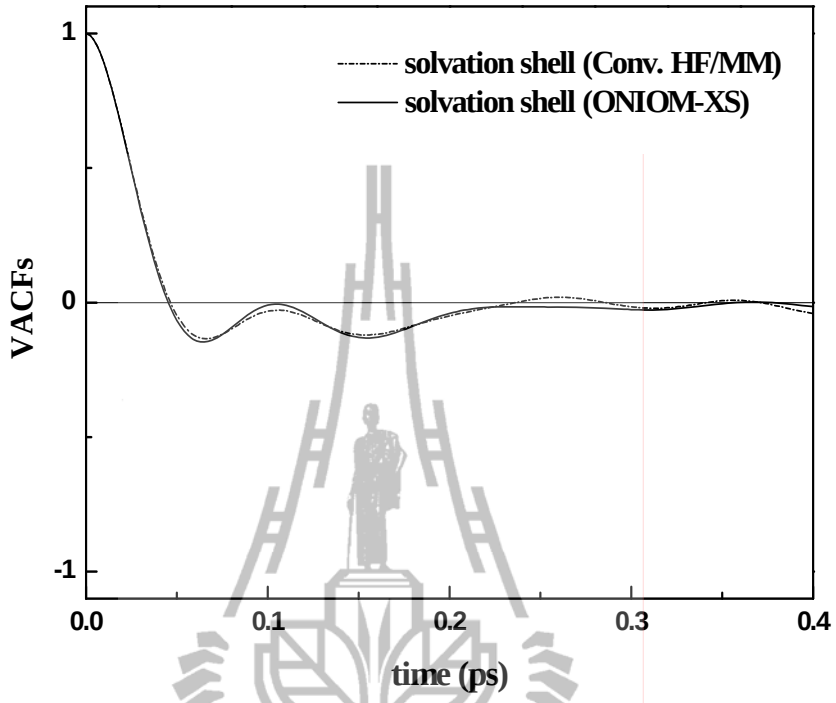

Figure 4.14 Velocity autocorrelation functions of the center-of-mass of first-shell waters for the Ca^{2+}-H_2O system.

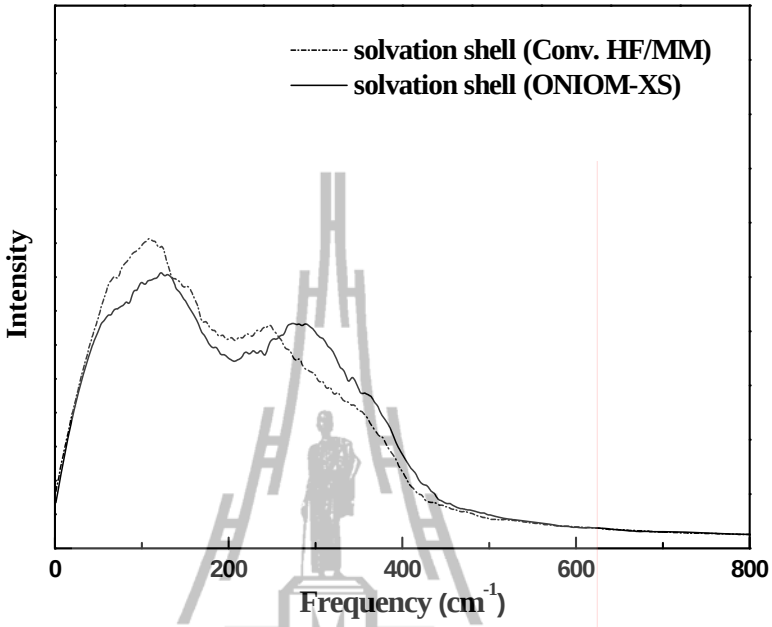

Figure 4.15 Fourier transforms of the translational motions of first-shell waters for the Ca^{2+}-H_2O system, calculated from the center-of-mass VACFs of waters.

4.7.2 Librational motions

To describe the librational motions of waters, the three axis, η, ξ and ζ, were chosen to be identical to the three principal moments of inertia employed in the description of the rotations of the rigid molecule, as shown in Figure 4.16,

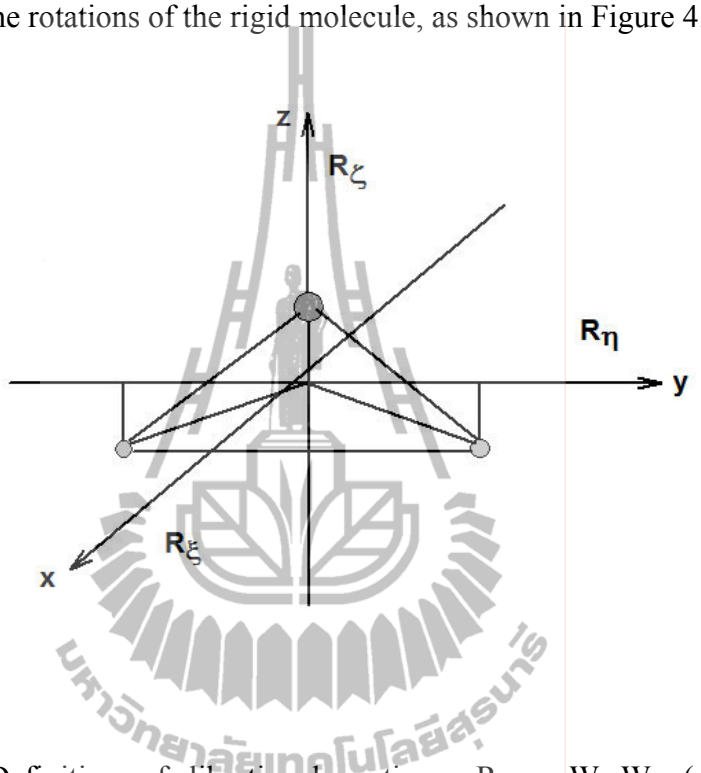

Figure 4.16 Definition of librational motions; R_ξ = W_1-W_2 (rotation around approximated x axis), R_η = R_1+R_2 (rotation around approximated y axis) and R_ζ = R_1-R_2 (rotation around approximated z axis). For the description of W and R, see Figure 4.11.

By this scheme, the three normalized autocorrelation functions can be calculated from

$$C_{R_\xi R_\xi}(t) = \frac{\sum_j \sum_{i=1}^{N_{H_2O}} \left[R_\xi^i(t_j) R_\xi^i(t_j + t)\right]}{\sum_j \sum_{i=1}^{N_{H_2O}} \left[R_\xi^i(t_j) R_\xi^i(t_j)\right]}$$

$$C_{R_\eta R_\eta}(t) = \frac{\sum_j \sum_{i=1}^{N_{H_2O}} \left[R_\eta^i(t_j) R_\eta^i(t_j + t)\right]}{\sum_j \sum_{i=1}^{N_{H_2O}} \left[R_\eta^i(t_j) R_\eta^i(t_j)\right]} \qquad (4.13)$$

$$C_{R_\zeta R_\zeta}(t) = \frac{\sum_j \sum_{i=1}^{N_{H_2O}} \left[R_\zeta^i(t_j) R_\zeta^i(t_j + t)\right]}{\sum_j \sum_{i=1}^{N_{H_2O}} \left[R_\zeta^i(t_j) R_\zeta^i(t_j)\right]}$$

The VACFs and their corresponding Fourier transformations for the librational motions of first-shell waters are shown in Figures 4.17 and 4.18 for the system of K^+-H_2O, and in Figures 4.19 and 4.20 for the system of Ca^{2+}-H_2O, respectively. Overall, the results obtained by the conventional HF/MM and ONIOM-XS simulations are not much difference. For both the K^+-H_2O and Ca^{2+}-H_2O systems, the conventional HF/MM and ONIOM-XS simulations suggest that the VACFs around the approximated ζ axis decay faster than the motions around the approximated ξ and η and hence give the peaks at the highest frequencies. Comparing between the K^+-H_2O and Ca^{2+}-H_2O systems, the shift of the peak positions for water molecules in the hydration shell of ions is related to the strength of ion-water interactions. In the case of Ca^{2+} (Figures 4.19 and 4.20), the influence of the ion shift the peaks to higher frequencies due to the stronger interactions between ion and water, *i.e.*, compared to the K^+-H_2O interactions.

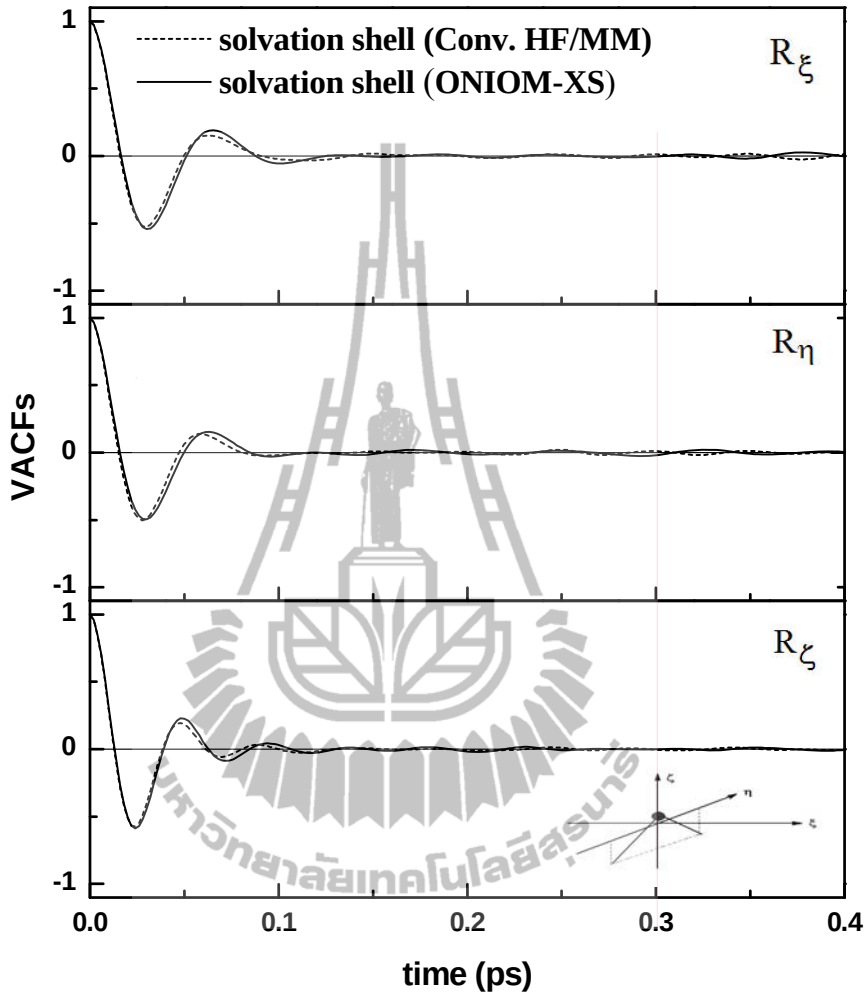

Figure 4.17 Velocity autocorrelation functions of water around the approximated ξ, η and ζ axes, for the system of K^+-H_2O.

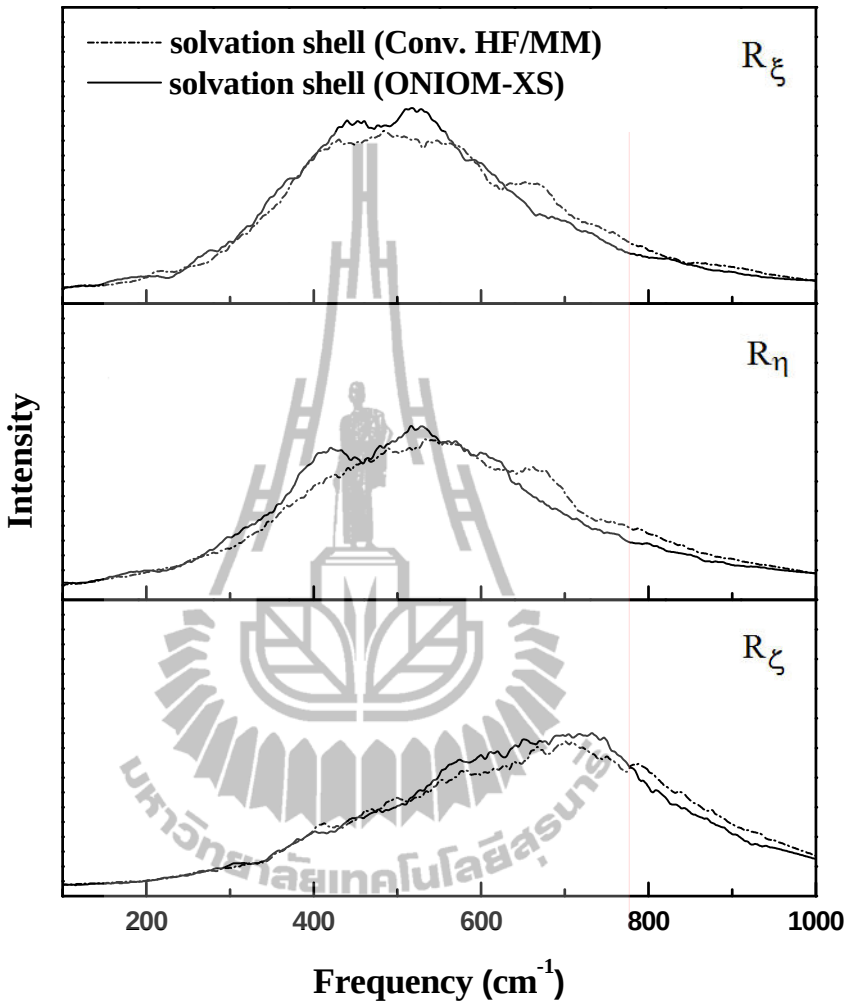

Figure 4.18 Fourier transforms of the librational motions of water for the system of K^+-H_2O, calculated from the VACFs of water around the approximated ξ, η and ζ axes.

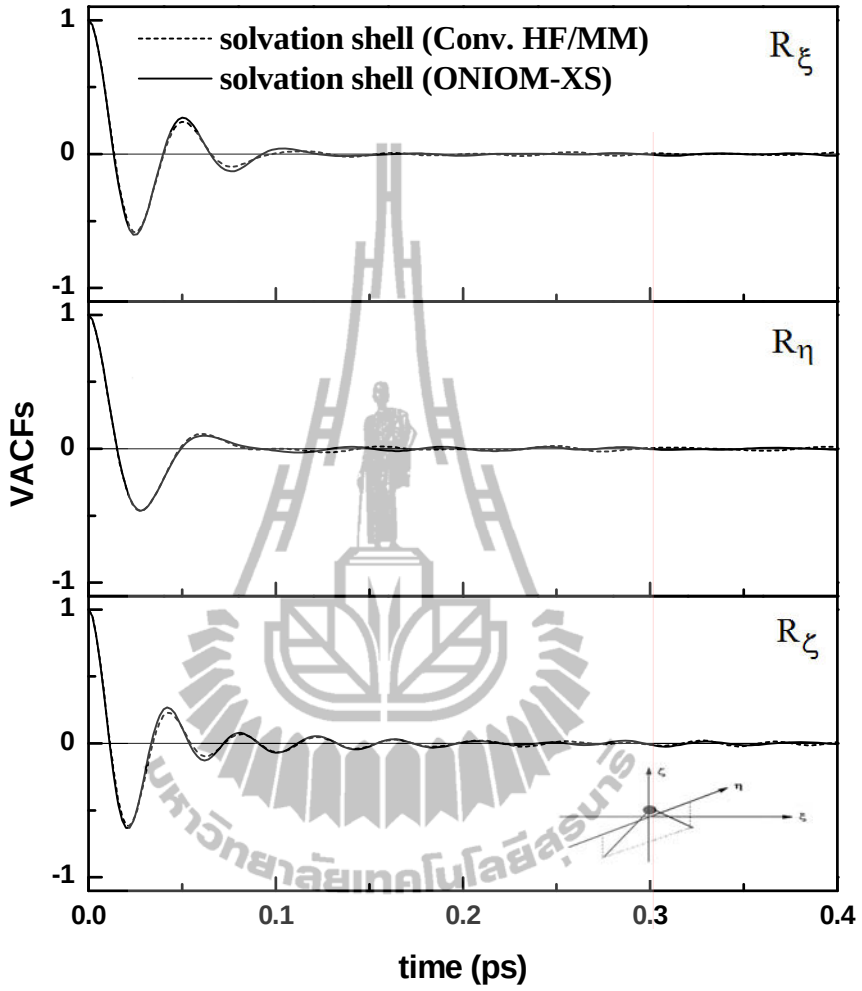

Figure 4.19 Velocity autocorrelation functions of water around the approximated ξ, η and ζ axes, for the system of Ca^{2+}-H_2O.

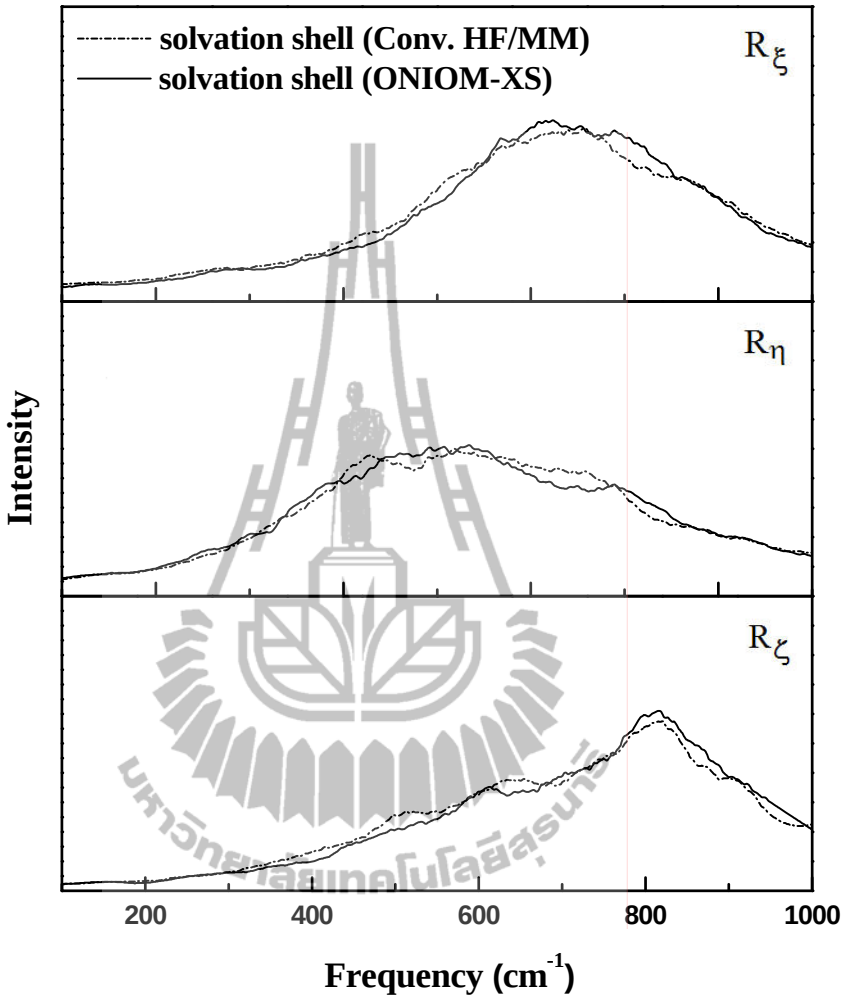

Figure 4.20 Fourier transforms of the librational motions of water for the system of Ca^{2+}-H_2O, calculated from the VACFs of water around the approximated ξ, η and ζ axes.

4.7.3 Vibrational motions

According to Figure 4.11, the three quantities, Q_1, Q_2 and Q_3 are defined as,

$$\begin{aligned} Q_1 &= U_1 + U_2, \\ Q2 &= W_1 + W_2, \\ Q3 &= U_1 + U_2, \end{aligned} \tag{4.14}$$

which correspond to the symmetric stretching and bending and asymmetric stretching motions of water molecule, respectively. The three normalized autocorrelation functions can be written as

$$C_{Q_k Q_k}(t) = \frac{\sum_j \sum_{i=1}^{N_{H_2O}} \left[Q_k^i(t_j) Q_k^i(t_j + t) \right]}{\sum_j \sum_{i=1}^{N_{H_2O}} \left[Q_k^i(t_j) Q_k^i(t_j) \right]} \tag{4.15}$$

where k = 1.2.3.

Fourier transforms of VACFs for obtaining infrared spectra are usually discussed in terms of shift of peak maxima as a result of the ionic influence. Due to rather constant systematic errors of Hatree-Fock frequencies, a scaling factor of 0.89 was proposed to scale the computed frequencies to be in agreement with the experiment (DeFrees and McLean, 1985). Therefore, all *ab initio* results in this work were scaled with this proposed factor. In addition, the normalized velocity autocorrelation functions of the approximate normal coordinates of water in the bulk are assumed to be not significantly different since there is only one ion contained in the system.

The normalized VACFs of the approximate normal coordinates of water in the hydration shell of ions, as obtained by the conventional HF/MM and ONIOM-XS simulations, are depicted in Figures 4.21 and 4.22 for the system of K^+-H_2O, and in Figures 4.23 and 4.24 for the system of Ca^{2+}-H_2O, respectively. Figures 4.25 and 4.26 show the corresponding bending and stretching frequencies, calculated separately for water in the bulk and in the hydration shell of the ions. The intramolecular vibrational frequencies of water obtained from various simulations and experiments are given in Tables 4.7 and 4.8 for the systems of K^+-H_2O and Ca^{2+}-H_2O, respectively. In this work, it should be noted that the shift of bending and stretching vibration of water molecules in the bulk and in the hydration shell of ions can not be directly compared since water molecules in the hydration shell of ions are treated by quantum mechanics, while those in the bulk are described by means of MM potentials. Instead, the comparison will be made with respect to the observed difference between the conventional HF/MM and ONIOM-XS data. For K^+-H_2O system, the bending frequency predicted by the conventional HF/MM and ONIOM-XS simulations are identical, while the ONIOM-XS gives a significant blue-shift for both the symmetric and asymmetric stretching frequencies. In the case of Ca^{2+}-H_2O system, the bending frequency predicted by the conventional HF/MM and ONIOM-XS simulations are also identical, but the ONIOM-XS gives a significant red-shift for both the symmetric and asymmetric stretching frequencies, which is in contrast to the K^+-H_2O system. The observed differences between the conventional HF/MM and ONIOM-XS simulations clearly confirm the efficiency of the ONIOM-XS technique in providing a more accurate description of the K^+ and Ca^{2+} hydrates.

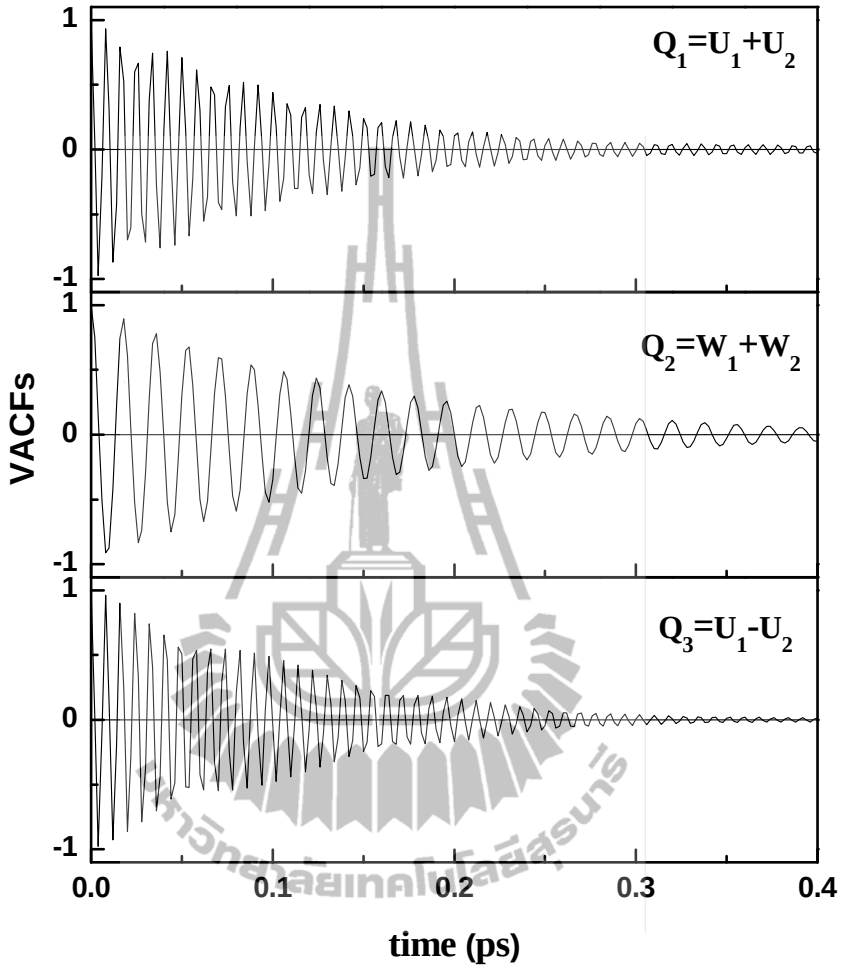

Figure 4.21 Normalized autocorrelation functions of the approximate normal coordinates for water in the hydration shell of K^+, as obtained from the conventional HF/MM simulation of K^+-H_2O system.

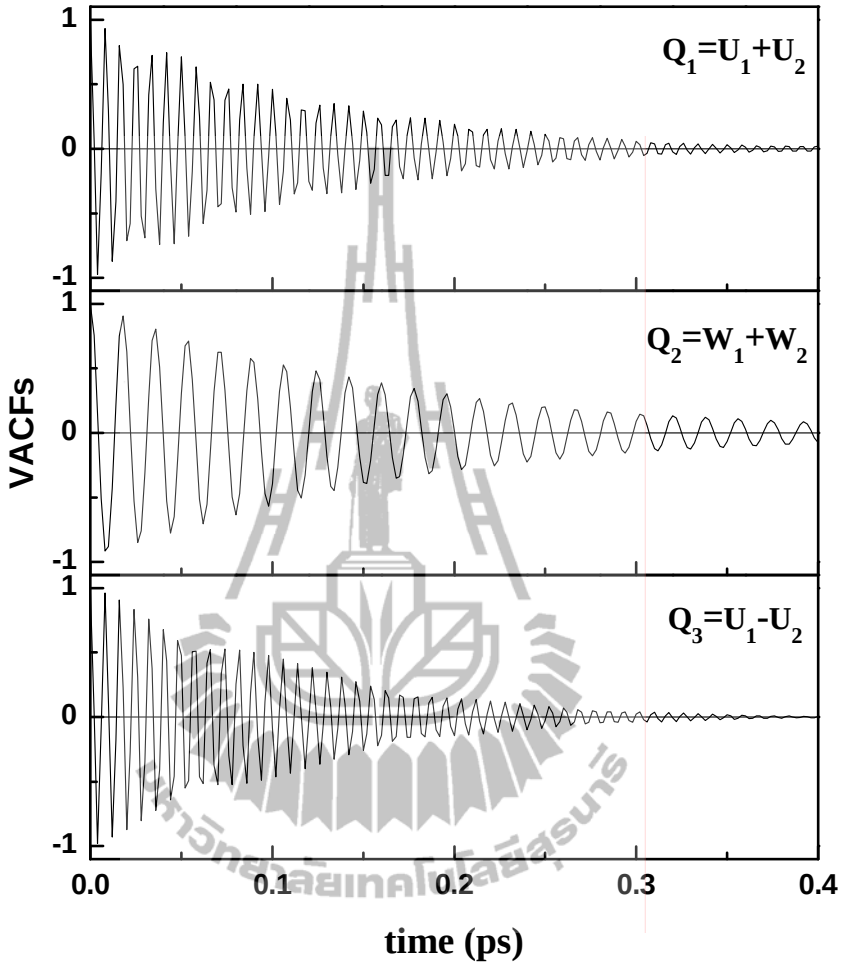

Figure 4.22 Normalized autocorrelation functions of the approximate normal coordinates for water in the hydration shell of K^+, as obtained from the ONIOM-XS simulation of K^+-H_2O system.

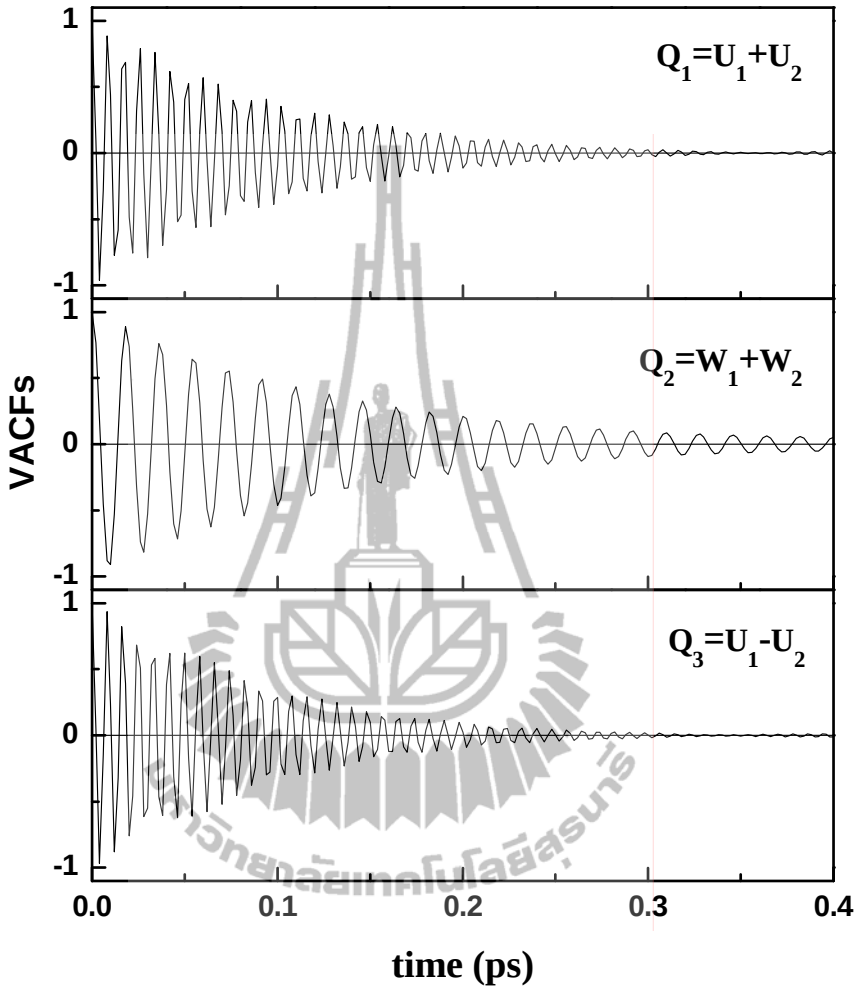

Figure 4.23 Normalized autocorrelation functions of the approximate normal coordinates for water in the hydration shell of Ca^{2+}, as obtained from the conventional HF/MM simulation of Ca^{2+}-H_2O system.

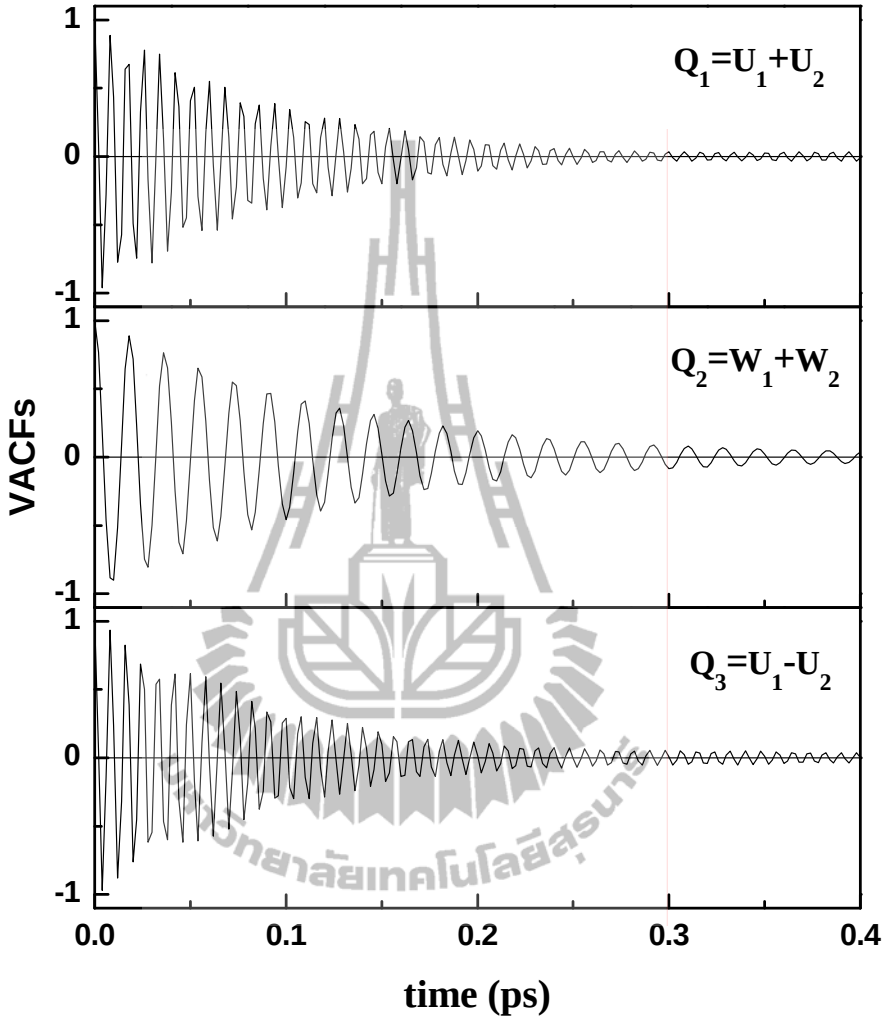

Figure 4.24 Normalized autocorrelation functions of the approximate normal coordinates for water in the hydration shell of Ca^{2+}, as obtained from the ONIOM-XS simulation of Ca^{2+}-H_2O system.

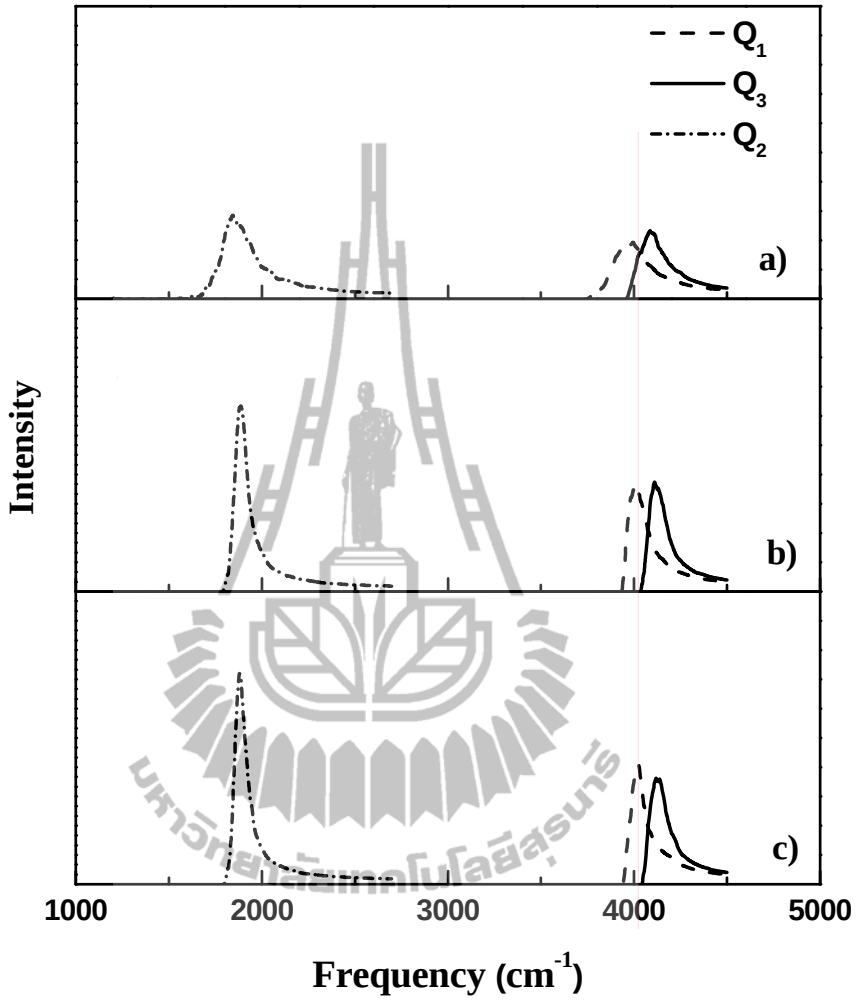

Figure 4.25 Fourier transforms of the hydrogen velocity autocorrelation functions of water in the a) bulk (conventional HF/MM), b) hydration shell of K^+ (conventional HF/MM) and c) hydration shell of K^+ (ONIOM-XS).

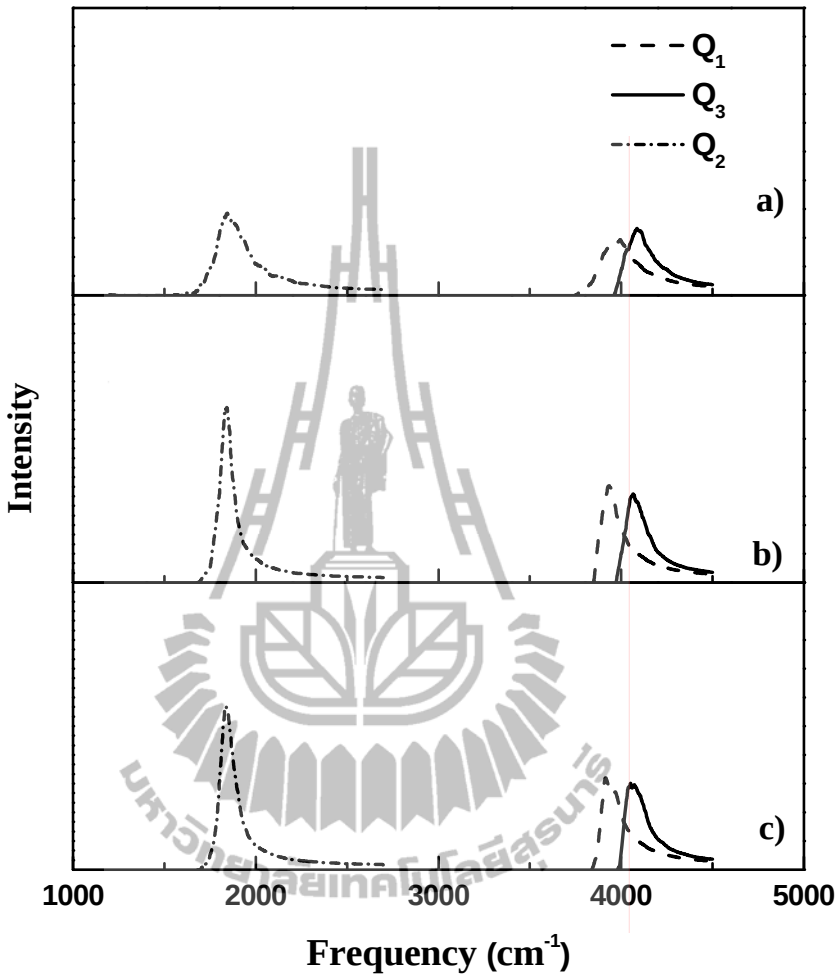

Figure 4.26 Fourier transforms of the hydrogen velocity autocorrelation functions of water in the a) bulk (conventional HF/MM), b) hydration shell of Ca^{2+} (conventional HF/MM) and c) hydration shell of Ca^{2+} (ONIOM-XS).

Table 4.7 Comparison of the intramolecular vibrational frequencies of water obtained from various simulations and experiment, concerning for K^+ in water. (Q_1, Q_2 and Q_3 corresponding to the symmetric stretching, bending, and asymmetric stretching vibrations, respectively)

Phase	Frequency (cm^{-1})			References
	Q_1	Q_3	Q_2	
Bulk	3552	3640	1638	This work, Conventional HF/MM
	3475	3580	1715	(Bopp, 1986)
	3345*	3445*	1645*	(Murphy and Bernstein, 1972)
	3527		1715	(Probst, Bopp, Heinzinger and Rode, 1984)
Hydration shell	3561	3656	1674	This work, Conventional HF/MM
	3579	3667	1674	This work, ONIOM-XS

* experimental frequencies in liquid water

Table 4.8 Comparison of the intramolecular vibrational frequencies of water obtained from various simulations and experiment, concerning for Ca^{2+} in water. (Q_1, Q_2 and Q_3 corresponding to the symmetric stretching, bending, and asymmetric stretching vibrations, respectively)

Phase	Frequency (cm^{-1})			References
	Q_1	Q_3	Q_2	
Bulk	3552	3640	1638	This work, Conventional HF/MM
	3475	3580	1715	(Bopp, 1986)
	3345*	3345*	1645*	(Murphy and Bernstein, 1972)
	3527		1715	(Probst, Bopp, Heinzinger and Rode, 1984)
Hydration shell	3501	3619	1634	This work, Conventional HF/MM
	3483	3605	1634	This work, ONIOM-XS
	3160	3285	1685	(Bopp, 1986)
	3280		1689	(Probst, Bopp, Heinzinger and Rode, 1984)

* experimental frequencies in liquid water

4.7.4 Water exchange processes

In general, the mechanism of water exchange can be classified into five ways as proposed by Langford and Gray (Langford and Gray, 1996). An associative exchange (A) refers to situation where the external water molecule joins the complex before the departing water leaves. On the other hand, the dissociative exchange (D) is the one where the water molecule leaves the complex before the external water joins. In the case where an incoming and outgoing water molecule interchanges at the same time, the mechanism is called interchange mechanism (I), which can be subdivided into two classes depending on whether the exchange is associative-like (I_a) or dissociative-like (I_d) (see Figure 4.27).

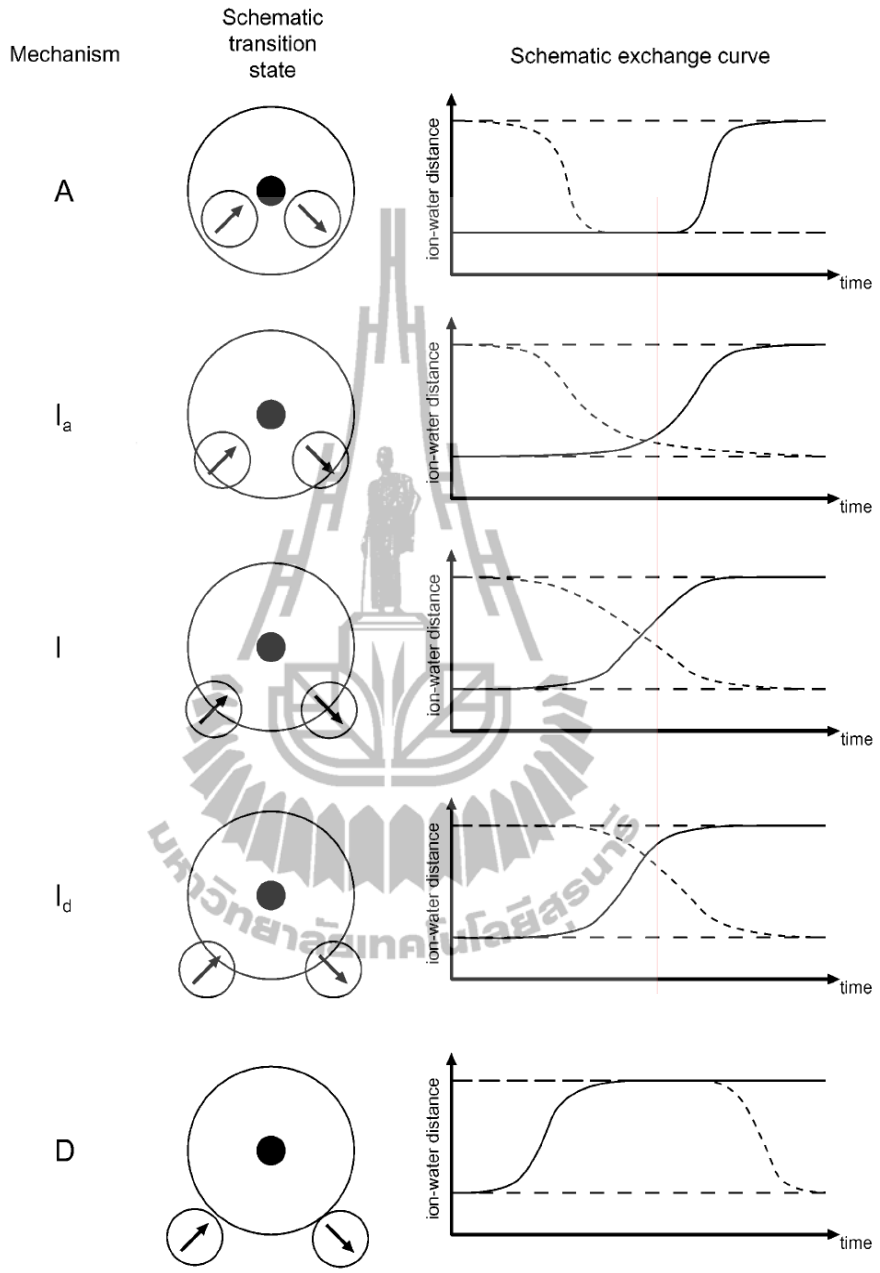

Figure 4.27 Representation of transition state of the five exchange classes. First column: classification of exchange mechanism. Second column: schematic illustration of the exchanges. Third column: ion-water distance exchange curve.

Figures 4.28 and 4.29 show the time dependence of the ion-O distance and number of first-shell waters obtained from the ONIOM-XS simulations of aqueous K^+ and Ca^{2+} solutions, respectively. For K^+ (Figure 4.28), it is obvious that water molecules surrounding the ion are quite labile, showing numerous water exchange processes during the ONIOM-XS simulation. Consequently, this results in the observed large variation of the K^+ coordination numbers, ranging from 4 to 9. Such phenomenon is understandable since the K^+-water interactions are relatively weak and are energetically comparable with water-water interactions in bulk water. This clearly suggests an extremely fast dynamics of the hydrated K^+. In the case of Ca^{2+} (Figure 4.29), most of the first-shell waters are tightly bound to the ion, in which the $Ca^{2+}(H_2O)_7$ and $Ca^{2+}(H_2O)_8$ complexes are found to be the dominant species in aqueous solution. With regard to the relatively small number of water exchange processes, *i.e.*, compared to that of the K^+ ion, this clearly indicates that most of first-shell waters are tightly bound to the ion and thus yielding a well-defined first Ca^{2+} hydration shell.

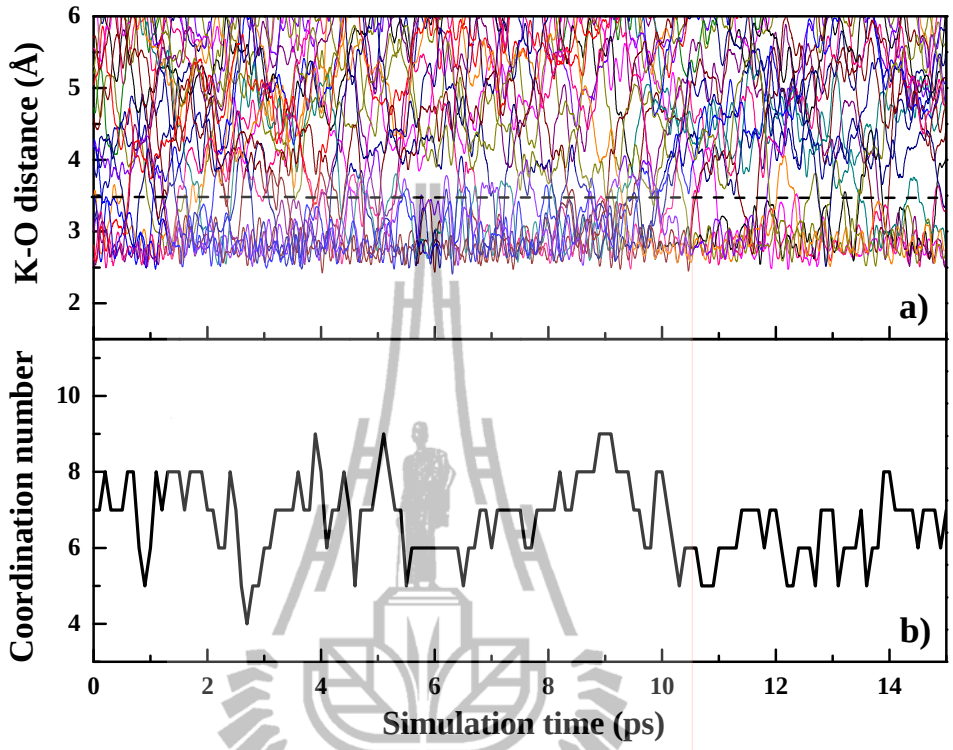

Figure 4.28 Time dependences of a) K^+---O distance and b) number of first-shell waters, as obtained from first 15 ps of the ONIOM-XS simulation. In Figure 4.28a), the dash line parallel to the x-axis indicates the first minimum of the K-O RDF.

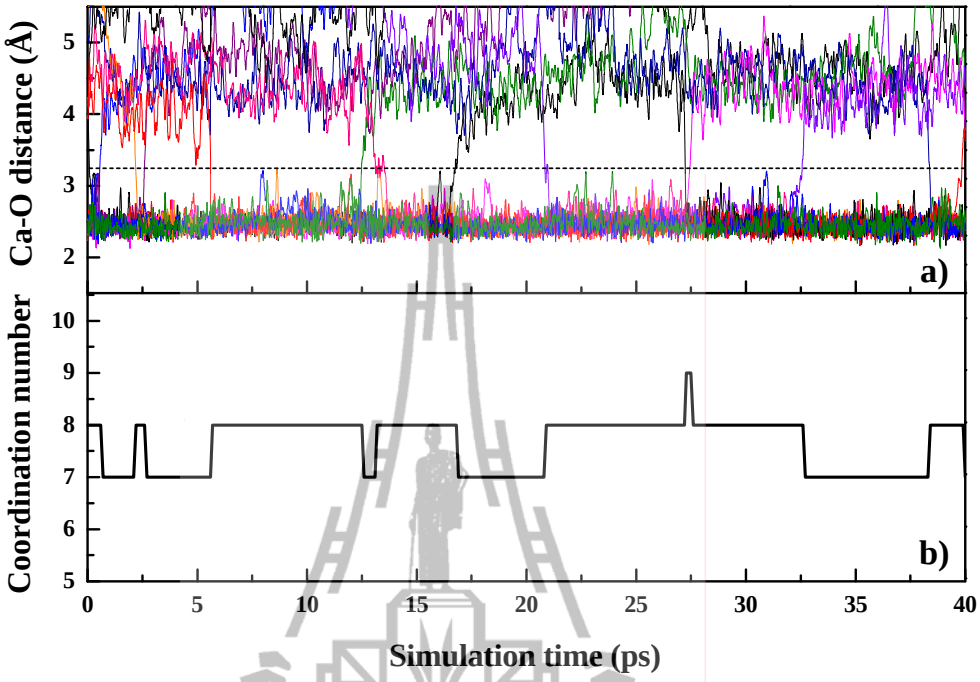

Figure 4.29 Time dependences of a) Ca^{2+}---O distance and b) number of first-shell waters, as obtained from 40 ps of the ONIOM-XS simulation. In Figure 4.29a), the dash line parallel to the x-axis indicates the first minimum of the Ca-O RDF.

The rate of water exchange processes were evaluated through *mean residence times* (MRTs) of water molecules surrounding the ions. In this work, the MRT data were calculated using the "direct" method (Hofer, Tran, Schwenk and Rode, 2004), as the product of the average number of water molecules in the first shell with the duration of the MD simulation, divided by the observed number of exchange events lasting a given time interval t^*,

$$MRT(\tau) = \frac{CN \times t_{sim}}{N_{ex}}, \tag{4.16}$$

where CN is the coordination number, t_{sim} is the simulation time and N_{ex} is the number of exchange events.

In general, it has been demonstrated that a t^* value of 0.0 ps is suitable for the estimation of hydrogen bond lifetimes, while a value of 0.5 ps is considered as a good measure for water exchange processes (Hofer, Tran, Schwenk and Rode, 2004). The calculated MRT data with respect to t^* values of 0.0 and 0.5 ps are summarized in Table 4.9, together with the corresponding data obtained from previous HF/MM works.

Table 4.9 Number of water exchange events (N_{ex}) and mean residence time of water molecules in the vicinity of K^+ and Ca^{2+} (τ), calculated within the first minimum of the K-O and Ca-O RDFs.

			$t^* = 0.0$ ps		$t^* = 0.5$ ps	
Atom/solute	CN	t_{sim}	$N_{ex}^{0.0}$	$\tau_{H_2O}^{0.0}$	$N_{ex}^{0.5}$	$\tau_{H_2O}^{0.5}$
Conventional HF/MM MD						
K^+	7.0	30.0	514	0.41	112	1.87
Ca^{2+}	7.8	40.0	26	12.00	8	39.00
ONIOM-XS MD						
K^+	6.3	30.0	445	0.42	105	1.80
Ca^{2+}	7.6	40.0	30	10.13	14	21.71

For K^+, although the conventional HF/MM and ONIOM-XS simulations reveal rather similar MRT values for both $t^* = 0.0$ and 0.5 ps, the amount of first-shell waters and the number of exchange events are somewhat different. In the case of Ca^{2+}, a significant difference between the conventional HF/MM and ONIOM-XS simulations is observed for $t^* = 0.5$ ps, in which the latter predicts a relatively large number of exchange events (of about two times) with the smaller MRT value (of about half) when compared with that of the conventional HF/MM simulation. With regard to this point, it should be demonstrated that the correct degree of lability of the hydration shell is a significant factor in determining the reactivity of ions in solution.

In particular for K^+, the detailed information of the water exchange processes is strongly related to the determination of the "structure-breaking" ability of this ion in aqueous solution. According to some unsolved problems in the conventional QM/MM scheme, the more sophisticated QM/MM MD simulation based on the ONIOM-XS method is highly recommended for studying such condensed-phase systems.

4.8 References

Adams, D. J., Adams, E. M. and Hills, G. J. (1979). The computer simulation of polar liquids. **Molecular Physics**. 38: 387 - 400.

Azam, S. S., Hofer, T. S., Randolf, B. R. and Rode, B. M. (2009). Hydration of sodium(I) and potassium(I) revisited: A comparative QM/MM and QMCF MD simulation study of weakly hydrated ions. **The Journal of Physical Chemistry A**. 113: 1827-1834.

Azam, S. S., Zaheer ul, H. and Fatmi, M. Q. (2010). Classical and QM/MM MD simulations of sodium(I) and potassium(I) ions in aqueous solution. **Journal of Molecular Liquids**. 153: 95-100.

Bopp, P. (1986). A study of the vibrational motions of water in an aqueous $CaCl_2$ solution. **Chemical Physics**. 106: 205-212.

Bopp, P., Jancsó, G. and Heinzinger, K. (1983). An improved potential for non-rigid water molecules in the liquid phase. **Chemical Physics Letters**. 98: 129-133.

DeFrees, D. J. and McLean, A. D. (1985). Molecular orbital predictions of the vibrational frequencies of some molecular ions. **The Journal of Chemical Physics**. 82: 333-341.

Hofer, T. S., Tran, H. T., Schwenk, C. F. and Rode, B. M. (2004). Characterization of dynamics and reactivities of solvated ions by *ab initio* simulations. **Journal of Computational Chemistry**. 25: 211-217.

Langford, C. H. and Gray, H. B. (1996). **Ligand Substitution Processes**. W.A. Benjamin: New York.

Murphy, W. F. and Bernstein, H. J. (1972). Raman spectra and an assignment of the vibrational stretching region of water. **The Journal of Physical Chemistry**. 76: 1147-1152.

Pálinkás, G., Radnai, T. and Hajdu, H. (1980). **Z. Naturforsch., Teil A, Phys. Phys. Chem. Kosmophys.** 35: 107-114.

Probst, M. M., Bopp, P., Heinzinger, K. and Rode, B. M. (1984). The effect of Ca^{2+} and Cl^{-} on the intramolecular vibrational frequencies of water. **Chemical Physics Letters**. 106: 317-320.

Rode, B. M., Schwenk, C. F., Hofer, T. S. and Randolf, B. R. (2005). Coordination and ligand exchange dynamics of solvated metal ions. **Coordination Chemistry Reviews**. 249: 2993-3006.

Rode, B. M., Schwenk, C. F. and Tongraar, A. (2004). Structure and dynamics of hydrated ions--new insights through quantum mechanical simulations. **Journal of Molecular Liquids**. 110: 105-122.

Stillinger, F. H. and Rahman, A. (1978). Revised central force potentials for water. **The Journal of Chemical Physics**. 68: 666-670.

Tongraar, A., Liedl, K. R. and Rode, B. M. (1997). Solvation of Ca^{2+} in water studied by Born-Oppenheimer *ab initio* QM/MM dynamics. **The Journal of Physical Chemistry A**. 101: 6299-6309.

Tongraar, A., Liedl, K. R. and Rode, B. M. (1998). Born−Oppenheimer *ab initio* QM/MM dynamics simulations of Na^+ and K^+ in water: From structure making to structure breaking effects. **The Journal of Physical Chemistry A**. 102: 10340-10347.

CHAPTER V

CONCLUSION

In this work, the hydration structure and dynamics of K^+ and Ca^{2+} in water were investigated by means of conventional QM/MM MD and QM/MM MD based on ONIOM-XS method (which is abbreviated as ONIOM-XS MD). The main objective of this work is to investigate the validity of the conventional QM/MM technique for the treatment of such particular systems, by comparing the QM/MM results to those obtained by the more accurate ONIOM-XS MD technique. By the QM/MM approach, the most interesting region, *i.e.*, the sphere which includes the ion and its surrounding water molecules, is treated at HF levels of accuracy using DZV+ basis set for water and LANL2DZ basis set for K^+ and Ca^{2+}, while the rest of the system is described by classical pair potentials. From the detailed analyses of the ONIOM-XS MD trajectories, the average hydration numbers for K^+ and Ca^{2+} were found to be 6.3 and 7.6, respectively, compared with the corresponding values of 7.0 and 7.8 derived from the conventional QM/MM simulations. A significant difference between the conventional QM/MM and ONIOM-XS simulations is also found in the comparison of dynamical data. The overall difference clearly indicates the deficiency of the conventional QM/MM scheme and, therefore, a more accurate QM/MM MD technique based on the ONIOM-XS method can be seen as a more suitable simulation approach, which can provide more reliable data on the structure and dynamics of these hydrated ions.

APPENDICES

APPENDIX A

THEORETICAL AND EXPERIMENTAL OBSERVATIONS DATA

Table A.1 Theoretical observations on K^+ solvation in aqueous solutions.

solute	ion/water ratio	method	*CN*	r_{max}	r_{min}	year
K^+	1/215	MC (QCDF)	6.3	2.71	-	1981
K^+	1/125	MD (MCY)	7.5	2.76	-	1983
K^+	1/215	MD (SPC/E)	7.2	2.80	3.65	1996
K^+	1/525	MD(TIP3P)	7.6	2.90	3.80	1996
K^+	1/199	MD (CF2)	7.8	2.78	3.40	1998
K^+	1/199	QM/MM MD (LANL2DZ)	8.3	2.81	3.72	1998
K^+	1/59	CP-MD (BLYP)	6.7	2.81	3.75	1999
K^+	1/216	MD (AMOEBA)	7.0	2.60	-	2003
K^+	1/216	MD (OPLS-AA)	6.6	2.64	-	2003
K^+	1/216	MD (CHARMM27)	6.9	2.62	-	2003
K^+	1/32	CP-MD (PW91)	4+2	2.80	-	2004
K^+	1/500	MD (AH/SWM4-DP)	6.9	2.74	3.55	2006

Table A.2 Experimental observations on K^+ solvation in aqueous solutions.

solute	molarity (M)	method	*CN*	r_{max}	r_{min}	year
KOH	1.0	XRD	4.0	-	-	1958
KCl	2.0	XRD	6.0	2.80	-	1980
KCl	4.0	XRD	6.0	2.80	-	1980
KF	1.2	ND	6.4	2.65	-	2006
KF	2.4	ND	6.2	2.65	-	2006
KF	4.8	ND	5.8	2.65	-	2006
KCl	1.2	ND	6.2	2.65	-	2006
KCl	2.4	ND	5.5	2.65	-	2006
KCl	4.8	ND	5.6	2.65	-	2006
KBr	1.2	ND	5.9	2.65	-	2006
KBr	2.4	ND	5.6	2.65	-	2006
KBr	4.8	ND	5.5	2.65	-	2006
KI	1.2	ND	6.0	2.65	-	2006
KI	2.4	ND	5.5	2.65	-	2006
KI	4.8	ND	5.9	2.65	-	2006
KCl	2.5	EXAFS	6.1	2.73	-	2006

Table A.3 Theoretical observations on Ca^{2+} solvation in aqueous solutions.

solute	ion/water ratio	method	*CN*	r_{max}	r_{min}	year
Ca^{2+}	1/205	MC (MCOH)	7.0	2.40	-	1995
Ca^{2+}	-	MD (SPC/E)	7.9	2.50	-	1996
Ca^{2+}	1/525	MD (CHARMM22)	8.0	2.50	-	1996
Ca^{2+}	1/199	MD (Pair)	9.2	2.47	3.10	1997
Ca^{2+}	1/199	QM/MM MD (STO-3G)	10.0	2.38	2.90	1997
Ca^{2+}	1/199	QM/MM MD (LANL2DZ)	8.3	2.45	3.30	1997
Ca^{2+}	1/509	MD (Åquist)	8.0	2.40	3.33	2001
Ca^{2+}	1/509	MD (Bounds)	9.5	2.51	3.42	2001
Ca^{2+}	1/509	MD (Gramos)	8.0	2.46	3.31	2001
Ca^{2+}	1/199	MD (Pair+3-body)	7.1	2.50	-	2001
Ca^{2+}	1/199	QM/MM MD (HF/LANL2DZ)	7.6	2.46	-	2001
Ca^{2+}	1/199	QM/MM MD (DFT/LANL2DZ)	8.1	2.51	-	2001
Ca^{2+}	1/54	CP-MD (BLYP)	6.0	2.50	-	2002
Ca^{2+}	1/31	CP-MD (BLYP)	7.5	2.64	-	2003
Ca^{2+}	-	QMSTAT	6.9	2.50	-	2006
Ca^{2+}	1/58	CP-MD (BLYP)	6.5	2.39	-	2008
$CaCl_2$	2/58	CP-MD (BLYP)	6.0	2.39	-	2008
Ca^{2+}	2/62	CP-MD (BLYP)	6.0	2.39	-	2008

Table A.3 Theoretical observations on Ca^{2+} solvation in aqueous solutions (continued).

solute	ion/water ratio	method	*CN*	r_{max}	r_{min}	year
Ca^{2+}	1/199	QM/MM MD (HF/LANL2DZ)	7.4	2.45	-	2010
Ca^{2+}	1/1000	MD (Pair+3-body)	7.9	2.59	-	2010
Ca^{2+}	1/1000	QMCF MD (HF/ Ahlrichs pVDZ)	7.9	2.55	-	2010

Table A.4 Experimental observations on Ca^{2+} solvation in aqueous solutions.

solute	molarity (M)	method	*CN*	r_{max}	r_{min}	year
$CaCl_2$	1.0	XRD	6.0	2.42	-	1976
$CaCl_2$	2.0	XRD	6.0	2.42	-	1976
$CaCl_2$	4.5	XRD	6.0	2.42	-	1976
$CaCl_2$	4.5	ND	5.5	2.41	-	1980
$CaCl_2$	1.0	ND	10.0	2.46	-	1982
$CaCl_2$	2.8	ND	7.2	2.39	-	1982
$CaCl_2$	4.5	ND	6.4	2.40	-	1982
$CaCl_2$	1.1	XRD	6.9	2.39	-	1985
$Ca(NO_3)_2$	3.6	XRD	7.0	2.44	-	1997
$Ca(NO_3)_2$	6.0	XRD	7.0	2.45	-	1997
$CaCl_2$	0.12	EXAFS	8.0	2.46	-	2000
$CaCl_2$	2.0	XRD	6.0	2.46	-	2001
$CaBr_2$	1.5	XRD	8.0	2.46	-	2001
CaI_2	1.5	XRD	8.0	2.46	-	2001
$CaCl_2$	0.2	EXAFS	6.8	2.43	-	2003
$CaCl_2$	6.0	EXAFS	7.2	2.44	-	2003
$CaCl_2$	6.4	ND	7.0	2.41	-	2004
$CaCl_2$	4.0	ND	7.3	2.40	-	2004
$CaCl_2$	6.0	EXAFS	6.8	2.43	-	2006

APPENDIX B

LIST OF PRESENTATIONS

1. Supachai Wanprakhon and Anan Tongraar. (January 21-23, 2010). Structure of the hydrated Ca^{2+}: A QM/MM MD simulation based on ONIOM-XS method study. **Pure and Applied Chemistry International Conference (PACCON 2010)** Ubon Ratchathani University, Ubon Ratchathani, Thailand.

APPENDIX C

PUBLICATION

Chemical Physics Letters 517 (2011) 171–175

Contents lists available at SciVerse ScienceDirect

Chemical Physics Letters

journal homepage: www.elsevier.com/locate/cplett

Hydration structure and dynamics of K^+ and Ca^{2+} in aqueous solution: Comparison of conventional QM/MM and ONIOM-XS MD simulations

Supachai Wanprakhon [a], Anan Tongraar [a,*], Teerakiat Kerdcharoen [b]

[a] School of Chemistry, Institute of Science, Suranaree University of Technology, Nakhon Ratchasima 30000, Thailand
[b] Department of Physics and NANOTEC Center of Excellence, Faculty of Science, Mahidol University, Bangkok 10400, Thailand

ARTICLE INFO

Article history:
Received 23 July 2011
In final form 21 October 2011
Available online 25 October 2011

ABSTRACT

Molecular dynamics (MD) simulations based on the conventional QM/MM scheme and ONIOM-XS method have been performed to investigate structural and dynamical properties of K^+ and Ca^{2+} in water. Regarding the detailed analyses of the ONIOM-XS MD trajectories, the average hydration numbers for K^+ and Ca^{2+} were found to be 6.3 and 7.6, respectively, compared with the corresponding values of 7.0 and 7.8 derived by the conventional QM/MM simulations. Together with the significant difference found in the comparison of the dynamics details, the ONIOM-XS method clearly shows its capability in predicting more reliable detailed knowledge of these hydrated ions.

1. Introduction

Comprehensive information on the structure and dynamics of ions solvated in aqueous electrolyte solutions is essential in order to understand their crucial role in solution chemistry, biochemistry and pharmacology [1–3]. Among simple ions, potassium (K^+) and calcium (Ca^{2+}) are ubiquitous in nature, and the interactions of these ions with water are responsible for a diverse number of chemical and biological processes [4,5]. During the past decades, a number of experimental and theoretical attempts have been made to elucidate the details of these ions in aqueous solutions [6–27]. Nevertheless, an inhomogeneous picture, even for such fundamental properties as the average number of coordinating solvent molecules and the mean ion-oxygen nearest-neighbor distance, still exists. In experiments, large variations of the coordination numbers, ranging from 4 to 7 and from 5.5 to 10, were reported for K^+ [6–9] and Ca^{2+} [10–18], respectively. The observed difference in these data has been attributed mainly to the concentration dependence, as well as to the different experimental methods employed.

Theoretical studies of K^+ and Ca^{2+} in aqueous solutions, *i.e.*, in terms of Monte Carlo (MC) and molecular dynamics (MD) simulations, also predicted large variations of the coordination numbers, varying from 6.3 to 8.8 [19–24] and from 6 to 10 [10,11,14,19,25–27], respectively. With regard to earlier MC and MD studies [19,22–24,26], the observed discrepancy could be ascribed to the use of different molecular mechanical (MM) force fields in describing the system's interactions. In this respect, the quality of the simulation results depends strongly on the reliability of the ion–water and water–water potentials employed in the simulations. To accurately describe the properties of ions in aqueous solution, it has been demonstrated that the non-additive contributions as well as the polarization effects are significant and that the inclusion of these terms in the simulations through the quantum mechanical calculations is mandatory [28].

In terms of quantum-mechanics-based simulations, a well-known Car–Parrinello (CP) MD technique has been established for the study of solvated ions [29–31]. However, some limitations of the CP-MD technique come from the use of simple generalized gradient approximation (GGA) functionals such as BLYP and PBE and of the relatively small system size. As a consequence, a so-called combined quantum mechanics/molecular mechanics (QM/MM) technique has been proposed [32–34], and has been successfully applied for studying such systems [24–28,35–37]. By the QM/MM technique, the most interesting part of the system (*i.e.*, a sphere which includes the ion and its surrounding solvent particles) is treated quantum mechanically, while the rest of the system is handled by simple MM force fields. For the systems of K^+ and Ca^{2+} in aqueous solution, a series of QM/MM MD simulations have been carried out, providing more insights into the structure and dynamics of these hydrated ions [24–27]. Despite the technique's successes, however, there are some unsolved problems that undermine the validity of this approach. For example, according to the conventional QM/MM scheme, a smoothing function is applied only for the exchanging particles that are crossing the QM/MM boundary. Such treatment is not realistic since an immediate exchange of particles between the QM and MM regions also affects the forces acting on the remaining QM particles. In addition, the conventional QM/MM framework cannot clearly define the energy expression during the solvent exchange process [38,39].

To solve these problems, a more sophisticated QM/MM MD technique based on the ONIOM-XS method has been proposed

* Corresponding author. Fax: +66 44 224750.
E-mail address: anan_tongraar@yahoo.com (A. Tongraar).

0009-2614/$ - see front matter © 2011 Elsevier B.V. All rights reserved.
doi:10.1016/j.cplett.2011.10.048

[37,38]. This technique allows forces on all QM particles to be smoothed during particle exchange, and thus, clearly defines the system' energy expression. Recently, the ONIOM-XS MD technique has been successfully applied for systems of Li^+ [38] and Ca^{2+} [39] in liquid ammonia, proving its capability in providing reasonable energetic information and a coordination number. In this work, the ONIOM-XS MD technique will be applied for studying the hydration shell structure and dynamics of K^+ and Ca^{2+} in water. The ONIOM-XS results will be discussed and compared with those obtained from conventional QM/MM simulations, as well as with the available experimental data.

2. Method

Schematic details of the conventional QM/MM MD technique are available elsewhere in the literature [24–28,35–37], and therefore, only the QM/MM MD based on the ONIOM-XS method will be given here. In terms of the ONIOM-XS method, the system is comprised of a 'high-level' QM region, *i.e.*, a sphere which contains the ion and its surrounding solvent molecules, and the remaining 'low-level' MM bulk solvents. A thin switching shell located between the QM and MM regions is employed to detect the exchanging particles and help in smoothing the energy and forces of the combined system. Given n_1, l and n_2 as the number of particles in the QM region, the switching layer and the MM region, respectively, and $N(= n_1 + l + n_2)$ as the total number of particles, the potential energy of the system can be written in two ways based on the ONIOM extrapolation scheme [40]. If the switching layer is included into the high-level QM sphere, the energy expression is written as

$$E^{\mathrm{ONIOM}}(n_1+l;N) = E^{\mathrm{QM}}(n_1+l) - E^{\mathrm{MM}}(n_1+l) + E^{\mathrm{MM}}(N). \quad (1)$$

If the switching layer is considered as part of the 'low-level' MM region, the energy expression is

$$E^{\mathrm{ONIOM}}(n_1;N) = E^{\mathrm{QM}}(n_1) - E^{\mathrm{MM}}(n_1) + E^{\mathrm{MM}}(N). \quad (2)$$

With regard to Eqs. (1) and (2), E^{QM} and E^{MM} terms refer to the interactions obtained by the QM calculations and by the classical MM potentials, respectively. In this respect, the interactions between the QM and MM regions are also described by means of MM potentials, and thus, these contributions are already included into the $E^{\mathrm{MM}}(N)$. In practice, when a particle moves into the switching layer (either from QM or MM region), both Eqs. (1) and (2) must be evaluated. Then, the potential energy of the entire system is taken as a hybrid between both energy terms (1) and (2),

$$E^{\mathrm{ONIOM\text{-}XS}}(\{r_I\}) = (1-\bar{s}(\{r_I\}))\cdot E^{\mathrm{ONIOM}}(n_1+l;N) + \bar{s}(\{r_I\}) \cdot E^{\mathrm{ONIOM}}(n_1;N), \quad (3)$$

where $\bar{s}(\{r_I\})$ is an average over a set of switching functions for individual exchanging particles in the switching layer $s_i(x_i)$,

$$\bar{s}(\{r_I\}) = \frac{1}{l}\sum_{i=1}^{l} s_i(x_i), \quad (4)$$

In general, the switching function in Eq. (4) can have any form. Here, a polynomial expression is employed,

$$s_i(x_i) = 6\left(x_i - \frac{1}{2}\right)^5 - 5\left(x_i - \frac{1}{2}\right)^3 + \frac{15}{18}\left(x_i - \frac{1}{2}\right) + \frac{1}{2}, \quad (5)$$

where $x_i = ((r_i - r_0)/(r_1 - r_0))$, and r_0 and r_1 are the radius of the inner and outer surfaces of the switching shell, respectively, and r_i is the distance between the center of mass of the exchanging particle and the center of the QM sphere. The above polynomial form and parameter sets were derived to have an S-shape that converges to 0 and 1 at r_0 and r_1, respectively [38]. This polynomial form is preferred over the ST2 switching function [41] usually employed in the conventional QM/MM simulation because its first and second derivatives are both continuous. Please note that both energies and forces must be smoothed in the ONIOM-XS scheme, whereas only forces were handled in the conventional QM/MM scheme. The gradient of the energy can be written as

$$\nabla_R E^{\mathrm{ONIOM\text{-}XS}}(\{r_1\}) = (1-\bar{s}(\{r_1\}))\cdot\nabla_R E^{\mathrm{ONIOM}}(n_1+l;N) + \bar{s}(\{r_1\})\cdot\nabla_R E^{\mathrm{ONIOM}}(n_1;N) + \frac{1}{(r_1-r_0)}\nabla\bar{s}(\{r_1\})\cdot\left(E^{\mathrm{ONIOM}}(n_1;N) - E^{\mathrm{ONIOM}}(n_1+l;N)\right) \quad (6)$$

According to both conventional QM/MM and ONIOM-XS MD simulations, all interactions within the QM region were evaluated by performing *ab initio* calculations at the Hartree–Fock (HF) level of accuracy using DZV+ [42] and LANL2DZ [43,44] basis sets for H_2O and ions, respectively. Since the correlated QM calculations, even at the simple MP2-level, are still beyond our current computational feasibility, the use of the HF method has been well demonstrated in previous QM/MM studies [27,28,35,36]. In this respect, it should be realized that the HF scheme could produce an error due to the neglect of electron correlation effects. In recent QM/MM MD simulations of pure water [37], it has been shown that the HF method with a sufficiently large QM size could provide detailed information of liquid water in good agreement with the MP2/MM simulation and with experimental data concerning the H-bond structure and lifetime. For both aqueous K^+ and Ca^{2+} solutions, a QM radius of 4.2 Å and a switching width of 0.2 Å were chosen, corresponding to the ONIOM-XS parameters r_0 and r_1 of 4.0 and 4.2 Å, respectively. Compared with the conventional QM/MM scheme [24–28], these parameters correspond to the start and the end of the QM radius, *i.e.*, a defined QM/MM boundary where the smoothing applies. This QM size is assumed to be large enough to include most of the many-body contributions and the polarization effects, *i.e.*, at least within the first hydration shell of the ions. In this respect, the remaining interactions beyond the QM region could be well accounted for by the MM potentials. As can be seen in the next section (cf. Figures 1 and 2), the smooth shape of the ion–O radial distribution functions (RDFs) between 4.0 and 4.2 Å clearly support that transition of water molecules between the QM and MM regions occurs smoothly. A flexible model, which describes intermolecular [45] and intramolecular [46] interactions, was employed for water. This flexible water model allows explicit hydrogen movements and, thus, ensures a smooth transition when water molecules move from the QM region with its full flexibility to the MM region. The pair

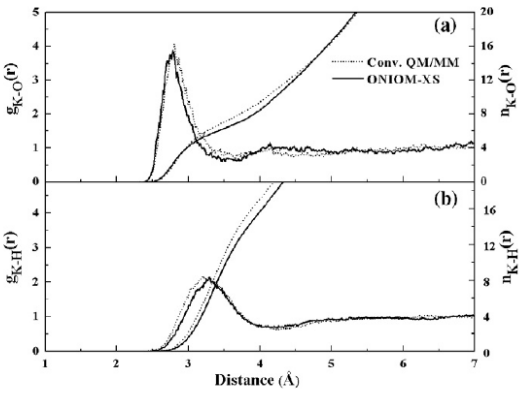

Figure 1. (a) K–O and (b) K–H radial distribution functions and their corresponding integration numbers, as obtained by the conventional QM/MM and ONIOM-XS MD simulations.

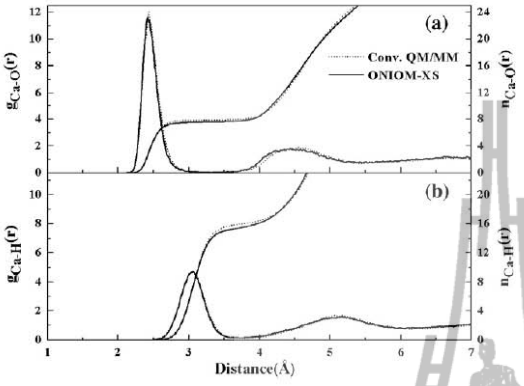

Figure 2. (a) Ca–O and (b) Ca–H radial distribution functions and their corresponding integration numbers, as obtained by the conventional QM/MM and ONIOM-XS MD simulations.

potential functions for describing K^+–H_2O and Ca^{2+}–H_2O interactions were obtained from previous works [24,26].

All MD simulations were performed in a canonical ensemble at 298 K with periodic boundary conditions. The system's temperature was kept constant using the Berendsen algorithm [47]. A periodic box, with a box length of 18.19 Å, contains one ion and 199 water molecules, corresponding to the experimental density of pure water. The reaction-field method [48] was employed for the treatment of long-range interactions. The Newtonian equations of motions were treated by a general predictor–corrector algorithm. The time step size was set to 0.2 fs, which allows for the explicit movement of the hydrogen atoms of water molecules. For the treatment of both aqueous K^+ and Ca^{2+} solutions, the conventional QM/MM and ONIOM-XS simulations were performed independently with the system's re-equilibration for 30 000 time steps, followed by another 150 000 (K^+) and 200 000 (Ca^{2+}) time steps to collect configurations every 10th step.

3. Results and discussion

The hydration shell structure of K^+ and Ca^{2+} are explained in terms of ion–O and ion–H RDFs and their corresponding integration numbers, as depicted in Figures 1 and 2, respectively. For the aqueous K^+ solution, the first K–O peaks obtained by both the conventional QM/MM and ONIOM-XS simulations are rather broad and are not well separated from the bulk, suggesting that water molecules surrounding the ion can easily exchange with bulk waters. The first K–O maximum peak predicted by the conventional QM/MM simulation is centered at 2.83 Å, whereas a slightly shorter distance of 2.78 Å is observed in the ONIOM-XS simulation. Integrations up to the first minimum of the K–O peaks yield the average coordination numbers of 7.0 and 6.3, respectively. With regard to the ONIOM-XS results, the first-shell coordination number and the K–O distance are closer to those of the X-ray diffraction study [9], which reported the K–O distance of 2.80 Å and the coordination number of 6. A further difference between the conventional QM/MM and ONIOM-XS simulations is recognizable in the K–H RDFs, in which the ONIOM-XS simulation reveals a slightly longer first K–H peak with a maximum at 3.28 Å, compared with the corresponding distance of 3.21 Å derived by the conventional QM/MM simulation. Overall, as compared with the conventional QM/MM results, the shape and position of the ONIOM-XS' K–O and K–H RDFs clearly reveal a more rigid structure of the K^+ first hydration shell. This finding clearly shows an important treatment of the ONIOM-XS method in obtaining a more reliable structural data for the K^+ hydrate.

In the case of Ca^{2+} (Figure 2), the results obtained by both the conventional QM/MM and ONIOM-XS simulations are almost identical, with the first Ca–O maximum peaks exhibited at about 2.44 Å. The shape and height of the Ca–O and Ca–H RDFs clearly indicate a strong 'structure-making' ability of Ca^{2+} in aqueous solution. The first Ca–O peaks are rather well separated from the outer region, giving the average coordination numbers of 7.8 and 7.6, respectively. The observed coordination numbers and the average Ca–O distances are in good accord with the extended X-ray absorption fine structure (EXAFS) measurements, in which the coordination numbers of Ca^{2+} were found to be of 6.8–8.0 with the Ca–O distances of 2.43–2.46 Å. The observed similarity of the conventional QM/MM and ONIOM-XS results is understandable since the ONIOM-XS method is expected to be more effective for the situation where the number of ligands that are crossing the QM/MM boundary is large, *i.e.*, a system where ion–water interactions are weak and water molecules surrounding the ion are labile. In this regard, it could be demonstrated that the conventional QM/MM scheme is reliable enough for the structural determination of such strong Ca^{2+}–water interactions, *i.e.*, a phenomenon where the immediate addition or deletion of particles in the QM region due to the solvent exchange is rare.

With regard to the QM/MM scheme, the selection of the QM size is found to be one of the main factors in obtaining different numbers of first-shell waters. For example, according to the analogous HF/MM simulations using similar basis sets, the coordination number of K^+ decreases significantly from 8.8 [20] and 8.3 [24] to the value of 7.0 in the present study according to the use of different QM radii of 3.8, 4.0 and 4.2 Å, respectively. Similarly, the coordination number of Ca^{2+} in water is found to decrease from 8.3 [26] to 7.8 in the present work according to the use of QM radii of 3.6 and 4.2 Å, respectively. In the earlier QM/MM studies, the size of the QM region was usually set with respect to only the first hydration sphere of the ions, *i.e.*, due to the restriction of CPU time. Regarding the results obtained by the present QM/MM simulations, it is obvious that the influence of non-additive interactions due to n-body effects beyond the first hydration shell of ions is significant, and that the use of a sufficiently large QM size is necessary in obtaining the correct coordination number of these hydrated ions. Recently, a lower K^+ coordination number of 6.2, which is close to the value of 6.3 obtained by the present ONIOM-XS simulation, was reported in the analogous QM/MM simulation with an enlarged QM radius of 6.0 Å [22]. This implies that the QM size with a radius of 4.2 Å employed in this work is considered to be large enough to achieve a sufficient level of accuracy in the QM/MM simulations once the ONIOM-XS method is employed.

To further analyze the difference between the conventional QM/MM and ONIOM-XS results, the probability distributions of the coordination numbers, calculated up to first minimum of the K–O and Ca–O RDFs, are plotted in Figure 3a and b, respectively. For K^+, the preferred coordination number is 7 (in addition to 8 and 6 in smaller amounts) in the conventional QM/MM simulation, whereas the value of 6 (followed by 7, 8 and 5 in decreasing amounts) is preferred according to the ONIOM-XS simulation. As can be seen in Figure 3a, the coordination number distributions for K^+ are rather broad, ranging from 5 to 10 (QM/MM) and from 4 to 9 (ONIOM-XS), indicating that a number of different hydrated K^+ species can simultaneously be formed in the solution. In the case of Ca^{2+}, although the preferred coordination number of 8 (followed by 7 in a smaller amount) is observed in both the conventional QM/MM and ONIOM-XS simulations, the probability distributions of the coordination numbers of 8 and 7 are significantly different, being of 81.9% and 16.7% and of 59.3% and

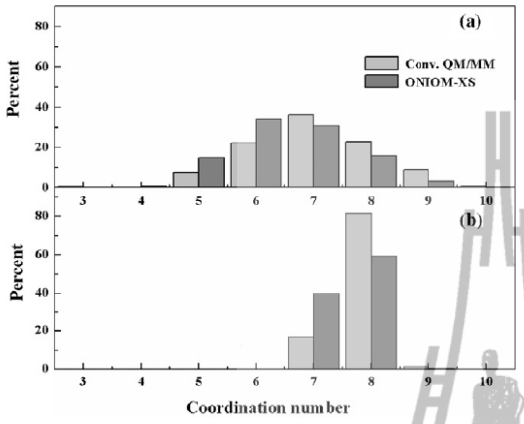

Figure 3. Distributions of the coordination numbers of (a) K^+ and (b) Ca^{2+}, calculated within the first minimum of the K–O and Ca–O RDFs, respectively.

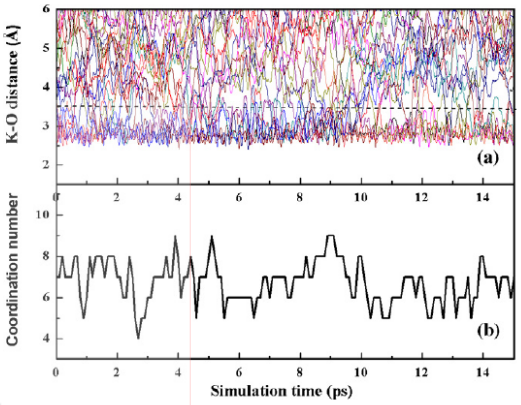

Figure 5. Time dependences of (a) K^+–O distance and (b) number of first-shell waters, as obtained from first 15 ps of the ONIOM-XS simulation. In Figure 5a, the dash line parallel to the x-axis indicates the first minimum of the K–O RDF.

40.0%, respectively. This supplies information that the ONOIM-XS treatment is essential in order to obtain the correct coordination number distributions of K^+ and Ca^{2+} hydrates. Further comparison on the orientation of first-shell waters, as obtained by the conventional QM/MM and ONIOM-XS simulations, is plotted in Figure 4a and b for the systems of K^+ and Ca^{2+}, respectively. In this context, the angle θ is defined by the ion–O axis and the dipole vector of first-shell water molecules. For K^+, the observed broad distributions of the θ angle clearly indicate weak K^+ hydration, *i.e.*, compared with the Ca^{2+} hydrate. As expected, the discrepancy between the conventional QM/MM and ONIOM-XS simulations is more significant than in the case of Ca^{2+}. This clearly supports the statement that the conventional QM/MM framework is probably useful for the structural determination of strong ion–water interactions, like Ca^{2+}–water, while a more sophisticated ONIOM-XS technique is necessary for the correct treatment of relatively weak ion–water interactions, such as in the case of K^+.

Besides the structural determination, it is of particular interest to evaluate the capability of the ONIOM-XS method in describing the dynamics details of these hydrated ions. Figures 5 and 6 show the time dependence of the ion–O distance and number of first-shell waters obtained from the ONIOM-XS simulations of aqueous K^+ and Ca^{2+} solutions, respectively. For K^+ (Figure 5), it is obvious that water molecules surrounding the ion are quite labile, showing numerous water exchange processes during the ONIOM-XS simulation. Consequently, this results in the observed large variation of the K^+ coordination numbers, ranging from 4 to 9. In the case of Ca^{2+} (Figure 6), most of the first-shell waters are tightly bound to the ion, in which the $Ca^{2+}(H_2O)_7$ and $Ca^{2+}(H_2O)_8$ complexes are found to be the dominant species in aqueous solution. The rates of water exchange processes at K^+ and Ca^{2+} were evaluated through mean residence times (MRTs) of water molecules surrounding the ions. In this work, the MRT data were calculated using the 'direct' method [49], as the product of the average number of water molecules in the first shell with the duration of the MD simulation, divided by the observed number of exchange events lasting a given time interval t^*. In general, it has been demonstrated that a t^* value of 0.0 ps is suitable for the estimation of hydrogen bond lifetimes, while a value of 0.5 ps is considered as a good measure for water exchange processes [49]. The calculated MRT data with respect to t^* values of 0.0 and 0.5 ps are summarized in Table 1, together with the corresponding data obtained from previous QM/MM works.

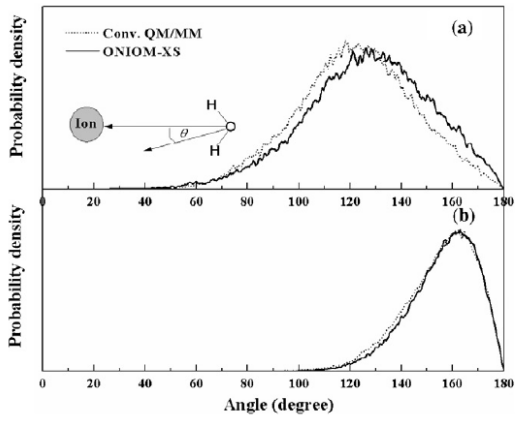

Figure 4. Probability distributions of θ angle in the first hydration shell of (a) K^+ and (b) Ca^{2+}, calculated within the first minimum of the K–O and Ca–O RDFs, respectively.

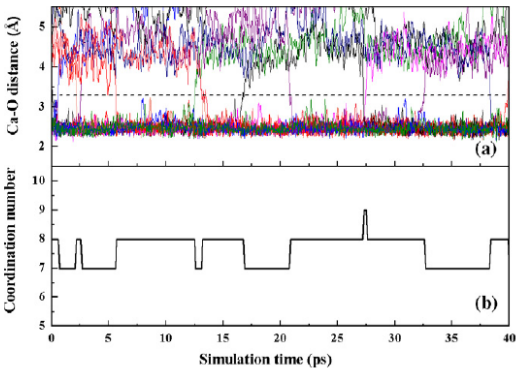

Figure 6. Time dependences of (a) Ca^{2+}–O distance and (b) number of first-shell waters, as obtained from 40 ps of the ONIOM-XS simulation. In Figure 6a, the dash line parallel to the x-axis indicates the first minimum of the Ca–O RDF.

Table 1
Number of water exchange events (N_{ex}) and mean residence time of water molecules in the vicinity of K^+ and Ca^{2+} (τ), calculated within the first minimum of the K–O and Ca–O RDFs.

Atom/solute	CN	t_{sim}	$t^* = 0.0$ ps		$t^* = 0.5$ ps		Ref.
			$N_{ex}^{0.0}$	$\tau_{H_2O}^{0.0}$	$N_{ex}^{0.5}$	$\tau_{H_2O}^{0.5}$	
Conventional QM/MM MD							
K^+	7.0	30.0	514	0.41	112	1.87	This work
	8.0	12.0	295	0.3	48	2.0	[50]
	8.8	12.0	189	0.47	26	3.4	[20]
Ca^{2+}	7.8	40.0	26	12.00	8	39.00	This work
	7.8	21.8	8	21.3	4	42.6	[49]
ONIOM-XS MD							
K^+	6.3	30.0	445	0.42	105	1.80	This work
Ca^{2+}	7.6	40.0	30	10.13	14	21.71	This work

For K^+, although the conventional QM/MM and ONIOM-XS simulations reveal rather similar MRT values for both $t^* = 0.0$ and 0.5 ps, the amount of first-shell waters and the number of exchange events are somewhat different. In the case of Ca^{2+}, a significant difference between the conventional QM/MM and ONIOM-XS simulations is observed for $t^* = 0.5$ ps, in which the latter predicts a relatively large number of exchange events (of about two times) with the smaller MRT value (of about half) when compared with that of the conventional QM/MM simulation. With regard to this point, it should be demonstrated that the correct degree of lability of the hydration shell is a significant factor in determining the reactivity of ions in solution. In particular for K^+, the detailed information of the water exchange processes is strongly related to the determination of the 'structure-breaking' ability of this ion in aqueous solution. According to some unsolved problems in the conventional QM/MM scheme, the more sophisticated QM/MM MD simulation based on the ONIOM-XS method is highly recommended for studying such condensed-phase systems.

4. Conclusions

In this work, the hydration structure and dynamics of K^+ and Ca^{2+} in water were investigated by means of conventional QM/MM and ONIOM-XS MD simulations. From the detailed analyses of the ONIOM-XS MD trajectories, the average hydration numbers for K^+ and Ca^{2+} were found to be 6.3 and 7.6, respectively, compared with the corresponding values of 7.0 and 7.8 derived from the conventional QM/MM simulations. A significant difference between the conventional QM/MM and ONIOM-XS simulations is also found in the comparison of dynamical data. The overall difference clearly indicates the deficiency of the conventional QM/MM scheme and, therefore, a more accurate QM/MM MD technique based on the ONIOM-XS method can be seen as a more suitable simulation approach, which can provide more reliable data on the structure and dynamics of these hydrated ions.

Acknowledgments

This work was supported by the Thailand Research Fund (TRF), under the Royal Golden Jubilee Ph.D. Program (Contract number PHD/0123/2549). A.T. also acknowledges support by the Synchrotron Light Research Institute (SLRI) and Suranaree University of Technology (SUT). T.K. acknowledges financial support from Mahidol University.

References

[1] H. Frank, Chemical Physics of Ionic Solutions, John Wiley & Sons, New York, 1956.
[2] E. Clementi, Determination of Liquid Water Structure, Coordination Number of Ions and Solvation for Biological Molecules, Springer-Verlag, New York, 1976. p. 107.
[3] N.J. Birch, J.D. Phillips, Adv. Inorg. Chem. 36 (1991) 49.
[4] E.R. Stadtman, Annu. Rev. Biochem. 62 (1993) 797.
[5] R.P. Wayne, Chemistry of Atmospheres, Oxford University Press, Oxford, 2000.
[6] Y. Marcus, Chem. Rev. 88 (1988) 1475.
[7] L.X. Dang, G.K. Schenter, V.-A. Glezakou, J.L. Fulton, J. Phys. Chem. B 110 (2006) 23644.
[8] G.W. Brady, J. Chem. Phys. 28 (1958) 464.
[9] G. Pálinkás, T. Radnai, F. Hajdu, Z. Naturforsch 35a (1980) 107.
[10] T. Todorava, P.H. Hünenberger, J. Hutter, J. Chem. Theory Comput. 4 (2008) 779.
[11] F. Jalilehvand, D. Spångberg, P. Lindqvist-Reis, K. Hermansson, I. Persson, M. Sandström, J. Am. Chem. Soc. 123 (2001) 431.
[12] Y.S. Badyal, A.C. Barnes, G.J. Cuello, J.M. Simonson, J. Phys. Chem. A 108 (2004) 11819.
[13] G. Licheri, G. Piccaluga, G. Pinna, J. Chem. Phys. 64 (1976) 2437.
[14] T. Megyes, I. Bakó, S. Bálint, T. Grósz, T. Radnai, J. Mol. Liq. 129 (2006) 63.
[15] S. Cummings, J. Enderby, R. Howe, J. Phys. C 13 (1980) 1.
[16] N. Hewish, G. Neilson, J. Enderby, Nature 297 (1982) 138.
[17] D. Spangberg, K. Hermansson, P. Lindqvist-Reis, F. Jalilehvand, M. Sandström, I. Persson, J. Phys. Chem. B 104 (2000) 10467.
[18] J. Fulton, S. Heald, Y. Badyal, J. Simonson, J. Phys. Chem. A 107 (2003) 4688.
[19] S. Obst, H. Bradaczek, J. Phys. Chem. 100 (1996) 15677.
[20] S.S. Azam, Zaheer-ul-Haq, M.Q. Fatmi, J. Mol. Liq. 153 (2010) 95.
[21] M. Mezei, D.L. Beveridge, J. Chem. Phys. 74 (1981) 6902.
[22] S.S. Azam, T.S. Hofer, B.R. Randolf, B.M. Rode, J. Phys. Chem. A 113 (2009) 1827.
[23] S.H. Lee, J.C. Rasaiah, J. Phys. Chem. 100 (1996) 1420.
[24] A. Tongraar, K.R. Liedl, B.M. Rode, J. Phys. Chem. A 102 (1998) 10340.
[25] C.F. Schwenk, H.H. Loeffler, B.M. Rode, J. Chem. Phys. 115 (2001) 10808.
[26] A. Tongraar, K.R. Liedl, B.M. Rode, J. Phys. Chem. A 101 (1997) 6299.
[27] C.F. Schewenk, B.M. Rode, Pure Appl. Chem. 76 (2004) 37.
[28] B.M. Rode, C.F. Schwenk, A. Tongraar, J. Mol. Liq. 110 (2004) 105.
[29] R. Car, M. Parrinello, Phys. Rev. Lett. 55 (1985) 2471.
[30] M.E. Tuckerman, D. Marx, M.L. Klein, M. Parrinello, Science 275 (1997) 817.
[31] D. Marx, J. Hutter, Modern Methods and Algorithms of Quantum Chemistry, in: J. Grotendorst (Ed.), NIC, FZ Jülich, 2000.
[32] A. Warshel, M. Levitt, J. Mol. Biol. 103 (1976) 227.
[33] U.C. Singh, P.A. Kollman, J. Comput. Chem. 7 (1986) 718.
[34] M.J. Field, P.A. Bash, M. Karplus, J. Comput. Chem. 11 (1990) 700.
[35] A. Tongraar, B.M. Rode, Chem. Phys. Lett. 403 (2005) 314.
[36] A. Payaka, A. Tongraar, B.M. Rode, J. Phys. Chem. A 114 (2010) 10443.
[37] D. Xenides, B.R. Randolf, B.M. Rode, J. Chem. Phys. 122 (2005) 174506.
[38] T. Kerdcharoen, K. Morokuma, Chem. Phys. Lett. 355 (2002) 257.
[39] T. Kerdcharoen, K. Morokuma, J. Chem. Phys. 118 (2003) 8856.
[40] M. Svensson, S. Humbel, R.D.J. Froese, T. Mutsubara, S. Sieber, K. Morokuma, J. Phys. Chem. 100 (1996) 19357.
[41] K. Tasaki, S. McDonald, J.W. Brady, J. Comput. Chem. 14 (1993) 278.
[42] T.H. Dunning Jr., P.J. Hay, Modern Theoretical Chemistry, III, Plenum, New York, 1976.
[43] P.J. Hay, W.R. Wadt, J. Chem. Phys. 82 (1985) 284.
[44] C.E. Check, T.O. Faust, J.M. Bailey, B.J. Wright, T.M. Gilbert, L.S. Sunderlin, J. Phys. Chem. A 105 (2001) 8111.
[45] F.H. Stillinger, A. Rahman, J. Chem. Phys. 68 (1978) 666.
[46] P. Bopp, G. Jancsó, K. Heinzinger, Chem. Phys. Lett. 98 (1983) 129.
[47] H.J.C. Berendsen, J.R. Grigera, T.P. Straatsma, J. Phys. Chem. 91 (1987) 6269.
[48] D.J. Adams, E.H. Adams, G.J. Hills, Mol. Phys. 38 (1979) 387.
[49] T.S. Hofer, H.T. Tran, C.F. Schwenk, B.M.J. Rode, Comput. Chem. 25 (2004) 211.
[50] A. Tongraar, B.M. Rode, Chem. Phys. Lett. 385 (2004) 378.

CURRICULUM VITAE

Mr. SUPACHAI WANPRAKHON

Education Background:

2002-2005 B.Sc. Second Class Honor (Chemistry), Ubon Ratchathani University, Ubon Ratchathani, Thailand

2006-2011 Ph.D. Candidate (Chemistry), Suranaree University of Technology, Nakhon Ratchasima, Thailand

Experiences:

2007-2009 Teaching Assistant, School of Chemistry, Institute of Science, Suranaree University of Technology, Nakhon Ratchasima, Thailand

Grant and Fellowships:

2007-2009 SUT Teaching Assistantship

2007-2011 The Royal Golden Jubilee (RGJ) Ph.D. Scholarship, Thailand Research Found (TRF)